

FINAL
N 7 3 3 0 6 7 3

GEOTECHNICAL ENGINEERING

MECHANICS OF WHEEL-SOIL INTERACTION

**CASE FILE
COPY**

by

H. JOHN HOVLAND

PREPARED FOR NASA HEADQUARTERS, WASHINGTON, D.C.
UNDER NASA GRANT NGR 05-003-406

APRIL 1973

SPACE SCIENCES LABORATORY



UNIVERSITY OF CALIFORNIA • BERKELEY

GEOTECHNICAL ENGINEERING

MECHANICS OF WHEEL-SOIL INTERACTION

FINAL REPORT FOR RESEARCH PHASE:

TRAFFICABILITY

by

H. John Hovland

Prepared for NASA Headquarters, Washington, D. C.
under NASA Grant NGR 05-003-406, "Lunar Soil
Properties and Soil Mechanics"

April, 1973

SPACE SCIENCES LABORATORY

SERIES 14 ISSUE 23

UNIVERSITY OF CALIFORNIA • BERKELEY

This report was prepared under NASA Grant NGR05-003-406, Lunar Soil Properties and Soil Mechanics, for the National Aeronautics and Space Administration. Technical liaison for this work was conducted by the Assistant Administrator for University Affairs. James K. Mitchell, Professor of Civil Engineering, served as Principal Investigator.

PREFACE

When man first invented the wheel, he did so without any theory. Several thousand years later, when man first went to the moon, he built the wheel for the Lunar Roving Vehicle (LRV), again without adequate theory. If man had waited for exact theory, the LRV probably would not have been carried to the moon.

So it seems that the existentialist is right in saying that existence precedes essence; that discovery proceeds from conceiving the physical phenomenon, to supplementing this phenomenon with explanation, usually expressed by mathematical abstractions. At least in wheel-soil interaction, wheels have preceded theory. Thus, a theoretical framework for a physical phenomenon which is known to exist can be useful, but it is not essential.

This philosophical argument presents a fundamental restriction to the value of any theory. There are, however, other less fundamental but more immediate restrictions.

In reviewing trafficability literature and in contemplating such phenomena during the past two years, the author (schooled primarily in soil mechanics) has become impressed with the complexity of the general problem of off-road mobility (see, for example, Bekker, 1969). This problem does not consist merely of a single, ideal wheel operating in an ideal environment, but of coupled wheels operating both in ruts made by preceding wheels and in virgin terrain. Further, the traverse over such a terrain is likely to include various soils, rocks, and bumps. The dynamic overall ride over such a terrain may, therefore, be only remotely related to theory developed for ideal wheel-soil conditions.

A general solution to a complex problem often results from research on separate aspects of the problem. This report presents a different and perhaps practically applicable theory on the very limited phenomenon of a rigid cylindrical wheel operating in a homogeneous soil. The developments are based on relatively simple considerations of statics and dynamics. Fundamental observations render the problem determinate. This leads to solutions of the sinkage and the pull which are likely to be within 15% of the correct value.

It is hoped that the theory presented in this report will be useful in evaluating and designing wheels for off-road mobility. Some new ideas are presented, and these need to be thoroughly checked and tested. It is hoped that concepts such as 1) the line of action of the resultant of radial stresses, 2) slip at a point, 3) the shear stress surface $\tau = f(\theta, s)$, 4) the closed-form approximate relation between contact angles and sinkage, 5) the general graphical solution for pull, 6) soil inertia forces, 7) equivalent cohesion, and 8) the performance surface, will inspire further thinking and relevant research.

The author wishes to express his appreciation to the National Aeronautics and Space Administration (NASA) for sponsoring this research. Special thanks go to Professor James K. Mitchell for his continued support and patience throughout the investigation, and for reviewing the manuscript. The author also gratefully acknowledges Mr. Dieter J. Schuring for reviewing Chapter 7 and Ms. Madeline Travers for editing the report. Finally, in one way or another, this treatise reflects understanding and experience accumulated in off-road mobility literature, without which this study would have been impossible.

TABLE OF CONTENTS

	<u>Page</u>
PREFACE	iii
CHAPTER 1 INTRODUCTION	1
CHAPTER 2 WHEEL-SOIL INTERACTION	3
CHAPTER 3 GENERAL WHEEL-SOIL INTERACTION THEORY	12
Dynamic Equilibrium	12
Force Component Equations	17
Slip and Instantaneous Wheel Velocity	19
The Friction Circle Method	22
Rigid Wheel in Cohesionless Soil	26
CHAPTER 4 APPROXIMATE WHEEL-SOIL INTERACTION THEORY	29
Line of Action of Resultant of Radial Stresses - A Fundamental Observation	29
Evidence in Support of this Observation	29
Cylindrical Wheel Rolling Down a Soil Slope	29
Spheres Rolling Down a Soil Slope	32
Experimental Data on the Line of Action of the Resultant of Radial Stresses	34
Theory	41
Forces Acting on a Wheel	41
Consideration of Magnitude and Direction of F	46
Inaccuracy Resulting from an Error in Selected Contact Angles	49
CHAPTER 5 WHEEL SINKAGE	52
Wheel Sinkage and Contact Angles	52
Pressure Sinkage Relations	54
CHAPTER 6 MOBILIZATION OF SHEAR STRESSES	66
Slip at a Point	66
Soil Displacement vs. Slip	69
Wheel-Soil Interface Strength Parameters	73
Shear Stress Surface	73

	<u>Page</u>
CHAPTER 7 SOIL INERTIA IN WHEEL-SOIL INTERACTION	78
Theoretical Analysis	78
Schuring's Analysis	90
Equivalent Cohesion	94
Discussion	95
CHAPTER 8 WHEEL-SOIL INTERACTION ANALYSIS	110
Summary	110
Analysis Procedure	114
Comparisons	118
Conclusions and Recommendations	121
REFERENCES	128
LIST OF SYMBOLS	130

CHAPTER 1. INTRODUCTION

A primary objective in off-road mobility is the design of a wheel which allows the most efficient transformation of mechanical energy of the engine to translational capability of the wheel. The most important single parameter in such a design is the pull, P , that the wheel can develop. This is defined as the pull that can be developed from the traction of a given wheel on a given soil for a certain input torque, T . In order to perform the desired design, it must be possible to predict this pull, either from theory or from experience.

Previous approaches to wheel-soil interaction have been either quasi-theoretical (Bekker, 1956) or empirical (U. S. Army Waterways Experiment Station [WES], 1954). One major shortcoming of the empirical approaches, and to a certain extent of the quasi-theoretical approaches, is the necessity to test a full size wheel. Adequate theory would considerably reduce the need for such expensive testing, although it would not do away with testing entirely.

A fairly substantial body of literature on wheel-soil interaction has accumulated over the years. An adequate review will not be attempted 1) because an excellent review is available (Bekker, 1969), and 2) because most of the previous approaches have little direct bearing on the developments presented in this report.

Because the wheel-soil interaction problem is indeterminate, and the torque input and wheel variables are rather specific, many investigators hoped that the secret to the solution could be found in the soil. Consequently, much recent research has dealt with methods of measuring and predicting soil flow and pressure distributions at the wheel soil contact. These investigations have resulted in a better understanding of the

wheel-soil interaction problem. They have also led to the conclusion that deformation processes in the soil are very complex, and that consequences of assumptions are difficult to evaluate.

This report presents both rigorous (general) theory and approximate theory for wheel-soil interaction. The purpose of the general theory is primarily to form a basis for further developments. The approximate theory forms the basis for a practical solution to the problem. It will be shown that two fundamental observations render the problem determinate:

1. The line of action of the resultant of radial stresses acting at the wheel soil interface approximately bisects the wheel-soil contact angle, θ_T , for all values of slip, s .
2. A shear stress surface, $\tau = f(\theta, s)$, can be hypothesized.

The influence of soil inertia forces is also evaluated. A concept of equivalent cohesion is introduced which allows a convenient experimental comparison for both cohesive and frictional soils. This theory compares favorably with previous analyses and experimental data, and shows that soil inertia forces influencing the motion of a rolling wheel can be significant. It is assumed that the inertia forces can be superimposed on forces resulting from a static analysis.

CHAPTER 2. WHEEL-SOIL INTERACTION

As a wheel moves on a deformable soil, a complex interaction takes place at the wheel-soil contact and in the adjacent soil. Fig. 2-1 illustrates a track and associated shear surfaces resulting from pulling a 24-inch (61-cm) diameter rigid spherical wheel on Yuma sand.

Model studies of this interaction (Hovland and Mitchell, 1972) show that the most noticeable features are:

1. Forward bending (movement) of initially vertical soil sections; some associated lateral movement.
2. Volume change in soil (compression directly under the wheel and dilation to the sides and front).
3. Shear surfaces, and sliding primarily forward along these surfaces.

To explain some of the details associated with general shear, the sequence of rolling and shearing is diagrammed in Fig. 2-2; (a) the soil before the wheel has rolled over it; (b) the shear surfaces and deformations that develop as the wheel rolls to the right, to position B; and (c) the appearance of the section after the wheel has rolled past.

Observations of particular interest are:

1. Shear surfaces do not appear to originate at the wheel surface (see Fig. 2-2b), as is often considered the case with shear under a loaded footing.
2. At the time a shear surface develops, its lower end is roughly parallel to the wheel surface. It diverges from a direction parallel to the wheel surface as it proceeds up and forward.
3. A wedge of soil is apparently pushed up and forward.

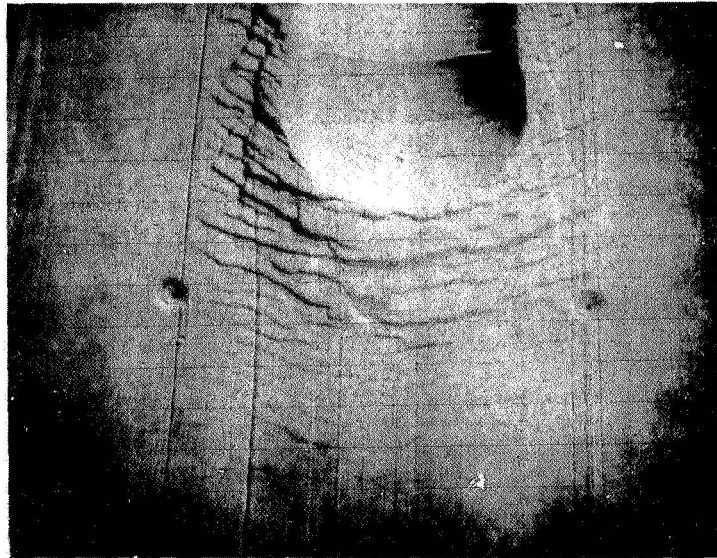


Fig. 2-1. Track and shear surfaces resulting from pulling a 24-inch diameter, 564-pound sphere on Yuma sand.

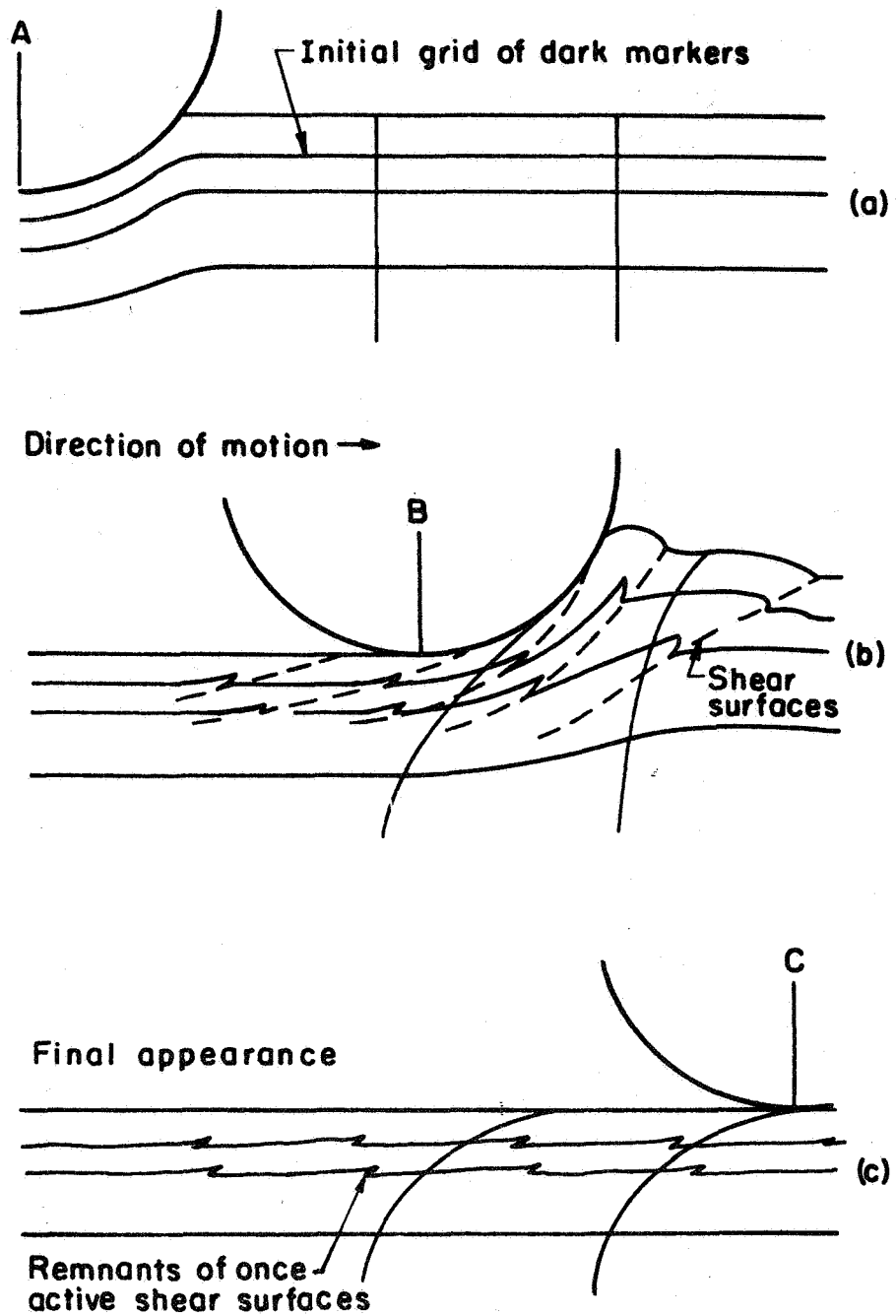


Fig. 2-2. Sequence of soil deformation and shear surface development under a rolling wheel.

4. Movement along any one shear surface is restricted, as implied by the relatively short but constant displacements.
5. Shear surfaces are spaced at relatively constant intervals as can be seen from the spacing of the teeth marks (compressed remnants of once active shear surfaces).

It is possible to conclude that the shearing process is not continuous, but consists of separate small shear phenomena spaced at relatively constant intervals with respect to space and time. The spacing of the shear surfaces as well as the amount of movement along any one shear surface is undoubtedly a function of soil type. Hence, although the rolling of a wheel may appear continuous to the naked eye, it is possible that the soil acceleration acting on the wheel changes slightly from one shear surface to the next.

The fact that shearing along any one shear surface appears to be restricted to a relatively small distance is perhaps associated with the change in direction of the shear surface with respect to the stress causing the movement. Most of the movement along a shear surface probably takes place when the surface is first formed. At that time, the shear surface is directed forward at an angle of $45^\circ - \phi/2$ to the direction of the major principal stress. As the wheel moves forward, the shear surface bends or turns toward a more vertical position. As the wheel passes, the shear surface is again bent down toward a final, more horizontal position (Fig. 2-2).

An instrumented spherical wheel, which was tested in Yuma sand, allowed further insight into wheel-soil interaction. The maximum radial wheel-soil contact pressure increased with increasing wheel load and then remained approximately constant, as shown in Fig. 2-3. This suggests

that the maximum radial pressure increases until the soil bearing capacity is reached. With further increase in wheel load, equilibrium is established by sinkage into the soil, with the load being distributed over a larger area. It is to be noted that, with the two lightest wheel loads, no distinct shear planes could be detected. Similar information can also be deduced from analysis by Vincent (1961) who noted that the rear wheel-soil contact angle for wheel loads too light to generate shear is relatively larger than the same angle for wheel loads heavy enough to generate shear.

The number of shear surfaces that could be distinguished in the forward shear zone (soil in front of wheel) were counted, and the results are presented in Fig. 2-4 as a function of track depth. The point on the horizontal axis of Fig. 2-4 corresponds to the 1200-Newton wheel load in Fig. 2-3.

The above discussion and data are primarily applicable to a spherical wheel rolling in sand. For such a soil, the interaction mechanism is dependent on the state of compaction. In a very loose state, the material would be compressible and the deformations would consist of both volume change and shearing distortion, but no general shear surfaces would develop. In a very dense state, general shear would be more significant, although volume change and shearing distortion would also take place. The usual case would involve all three phenomena; initial volume change accompanied by shearing distortion would be followed by general shear.

The following steps appear to be involved as a wheel rolls over a sand surface:

1. Compression occurs under the wheel.
2. Initially vertical soil sections are bent forward.

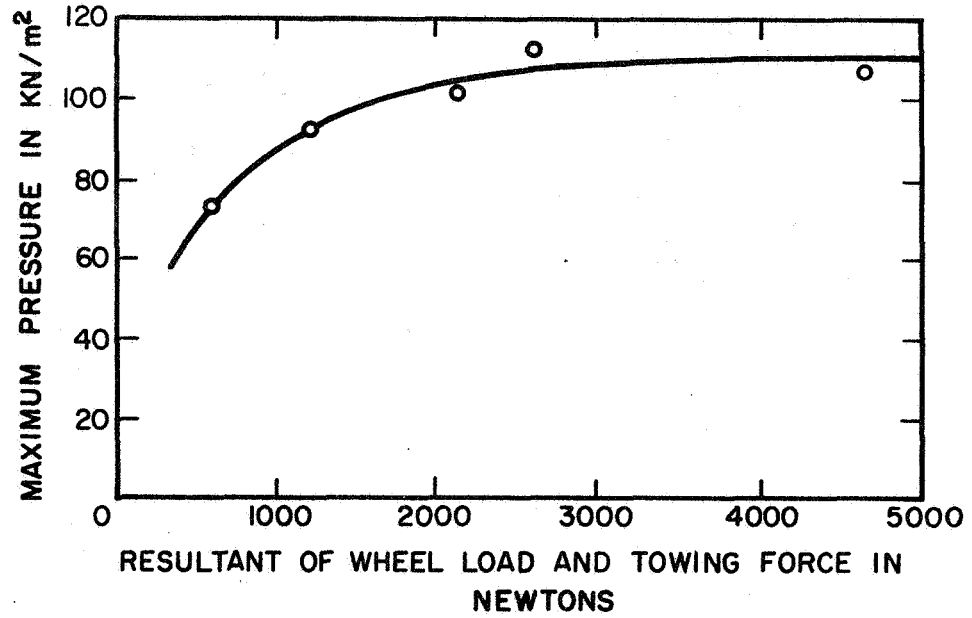


Fig. 2-3. Maximum pressure vs. resultant of wheel load and towing force.

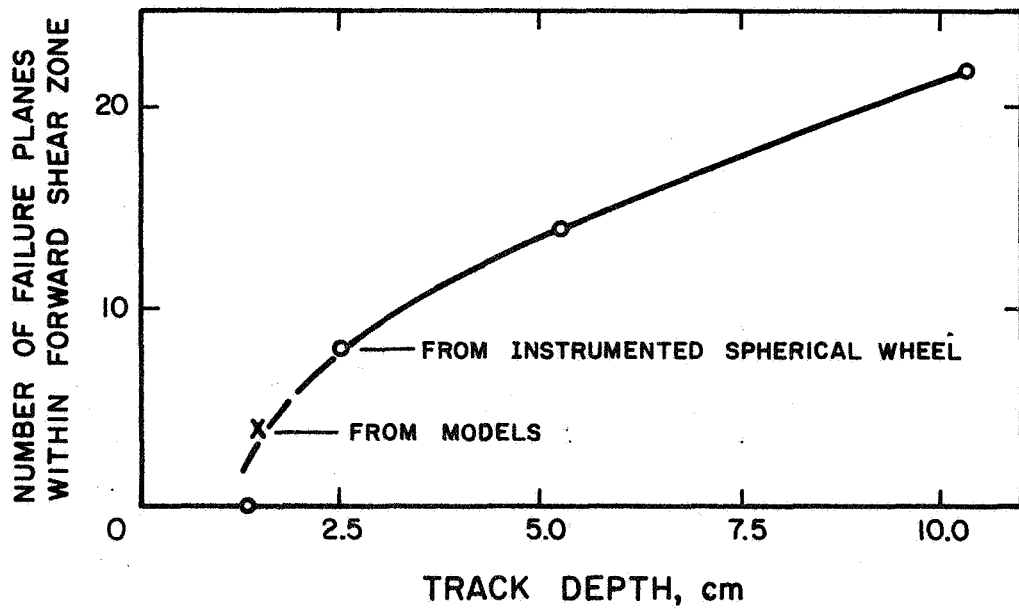
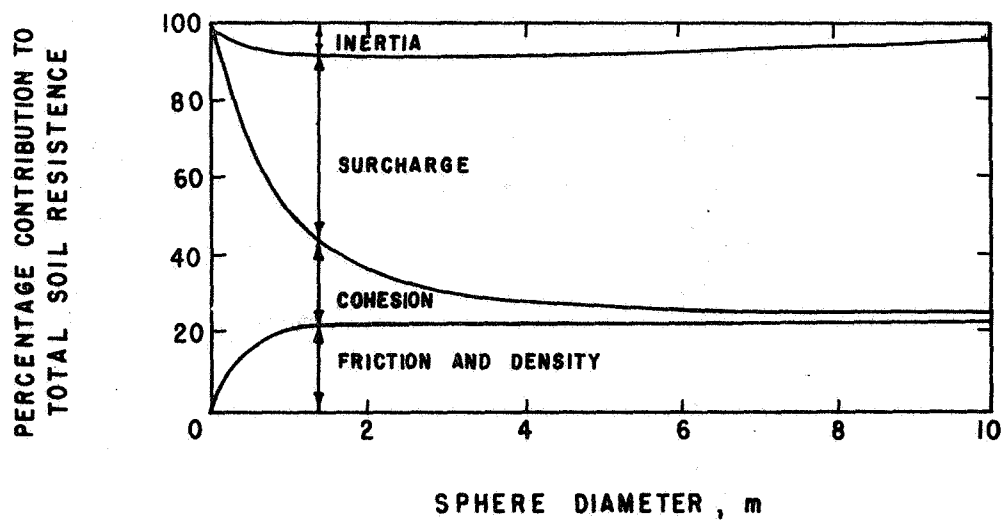


Fig. 2-4. Number of failure planes within the forward shear zone as a function of track depth.

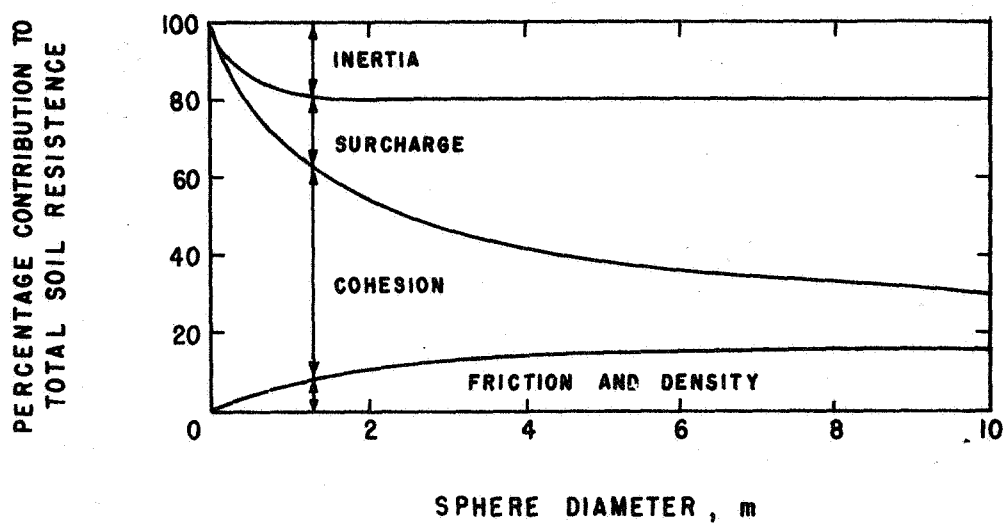
3. A horseshoe-shaped zone of dilation, which extends from the sides and around the front of the wheel, develops. This zone moves forward with the wheel. Some of the external evidence of this zone of dilation is the bow wave that forms in front of the wheel.
4. When volume changes and shearing distortion can no longer account for all the soil that must be displaced, shear surfaces develop. The development of shear surfaces is probably influenced by the magnitude of shearing distortion and the magnitude and direction of the major principal stress.
5. Sliding along the shear surfaces continues only for a short time and distances, as previously described.
6. After a certain distance, a new shear surface develops and the shearing cycle repeats itself.
7. As the wheel rolls forward, deformations assume a final position, and excess material from the bow wave is wasted to the sides to form the crests of the track.

Other experimenters have investigated wheel-soil interaction in clay (Yong and Webb, 1969; Yong and Windisch, 1970). These studies indicate that deformations are similar in clay although the elastic recovery or rebound is greater.

However, the relative importance of cohesion or friction depends on the nature of the phenomenon being investigated. A soil may be classified cohesionless by ordinary soil mechanics criteria, and yet for very small loaded areas cohesion may account for most of the resistance. Consider, for example, spheres rolling in a soil typical of lunar soil, with cohesion, c , of 20 psf (1 kN/m^2) and a friction angle, ϕ , of 37° . For analysis based on bearing capacity theory (Fig. 2-5), cohesion provides most of



a) Earth gravity.



b) Lunar gravity.

Fig. 2-5. Relative contribution to total soil resistance from cohesion, surcharge, friction and density, and soil inertia as a function of sphere diameter.

the resistance for a 10-cm in diameter sphere, while friction provides most of the resistance for a 2-m in diameter sphere. Fig. 2-5 also shows the relative contribution to total soil resistance (bearing capacity) from the various terms in the bearing capacity equation (Hovland, 1970), and it shows how these are influenced by the gravity field.

CHAPTER 3. GENERAL WHEEL-SOIL INTERACTION THEORY

The developments in this chapter form a basis for theory in subsequent chapters. It is hoped that these developments will also be of value to other wheel-soil interaction investigations which depend on a knowledge of the distribution of normal and shear stresses along the wheel-soil interface.

DYNAMIC EQUILIBRIUM

A free-body diagram of a wheel and all the forces and pressures acting on it are shown in Fig. 3-1. The symbols are defined below:

- a = linear acceleration of wheel
- u = angular acceleration of wheel
- m = mass of wheel, W/g
- W = wheel load or weight
- g = acceleration of gravity
- v = linear velocity of wheel
- ω = angular velocity of wheel
- I = mass moment of inertia of wheel
- T = input torque
- P = output pull, pull developed by the input torque and the wheel-soil traction
- dN = differential normal force
- dF = differential shear force
- dR = differential resultant
- F_a = algebraic sum of shear forces along the wheel-soil contact
- R_a = algebraic sum of resultants dR
- R = vectorial sum of resultants dR
- r = wheel radius

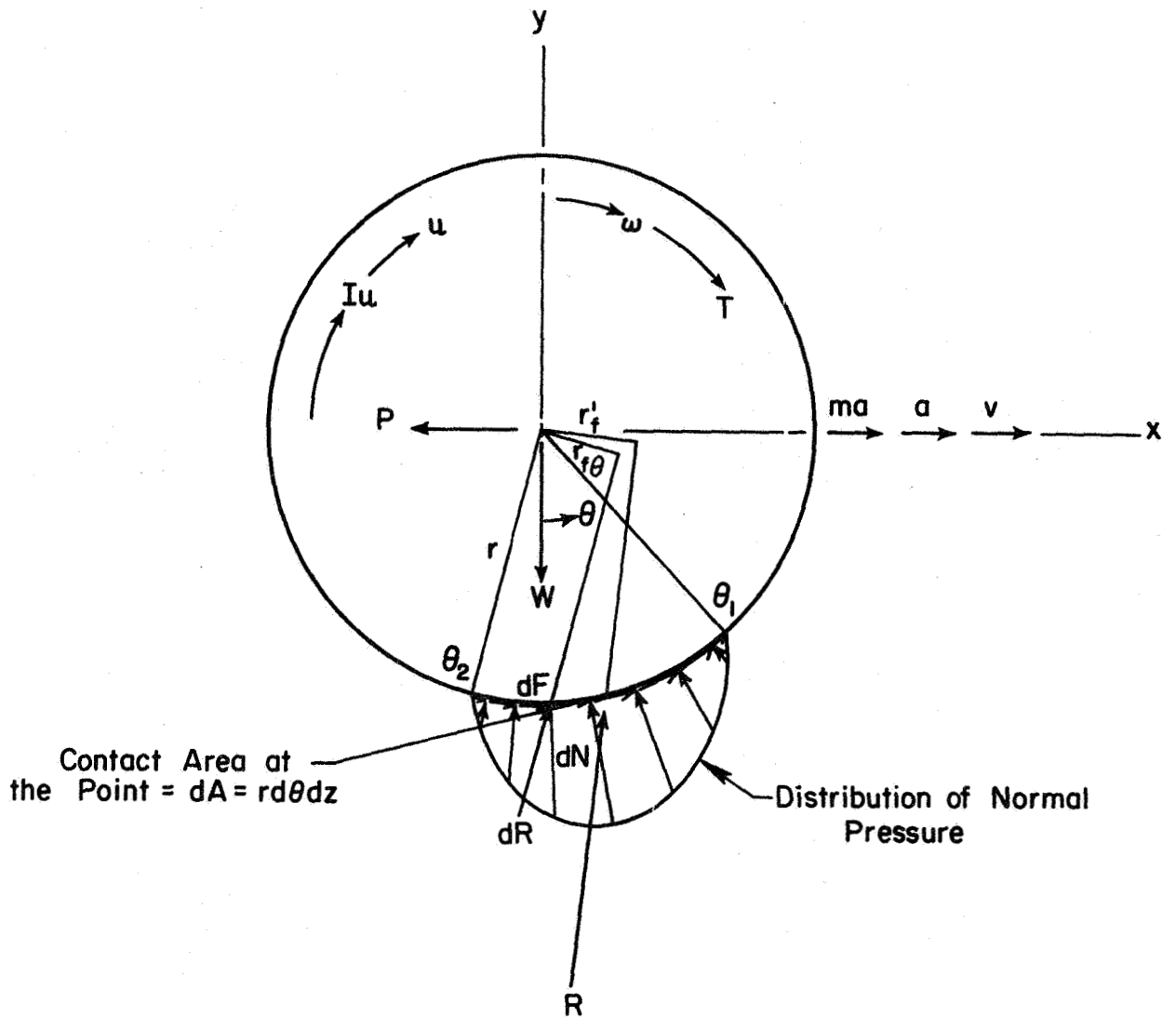


Fig. 3-1. Free body diagram of wheel.

$r_{f\theta}$ = moment arm of any dR

r_f' = moment arm of R

x, y, z = coordinates

θ = any central angle measured counterclockwise

θ_1 = angle between the vertical and front soil contact

θ_2 = angle between the vertical and rear soil contact.

For a rigid wheel rolling on an unyielding surface, the forces acting on the wheel can be represented graphically as shown in Fig. 3-2a. Analogously, for a wheel rolling on a deformable surface, the forces can be represented as shown in Fig. 3-2b. It is, therefore, valid to express the developed pull by

$$P = \sqrt{R^2 - W^2} \quad (3-1)$$

For the general case represented by Fig. 3-1,

$$P = \sqrt{R^2 - W^2} - ma \quad (3-2)$$

The unknown in equation (3-2) is the vectorial resultant of all forces acting at the wheel-soil contact, R , which is a function of the shear and normal stress distributions.

At any point on the contact surface, the normal stress may be defined as $\sigma_{\theta z}$ and the shear stress as

$$\tau_{\theta z} = c_{a\theta s} + \sigma_{\theta z} \tan \delta_{\theta s} \quad (3-3)$$

If we further include the possibility of a toroidal, or other than a cylindrical wheel, the radius may also be a function of z . (Such cases have usually been studied using the average wheel radius called the effective radius, r_e .) Then the total shear force along the wheel-soil contact is for the general case

a)
unyielding surface

b)
yielding surface

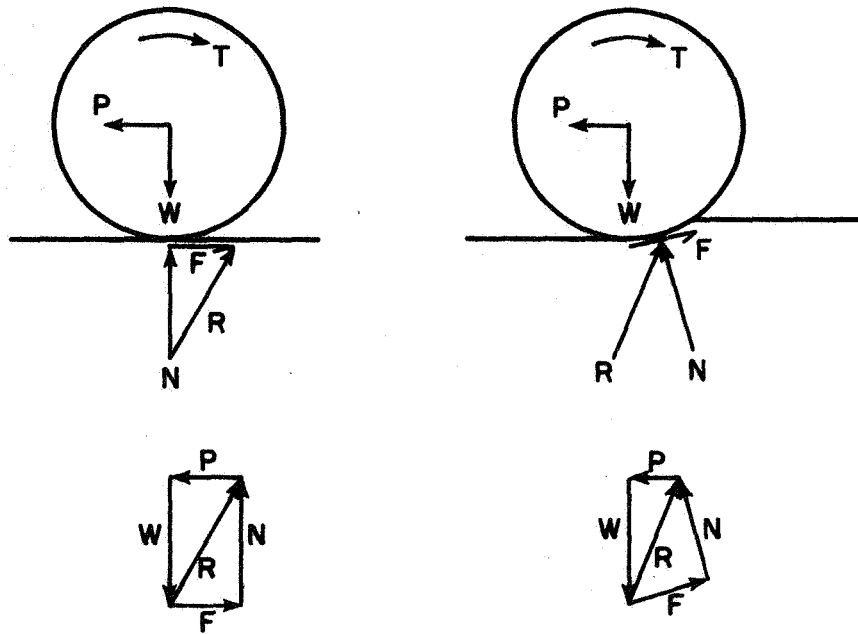


Fig. 3-2. Force polygons of forces acting on a wheel.

$$F_a = \iint r_z (c_{a\theta s} + \sigma_{\theta z} \tan \delta_{\theta s}) d\theta dz \quad (3-4)$$

In the above equations, the subscripts θ , s , and z indicate that the parameter having the subscripts is a function of the contact angle, θ , slip, s , and the dimension perpendicular to the plane of the paper, z . Also, in these equations, c_a = wheel-to-soil cohesion or adhesion and δ = the wheel-to-soil friction angle. The mobilization of c_a and δ will be considered later. They are in general much lower than the soil-to-soil cohesion, c , and the soil-to-soil angle of shearing resistance, ϕ .

Taking moments about the center of the wheel (Fig. 3-1) and noting that all the normal forces go through the center,

$$Rr_f' = F_a r = T - Iu \quad (3-5)$$

Thus we note that the quantity Rr_f' is determinable if either the total shear force, F_a , or the input torque, T , and the dynamics of the wheel are known. In this case,

$$R = \frac{1}{r_f'} (T - Iu) \quad (3-6)$$

If the input torque and wheel dynamics are not known, a more general and interesting case since it demonstrates the dependence on soil type, we have, from combining equations (3-4) and (3-5),

$$R = \frac{r}{r_f'} F_a = \frac{1}{r_f'} \iint r_z^2 (c_{a\theta s} + \sigma_{\theta z} \tan \delta_{\theta s}) d\theta dz \quad (3-7)$$

Combining equations (3-2) and (3-7) results in a general expression for the developed pull

$$(P+ma)^2 = \left[\frac{1}{r_f'} \iint r_z^2 (c_{a\theta s} + \sigma_{\theta z} \tan \delta_{\theta s}) d\theta dz \right]^2 - W^2 \quad (3-8)$$

which is valid for any pressure distribution and any soil obeying the Mohr-Coulomb failure criterion.

From this point the derivation will be continued for a cylindrical wheel, and it will be assumed that the pressure distribution is a representative average with respect to z . Equation (3-8) then reduces to

$$(P+ma)^2 = \left[\frac{r^2}{r_f} \int (c_{a\theta_s} + \sigma_{\theta} \tan \delta_{\theta_s}) d\theta \right]^2 - W^2 \quad (3-9)$$

It now remains to evaluate the force components associated with R , and r_f' .

FORCE COMPONENT EQUATIONS

Consider the wheel-soil contact shown in Fig. 3-3 and the forces acting there.

Depending on the sign of θ (the location on the wheel-soil contact of the point in question), the sign of the dN_y forces will always be positive, while the sign of the dF_y , dF_x , and dN_x forces will vary depending on θ and the state of slip of the wheel. By appropriately adding up all the x and y force components,

$$R^2 = (F_x + N_x)^2 + (F_y + N_y)^2 \quad (3-10)$$

the vectorial resultant.

The terms in equation (3-10) can be evaluated from:

$$dN = \sigma_{\theta} dA = r \sigma_{\theta} d\theta \quad (3-11)$$

$$dF = \tau_{\theta} dA = r \tau_{\theta} d\theta \quad (3-12)$$

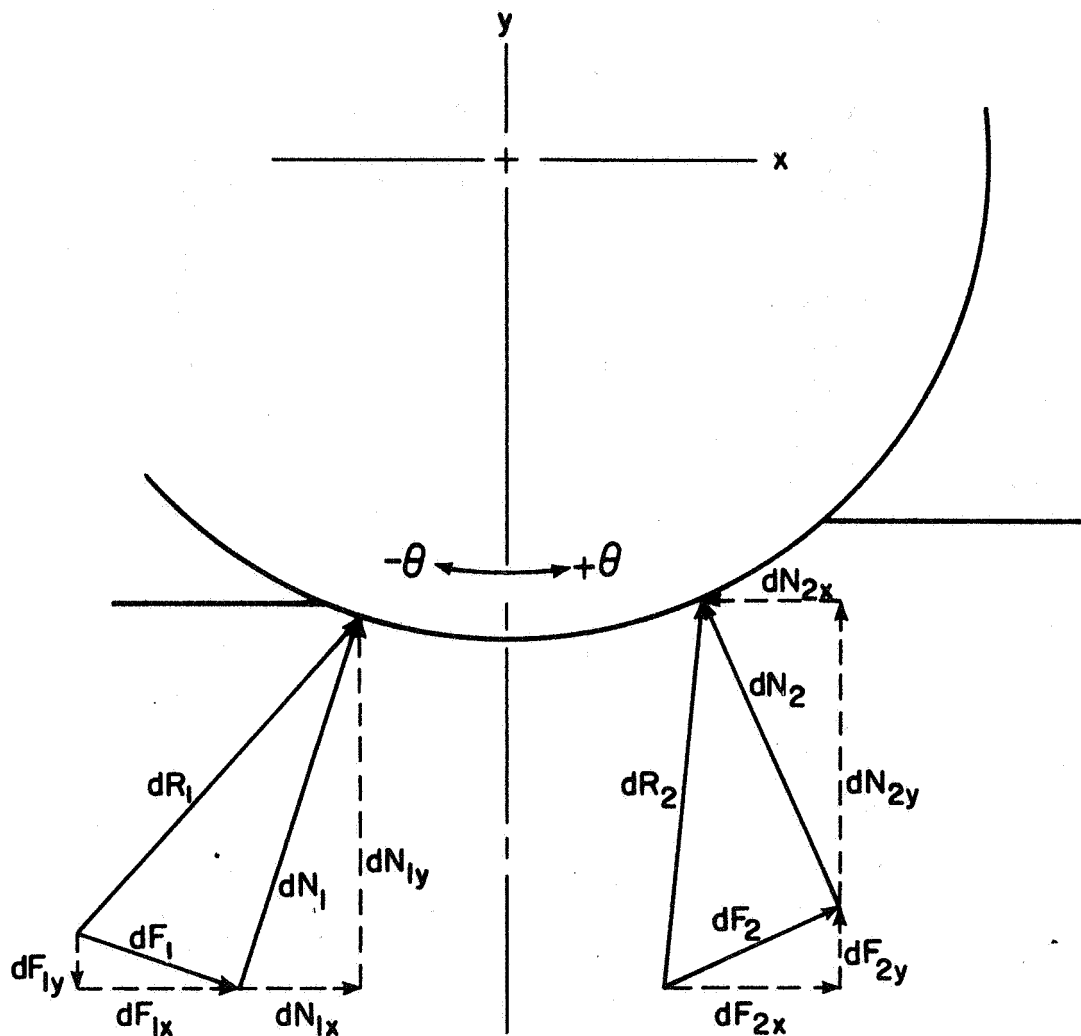


Fig. 3-3. Forces broken to x and y components.

$$\begin{aligned}
 F_x &= r \int \tau_\theta \cos\theta d\theta \\
 N_x &= -r \int \sigma_\theta \sin\theta d\theta \\
 F_y &= r \int \tau_\theta \sin\theta d\theta \\
 N_y &= r \int \sigma_\theta \cos\theta d\theta
 \end{aligned}
 \tag{3-13}$$

SLIP AND INSTANTANEOUS WHEEL VELOCITY

The instantaneous velocity of the wheel, can be easily determined (see also Andreyer, Sitkei, and Janosi (Bekker, 1969)).

Velocity components of a rolling wheel are shown in Fig. 3-4. The wheel is moving to the right with a velocity, $v_{c/x}$, of the center of the wheel with respect to an instantaneous coordinate system, x , fixed to a far point in the soil. Point, p , has a tangential velocity with respect to the center of the wheel of $v_{p/c}$. The desired velocity, $v_{p/x}$, is that of the point p with respect to x and it is the vector sum of $v_{p/c}$ and $v_{c/x}$.

$$\bar{v}_{p/x} = \bar{v}_{p/c} + \bar{v}_{c/x} \tag{3-14}$$

or.

$$v_{p/x} = \sqrt{(v_{c/x} - v_{p/c} \cos\theta)^2 + (v_{p/c} \sin\theta)^2} \tag{3-15}$$

Slip may be defined as

$$i = \frac{DR - DT}{DR} \tag{3-16}$$

where DR = distance wheel would have revolved had it been rolling on a hard surface without slip, and DT = distance wheel actually travelled. Then

$$\frac{DT}{DR} = (1 - i) \tag{3-17}$$

but also,

$$\frac{DT}{DR} = \frac{v_{c/x} t}{v_{p/c} t} = \frac{v_{c/x}}{v_{p/c}} \quad (3-18)$$

where t = time; therefore,

$$v_{c/x} = v_{p/c} (1 - i) \quad (3-19)$$

Substituting equation (3-19) into equation (3-15) gives

$$v_{p/x} = v_{p/c} \sqrt{[(1-i) - \cos\theta]^2 + \sin^2\theta} \quad (3-20)$$

which defines the magnitude of the instantaneous velocity of any point on the wheel periphery.

The direction of $v_{p/x}$ can also be determined. First, let

$$A_1 = A_2 - \theta \quad (3-21)$$

$$A_2 = \tan^{-1} \left(\frac{v_{c/x} - v_{p/c} \cos\theta}{v_{p/c} \sin\theta} \right) \quad (3-22)$$

$$-A_1 = \theta - \tan^{-1} \left(\frac{v_{c/x} - v_{p/c} \cos\theta}{v_{p/c} \sin\theta} \right) \quad (3-23)$$

Substituting equation (3-19) into equation (3-23), and simplifying gives

$$-A_1 = \theta - \tan^{-1} \left(\frac{(1-i) - \cos\theta}{\sin\theta} \right) \quad (3-24)$$

To establish a graphical solution for the instantaneous center of rotation, it would be interesting to determine at what vertical distance, y , from the bottom dead center of the wheel a line drawn at an angle A_1 to the tangent at a point would intersect a vertical drawn through C. Referring again to Fig. 3-4,

$$y = d - z \quad (3-25)$$

but

$$\begin{aligned} d &= r \sin \theta \tan(\theta + A_1) \\ &= r \sin \theta \tan A_2 \\ A_2 &= \tan^{-1} \left(\frac{(1-i) - \cos \theta}{\sin \theta} \right) \\ z &= r(1 - \cos \theta) \end{aligned}$$

With these substitutions

$$y = r \sin \theta \tan \left[\tan^{-1} \left(\frac{(1-i) - \cos \theta}{\sin \theta} \right) \right] - r(1 - \cos \theta) \quad (3-26)$$

Simplifying

$$\frac{y}{r} = \sin \theta \left(\frac{(1-i) - \cos \theta}{\sin \theta} \right) - 1 + \cos \theta$$

$$\text{or} \quad \frac{y}{r} = -i \quad (3-27)$$

This equation shows that the instantaneous center of rotation is located a vertical distance, ri , from the bottom dead center of the wheel-soil contact. For positive slip ($+i$), a distance $+y = +ri$ above, and for negative slip ($-i$), a distance $-y = -ri$ below the bottom dead center of the wheel.

Therefore, the magnitude of the velocity of any point along the wheel periphery with respect to a fixed coordinate system in the soil can be determined from equation (3-20), and the direction of the same velocity can be determined using equation (3-24) or graphically using the instantaneous center of rotation.

THE FRICTION CIRCLE METHOD

The forces acting along a sliding contact are illustrated in Fig. 3-5.

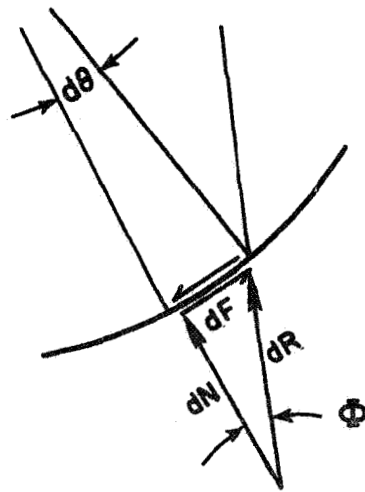


Fig. 3-5. Forces acting along a sliding contact.

Clearly the direction of dR for any differential contact area, dA , is defined by the angle, Φ .

$$\tan\Phi = \frac{dF}{dN} = \frac{\tau_{\theta}dA}{\sigma_{\theta}dA} = \left(\frac{c_a}{\sigma_{\theta}} + \tan\delta\right) \quad (3-28)$$

Then, the moment arm of any dR (Fig. 3-1) must be

$$r_{f\theta} = r\sin\Phi \quad (3-29)$$

Noting that if the ratio c_a/σ_{θ} in equation (3-28) is insignificant or zero, and if we have soil-to-soil sliding with friction angle ϕ rather than δ ,

$$r_{f\theta} = r\sin\Phi = r\sin(\tan^{-1}\tan\phi) = r\sin\phi = r_f \quad (3-30)$$

Equation (3-30) defines the radius of the friction circle as used by Taylor (1937). (Taylor first introduced the friction circle method for the analysis of the stability of cohesionless embankments.) In equation (3-30), $r_{f\theta}$ is independent of θ and therefore equal to r_f .

Combining equations (3-4) and (3-29) we obtain

$$\frac{r'_f}{r_{f\theta}} = \frac{1}{\sin\Phi} \frac{F}{R} \quad (3-31)$$

Equation (3-31) expresses the extent by which the moment arm to the resultant R differs from the moment arm to a dR force. That there is a difference between r'_f and $r_{f\theta}$ can be clearly illustrated for $c_a = 0$ as shown in Fig. 3-6. Whereas all the dR forces in Fig. 3-6 are tangent to the friction circle with radius $r_{f\theta}$, the resultant of any two dR forces, such as dR_{12} , acts at a slightly greater distance, r'_{f12} . Analogously, the resultant of all dR forces will also act at a somewhat greater distance, r'_f . The difference is anticipated to be small, however, and the correction factor, $r'_f/r_{f\theta}$, will be evaluated for certain cases of interest.

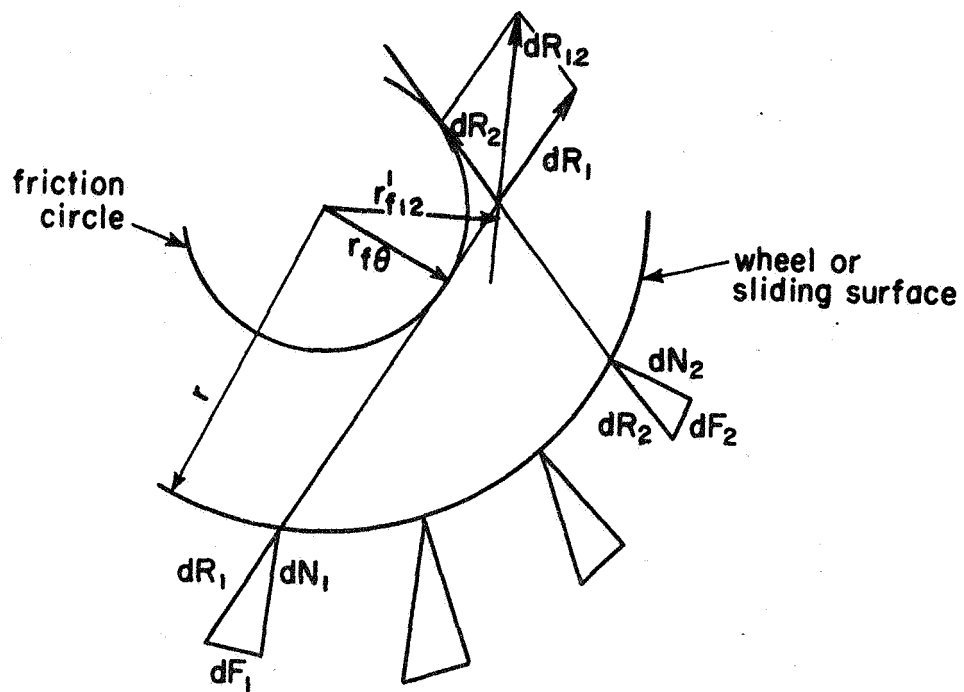


Fig. 3-6. The friction circle method, $c_a = 0$.

RIGID WHEEL IN COHESIONLESS SOIL

For a rigid cylindrical wheel driven at constant velocity in a cohesionless soil for which $c_a = 0$, equation (3-9) reduces to

$$P^2 = \left[\frac{r^2}{r_f} \int \tan \delta_{\theta_s} \sigma_{\theta} d\theta \right]^2 - W^2 \quad (3-32)$$

and equation (3-31) becomes

$$\frac{r'_f}{r_f} = \frac{1}{\sin \delta_{\theta_s}} \frac{F_a}{R} \quad (3-33)$$

Using equations (3-5) and (3-33), equation (3-32) can be expressed in terms of the r'_f/r_f ratio

$$P^2 = \left[\frac{r}{r'_f/r_f} \int \frac{\sigma_{\theta}}{\cos \delta_{\theta_s}} d\theta \right]^2 - W^2 \quad (3-34)$$

Using the force component equations (3-10), (3-12) and (3-13), the correction ratio, r'_f/r_f , can be solved from equation (3-33) for any integrable distribution of radial pressure at the wheel-soil contact. For a constant pressure distribution, for example, equation (3-33) reduces to

$$\frac{r'_f}{r_f} = \frac{\theta_T}{\sqrt{2} \sqrt{1 - \cos \theta_T}} \quad (3-35)$$

which is identical to Taylor's solution (θ_T = total wheel-soil contact angle). Taylor (1937) presents values of this correction ratio (Fig. 3-7) for both a constant and a sinusoidal pressure distribution. A constant pressure distribution is a good approximation for a pure clay; a sinusoidal pressure distribution is a good approximation for a pure sand. Other pressure distributions would likely lead to some intermediate correction.

Since Fig. 3-7 shows that the correction factor is very small (1-6%) for either case, for contact angles less than 70° , we may consider equation (3-34) a nearly rigorous solution for the pull that can be developed in a cohesionless soil.

The theoretical developments presented in this chapter are all based on the Mohr-Coulomb failure criterion, and depend on a knowledge of the shear and normal stress distributions along the wheel-soil contact. It is recognized that these pressure distributions are difficult to determine. In the next chapter it will be shown that, for all practical purposes, certain observations make it possible to bypass the difficult question of pressure distributions.

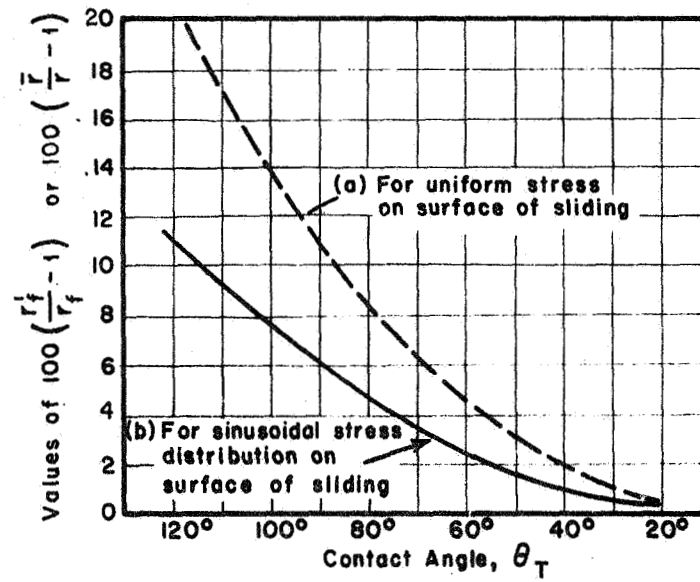


Fig. 3-7. Correction to be used with the friction circle method.

(Taylor, 1937)

CHAPTER 4. APPROXIMATE WHEEL-SOIL INTERACTION THEORY

LINE OF ACTION OF RESULTANT OF RADIAL STRESSES--A FUNDAMENTAL OBSERVATION

The line of action of the resultant of radial stresses approximately bisects the wheel-soil contact angle, θ_T , for all values of slip, s .

This observation is supported by:

- a) A rational argument based on a cylindrical wheel rolling down a soil slope at constant velocity
- b) An empirical argument based on data from spheres rolling down a soil slope at constant velocity
- c) Test data from many wheel-soil interaction experiments.

A relatively simple approximate theory is then developed.

EVIDENCE IN SUPPORT OF THIS OBSERVATION

Cylindrical Wheel Rolling Down a Soil Slope

A cylindrical wheel rolling down a soil slope is shown in Fig. 4-1.

The symbols in Fig. 4-1 are defined as follows:

- W = weight of wheel
- m = mass of wheel
- R = resultant soil reaction force
- R_x = component of R parallel to slope
- R_y = component of R normal to slope
- r = radius of wheel
- r'_f = distance from center of wheel to line of action of R
- I = moment of inertia of wheel
- a = linear acceleration of wheel
- u = angular acceleration of wheel

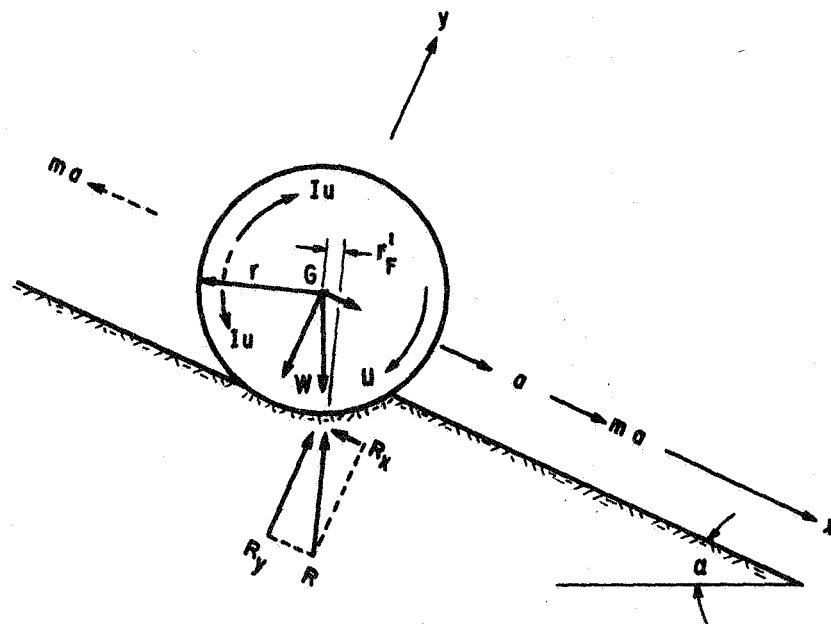


Fig. 4-1. Dynamic equilibrium of a cylindrical wheel rolling down a soil slope.

x, y = coordinate directions

α = slope angle

Negative slip usually takes place as a wheel rolls freely down a slope, and, therefore, $a \neq ur$.

Applying Newton's Second Law, using the method of dynamic equilibrium, ma and Iu are considered acting opposite to their actual sense, as shown by the dotted arrows in Fig. 4-1. We then have

$$+\uparrow \sum R_y = 0 = R_y - W \cos \alpha, \quad R_y = W \cos \alpha \quad (4-1)$$

$$+\rightarrow \sum R_x = 0 = W \sin \alpha - R_x - ma, \quad R_x = W \sin \alpha - W \frac{a}{g} \quad (4-2)$$

$$+\curvearrowright \sum M_G = 0 = R r_f - Iu, \quad R = \frac{2}{5} W \frac{r^2}{r_f} \frac{u}{g} \quad (4-3)$$

The resultant, R , in terms of R_y and R_x , is

$$R^2 = R_x^2 + R_y^2 \quad (4-4)$$

Substituting R_y and R_x from equations (4-1) and (4-2) into equation (4-4) gives

$$R = W \left[\left(\sin \alpha - \frac{a}{g} \right)^2 + \cos^2 \alpha \right]^{1/2} \quad (4-5)$$

If a and u were established experimentally (this can be easily done by taking movies of the rolling wheels), R and r_f could be determined from equations (4-3) and (4-5). This would give the magnitude and direction of the resultant soil reaction, R , as well as its point of action on the wheel surface.

For constant velocity rolling, ($a = 0$), equation (4-5) shows that $R = W$, and has the same line of action. Net shear stresses at the wheel-soil contact must be zero since moments about the wheel center are zero. Because soil contact pressure tends to distribute itself about the point

of application of the load, W , the resultant of soil stresses, R , must pass approximately through the middle of the wheel-soil contact area.

Further, the continuous process of rolling requires that the line between the wheel center and the wheel-soil rear contact be nearly perpendicular to the slope. (Soil exhibits some rebound, and the line between the wheel center and the wheel-soil rear contact deviates from a perpendicular by θ_2). These conditions are illustrated in Fig. 4-2. From these conditions a unique relationship can be established between track geometry and slope angle. If the line between the front and the rear wheel-soil contacts is horizontal,

$$\frac{z}{r} = 1 - \cos(2\alpha + \theta_2) \quad (4-6)$$

It has been argued that for a cylindrical wheel rolling at constant velocity down a slope, the resultant of radial contact stresses bisects the wheel-soil contact angle, θ_T , and a unique relationship exists between sinkage and slope angle (equation (4-6)), which is independent of wheel load. A free-body diagram of a wheel rolling on a horizontal surface would differ from the above case only with respect to the direction of W , resulting in $R = W/\cos\alpha$.

Therefore, a rational argument exists for the validity of the observation stated on page 29. What about experimental evidence?

Spheres Rolling Down a Soil Slope

For a sphere (spherical wheel) rolling down a soil slope, the track width, w , is related to the sinkage geometry (Fig. 4-2) by

$$\sin(2\alpha + \theta_2) = \frac{w/2}{r} = \frac{w}{D} \quad (4-7)$$

which, again, is a unique relationship independent of sphere load, for constant velocity rolling only.

Spheres rolled on Yuma sand provided an opportunity to test equation (4-7) for $\theta_2 = 0$. These experiments are described in detail by Hovland (1970). Fig. 4-3 shows the comparison. The agreement is best for loose, moist sand. In this material the tracks left by the rolling sphere had sharp, well-defined edges which could be accurately measured. The deviation is greatest for loose, dry sand where the tracks tended to cave or slump, and where the crest-to-crest track width, w , measured was undoubtedly somewhat greater than the track width at the time the sphere was in contact with the soil.

Experimental Data on Wheel-Soil Contact Angles and Radial Stresses

Physical reasoning would indicate that the resultant of radial stresses, at least for low values of slip, should approximately bisect the contact angle. The value of stress must be zero at the front contact and zero at the rear contact. For high positive or negative values of slip, however, this is not obvious. To compare data from various experiments for all values of slip, a redefinition of slip is first desirable.

The most common definition of slip, equation (3-16), is

$$i = \frac{DR - DT}{DR} = 1 - \frac{DT}{DR} \quad (3-16)$$

where DR = distance wheel periphery rolled, and DT = distance wheel traveled. Fig. 4-4a shows a plot of equation (3-16). A purely skidding wheel, $DT/DR = \infty$, would plot at $i = -\infty$. This is consistent with the instantaneous center of rotation, but not useful for developing theory valid for the whole slip range. Some investigators (for example, Sela, 1964) define

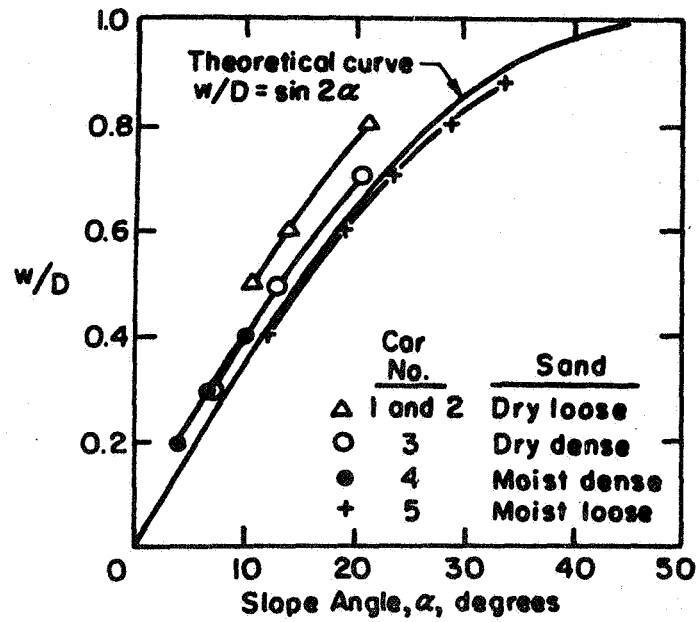
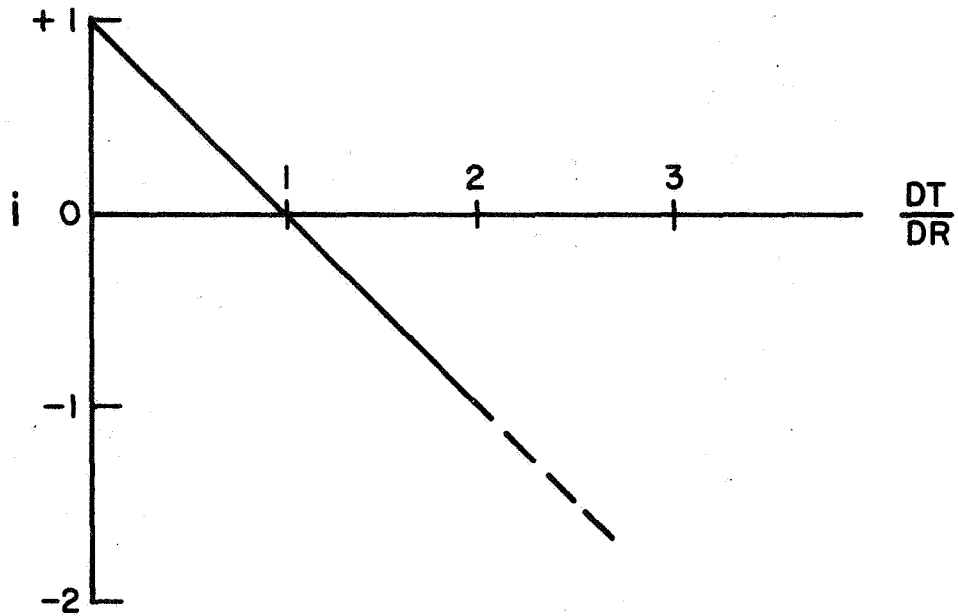
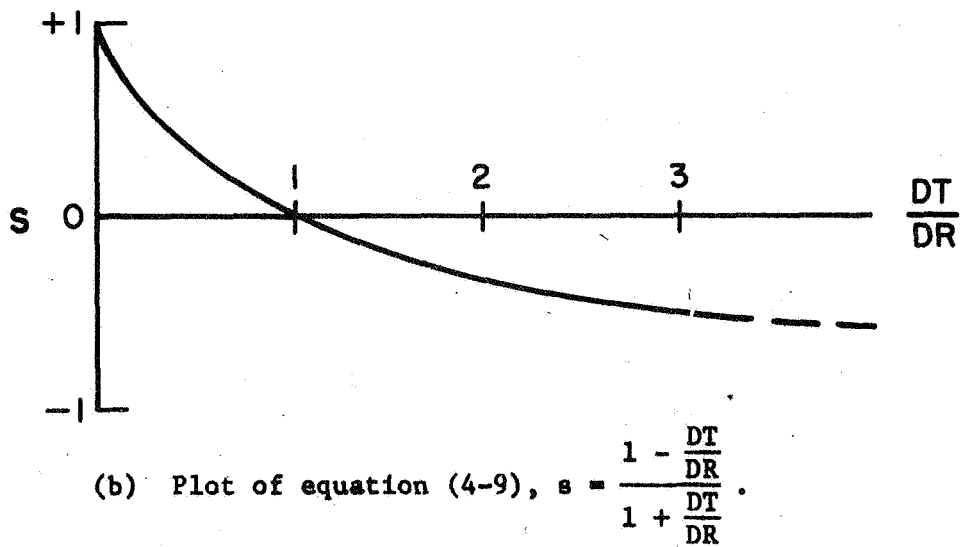


Fig. 4-3. w/D vs. slope angle, α , for constant velocity rolling.



(a) Plot of equation (3-16), $i = 1 - DT/DR$.



(b) Plot of equation (4-9), $s = \frac{1 - \frac{DT}{DR}}{1 + \frac{DT}{DR}}$.

Fig. 4-4. Illustration of definitions of slip.

positive slip by equation (3-16) but negative slip by

$$-i = \frac{DT - DR}{DT} = 1 - \frac{DR}{DT} \quad (4-8)$$

Therefore, it is necessary to have one mathematical expression which is valid for all values of slip. This is achieved by

$$s = \frac{DR - DT}{DR + DT} = \frac{1 - \frac{DT}{DR}}{1 + \frac{DT}{DR}} \quad (4-9)$$

The author prefers equation (4-9) because a purely spinning wheel has slip $s = +1$, and a purely skidding wheel has slip $s = -1$ (see also Fig. 4-4b). Since all definitions are functions of DT/DR , one can always go from one definition to another. Occasionally in the literature the definition for slip has not been explicitly stated. In such a case, it has been assumed that slip was defined by equation (3-16).

Of the data considered, Sela's (1964) showed the most consistent relationship and also extended over a larger range of slip values (Fig. 4-5). The data suggests that the position of the resultant of radial (normal) pressures, θ_N , moves slightly forward with increasing slip. All the data (Fig. 4-6) support the same trend.

A statistical analysis of all the points between $s = -.3$ and $s = +.3$ (Fig. 4-7) shows that the mean is 0.49 and the standard deviation is 0.06. Comparing information in Figs. 4-5, 4-6, and 4-7, an average drawn through Sela's data is about one standard deviation above the mean based on all the data, but the slope of the average line is about the same.

In order to use the data in Fig. 4-6, for example, it is necessary to separate out θ_1 and θ_2 . Considering θ_2 , when $s = -1$, θ_2 should equal zero, and when $s = +1$, θ_2 should approach θ_1 as slip sinkage increases. Thus, if θ_2/θ_T were plotted vs. slip, some kind of curve beginning with a

○ Sela, 1964
rigid wheels and dry sand

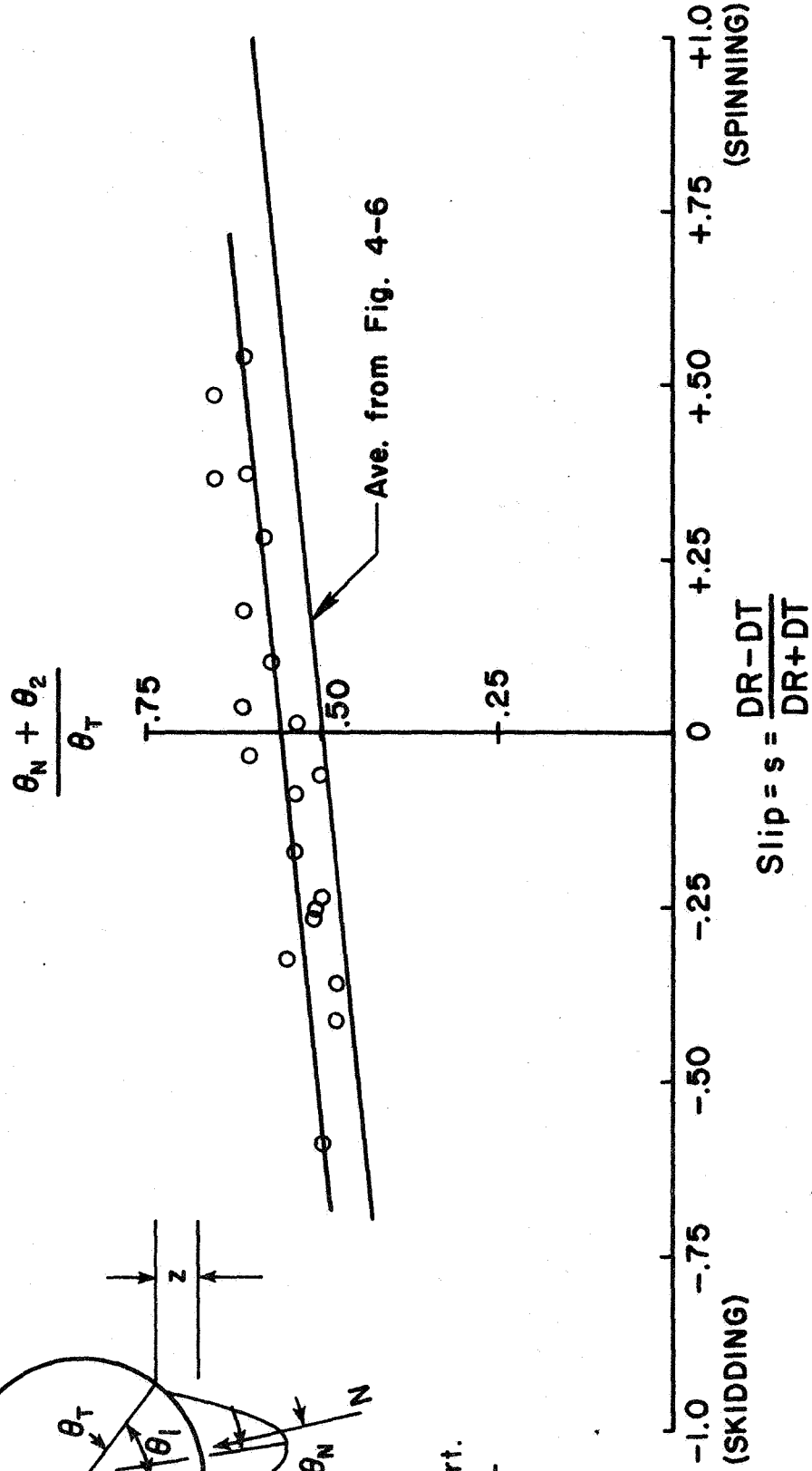
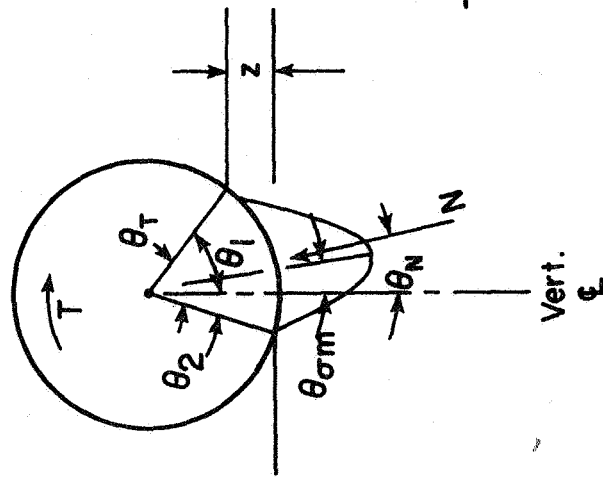


Fig. 4-5. Line of action of the resultant of radial stresses as a function of slip (Sela's, 1964 data).

- | | | | | | | | |
|---|------------------------|---------------------|------------|---|-------------------------|------------|----------------|
| ▽ | Uffelmann, 1961 | clay | rig. wheel | ○ | Sela, 1964 | sand | rig. wheel |
| × | Söhne and Sonnen, 1961 | silty sand | rig. wheel | ◇ | Onafeko and Reece, 1967 | sand | rig. wheel |
| △ | Vincent, 1961 | sand | pneu. tire | ● | Krick, 1969 | sandy loam | rig. and pneu. |
| □ | Smith (Schuring, 1966) | sand and sandy loam | rig. wheel | + | Hovland, 1971 | sand | rig. sphere |

○ centroid of points for intervals $s = .25$
 $\frac{\theta_N + \theta_2}{\theta_T}$

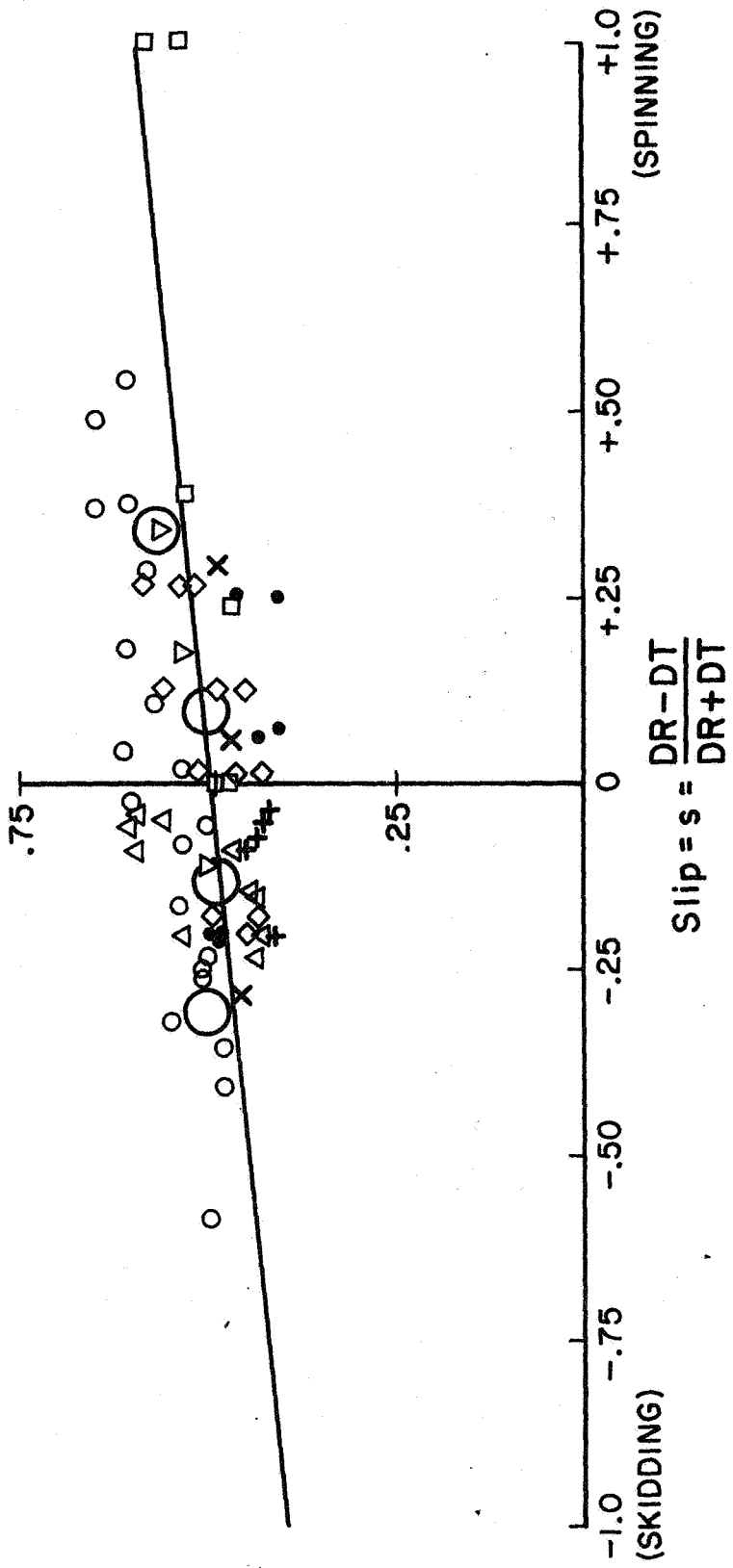


Fig. 4-6. Line of action of the resultant of radial stresses as a function of slip (all collected data).

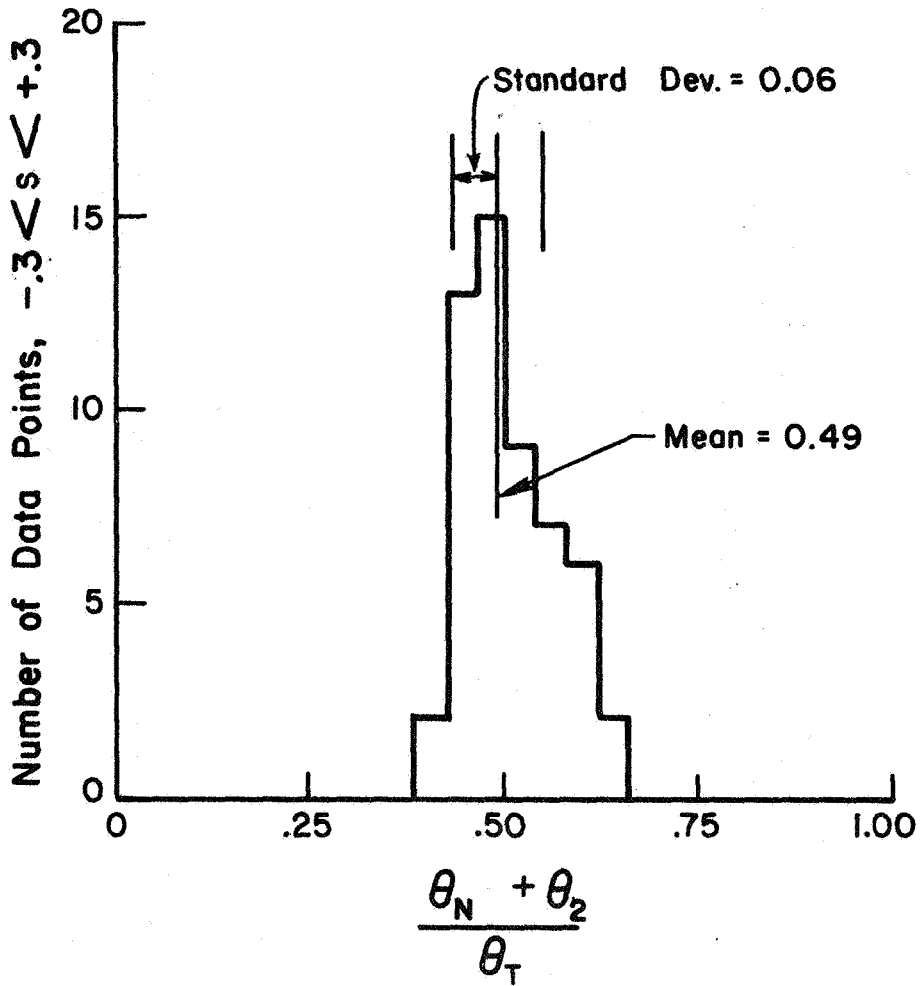


Fig. 4-7. Frequency distribution of the line of action of the resultant of radial stresses for data in the range $-0.3 \leq s \leq +0.3$.

low value of θ_2/θ_T in the negative slip range, and increasing with increasing slip should be expected. Fig. 4-8 shows an attempt to plot θ_2/θ_T vs. slip. The scatter does not invalidate the plot, but it does illustrate that much more detailed experiments are necessary to establish what influences θ_2 ; particular attention should be given to the influence of soil types.

Fig. 4-9 shows a plot of θ_N/θ_1 vs. slip. The plot in Fig. 4-6 shows a better correlation, however.

The data in Fig. 4-6 can be approximated by the line

$$\frac{\theta_N + \theta_2}{\theta_T} = \frac{\theta_N + \theta_2}{\theta_1 + \theta_2} = 0.5 + 0.1s \quad (4-10)$$

A curve through the centroid of points in Fig. 4-8 can be approximated by

$$s = -0.5 + 40 \left(\frac{\theta_2}{\theta_T} \right)^e \quad (4-11)$$

or

$$\frac{\theta_2}{\theta_T} = \frac{\theta_2}{\theta_1 + \theta_2} = \left(\frac{s + .5}{40} \right)^{1/e} \quad (4-12)$$

Combining equations (4-10) and (4-12)

$$\frac{\theta_N}{\theta_1} = (.5 + .1s) + \frac{(.5 - .1s)}{1 - \left(\frac{40}{s+.5} \right)^{1/e}} \quad (4-13)$$

Judging by the fit between the data and the curve (equation (4-13)) in Fig. 4-9, the equations appear to be adequate, and the curve in Fig. 4-8 is a good first approximation.

THEORY

Forces Acting on a Wheel

The forces acting on a wheel operating on a horizontal surface are

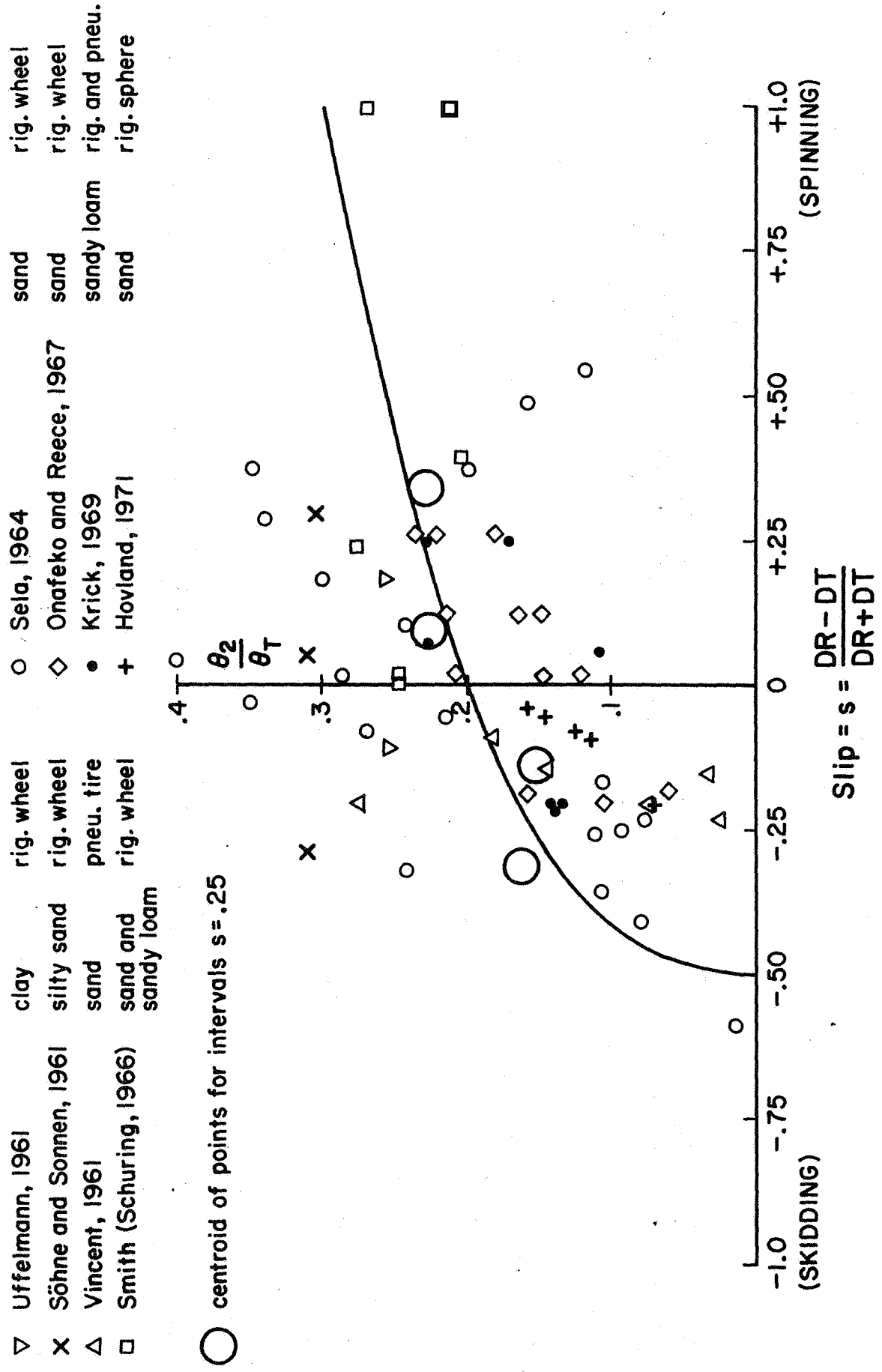


Fig. 4-8. Rear wheel-soil contact angle as a function of slip.

▽	Uffelmann, 1961	clay	rig. wheel	○	Sela, 1964	sand	rig. wheel
×	Söhne and Sonnen, 1961	silty sand	rig. wheel	◇	Onafeko and Reece, 1967	sand	rig. wheel
△	Vincent, 1961	sand	pneu. tire	●	Krick, 1969	sandy loam	rig and pneu.
□	Smith (Schuring, 1966)	sand and sandy loam	rig. wheel	+	Hovland, 1971	sand	rig. sphere

○ centroid of points for intervals $s = .25$

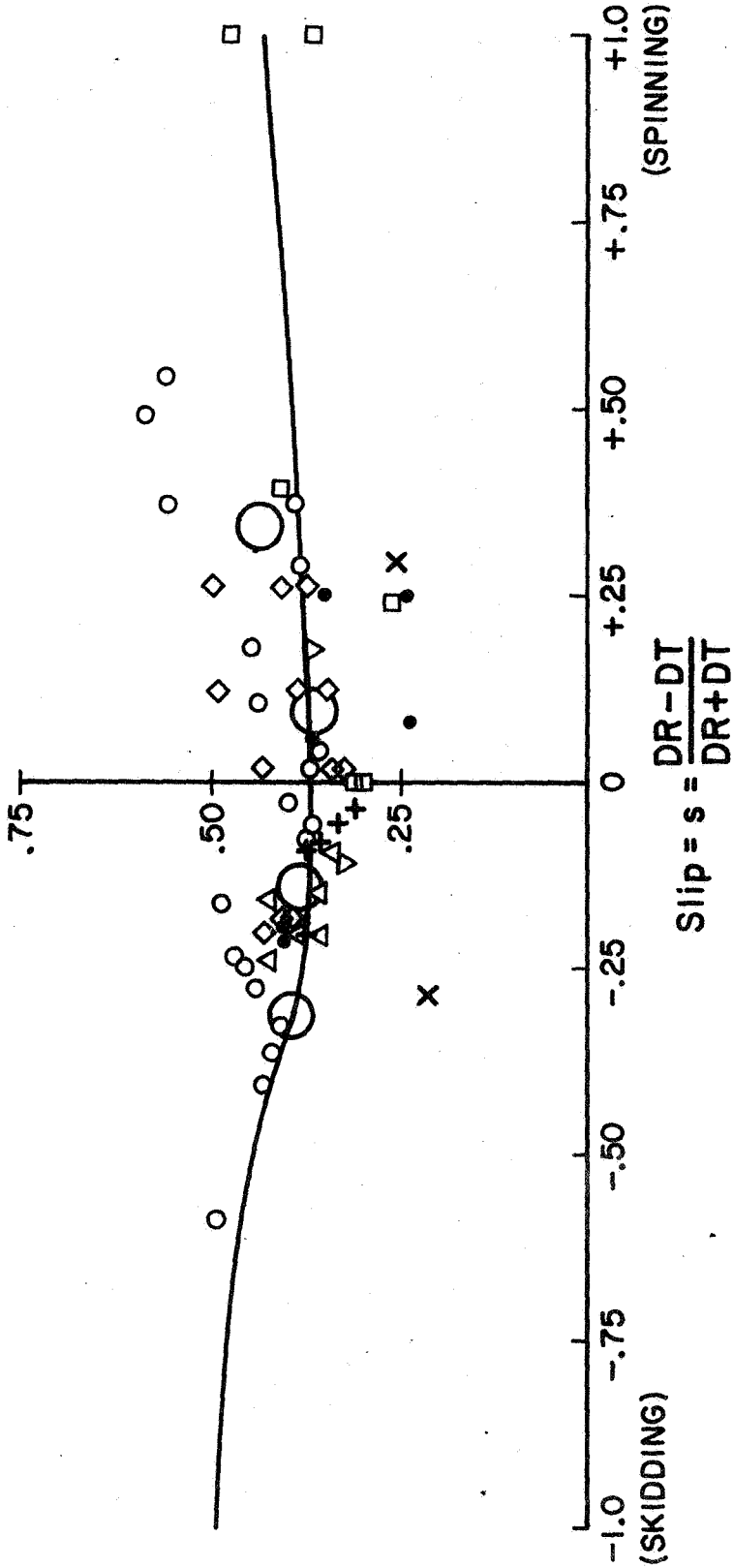


Fig. 4-9. The ratio of θ_N to front wheel-soil contact angle vs. slip.

shown in Fig. 4-10. Four cases are shown: 1) a driven wheel generating pull (+F, +P), 2) a self propelled wheel (+F, P = 0), 3) a towed wheel (F = 0, - P), and 4) a braked wheel (-F, = - P). As shown in Fig. 4-10, if θ_N and W are known and F is assumed to act perpendicular to N, the problem is determinate. Arguments and data were presented for θ_N in the previous section. F does not always act perpendicular to N, and a correction will be developed. Interestingly, the line of action of F is likely to deviate most from a perpendicular to N for low and moderate mobilizations of F. For high values of $\pm F$, when consequences of the deviation could be significant, F acts approximately perpendicular to N.

The following expressions can be written directly from Fig. 4-10:

$$R^2 = N^2 + F^2 \quad (4-14)$$

$$R^2 = P^2 + W^2 \quad (4-15)$$

$$N = W \cos \theta_N - P \sin \theta_N \quad (4-16)$$

In these equations, all forces are vectorial unless otherwise noted.

From equations (4-14) and (4-15),

$$P^2 = N^2 + F^2 - W^2 \quad (4-17)$$

The algebraic sum of shear stresses at the wheel-soil contact can be expressed by

$$F_a = N \tan \delta_{\theta s} + A c_{a \theta s} \quad (4-18)$$

where A = the wheel-soil contact area = $w \theta_T r$ (w = wheel width). (To abbreviate slightly the subsequent equations, the subscripts θ and s are omitted from δ and c_a).

Taking moments about the center of the wheel, the vectorial F is

$$F = \frac{F_a}{\bar{r}/r} \quad (4-19)$$

The correction ratio \bar{r}/r will be considered separately.

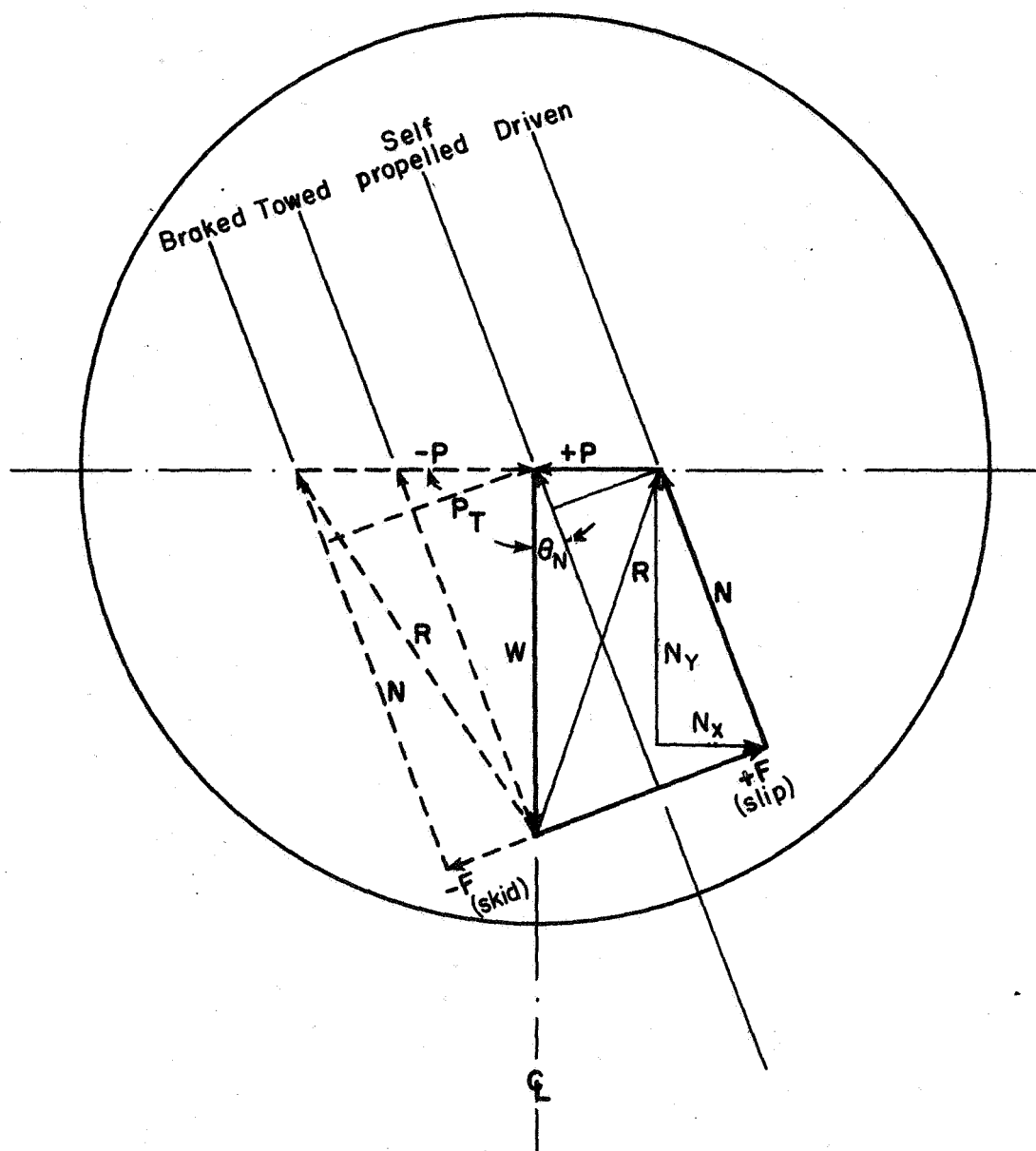


Fig. 4-10. Forces acting on a wheel operating on a horizontal surface.

Substituting equations (4-16), (4-18), and (4-19) into equation (4-17) gives

$$\left(\frac{P}{W}\right)^2 = \left(\cos\theta_N - \frac{P}{W} \sin\theta_N\right)^2 \left[1 + \left(\frac{\tan\delta}{\bar{r}/r}\right)^2\right] + 2 \left(\cos\theta_N - \frac{P}{W} \sin\theta_N\right) \frac{\tan\delta}{(\bar{r}/r)^2} \frac{Ac_a}{W} + \left(\frac{Ac_a}{W\bar{r}/r}\right)^2 - 1 \quad (4-20)$$

For a pure sand ($c_a = 0$), equation (4-20) becomes

$$\left(\frac{P}{W}\right)^2 = \left(\cos\theta_N - \frac{P}{W} \sin\theta_N\right)^2 \left[1 + \left(\frac{\tan\delta}{\bar{r}/r}\right)^2\right] - 1 \quad (4-21)$$

For a pure clay ($\delta = 0$), equation (4-20) becomes

$$\left(\frac{P}{W}\right)^2 = \left(\cos\theta_N - \frac{P}{W} \sin\theta_N\right)^2 + \left(\frac{Ac_a}{W\bar{r}/r}\right)^2 - 1 \quad (4-22)$$

For a towed wheel, net shear stresses are zero, which can also be accomplished by letting c_a and δ in equation (4-20) equal zero

$$\left(\frac{P}{W}\right)^2 = \left(\cos\theta_N - \frac{P}{W} \sin\theta_N\right)^2 - 1 \quad (4-23)$$

These equations are valid for all conditions illustrated in Fig. 4-10. Although the equations are lengthy, they are not difficult to solve; the variables are θ_N , δ , c_a , and θ_T . Testing yields δ , and c_a , for every case of interest. Anticipated sinkage and previous developments in this report yield θ_N and θ_T .

Consideration of Magnitude and Direction of F

It was noted by equation (4-18) that F_a in that equation was algebraic, and that, taking moments about the center of the wheel, the vectorial F is

$$F = \frac{F_a}{\bar{r}/r} \quad (4-19)$$

where \bar{r} = moment arm to action of F. Then

$$\frac{\bar{r}}{r} = \frac{F_a}{\sqrt{F_x^2 + F_y^2}} \quad (4-24)$$

or

$$\frac{\bar{r}}{r} = \frac{r \int \tau_\theta d\theta}{\sqrt{(r \int \tau_\theta \cos\theta d\theta)^2 + (r \int \tau_\theta \sin\theta d\theta)^2}} \quad (4-25)$$

For a constant shear stress distribution, equation (4-25) reduces to

$$\frac{\bar{r}}{r} = \frac{\theta_T}{\sqrt{2 - 2\cos T}} \quad (4-26)$$

which is identical to equation (3-37). Therefore, the same correction chart (Fig. 3-7) can be used.

For a sinusoidal shear stress distribution, equation (4-25) reduces to

$$\frac{\bar{r}}{r} = \frac{1 - \left(\frac{\theta_T}{\pi}\right)^2}{\cos \frac{\theta_T}{2}} \quad (4-27)$$

which is, again, the same correction obtained by Taylor (1937) the correction is found from Fig. 3-7.

The amount by which the direction of F deviates from a perpendicular to the direction of N is illustrated in Fig. 4-11. This deviation can be expressed by

$$|\theta_N + \theta_2 - \theta_F| = |\theta_N + \theta_2 - \tan^{-1} \frac{F_y'}{F_x'}| \quad (4-28)$$

where

$$\frac{F_y'}{F_x'} = \frac{r \int \tau_\theta \sin\theta d\theta}{r \int \tau_\theta \cos\theta d\theta} \quad (4-29)$$

Solving equation (4-28), using equation (4-29), for a constant and a sinusoidal shear stress distribution respectively, gives

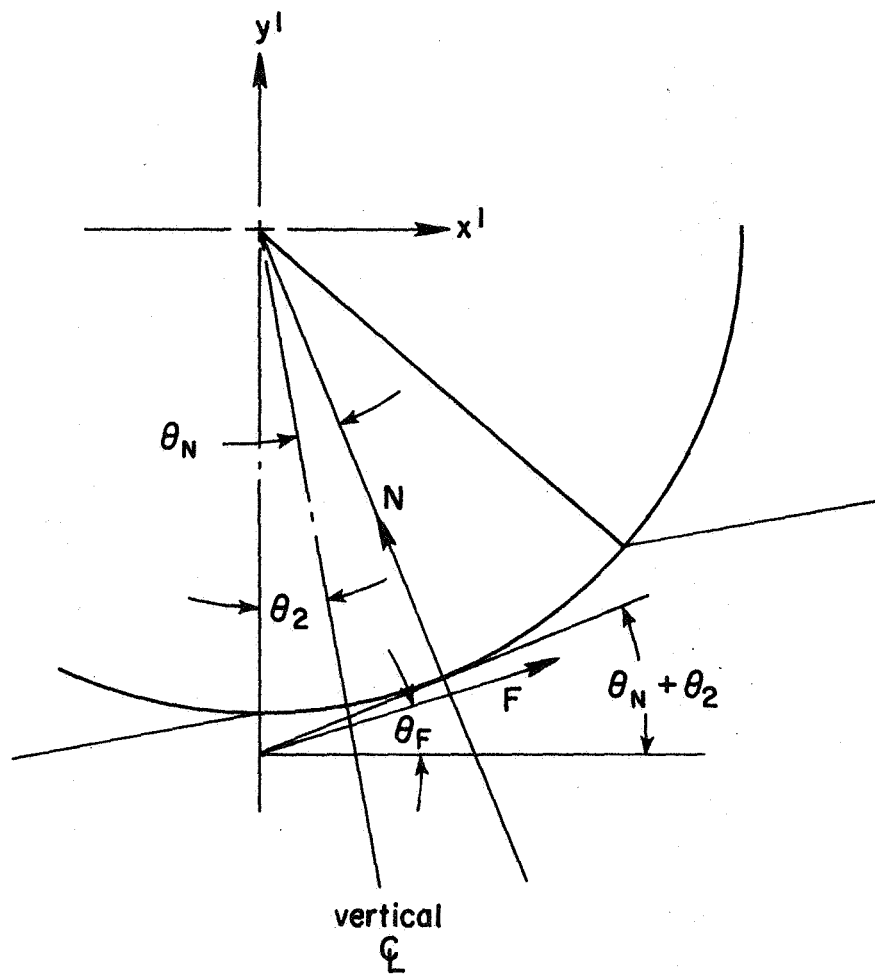


Fig. 4-11. The angle by which the direction of F deviates from a perpendicular to the direction of N .

$$\tau_{\theta} = \text{constant}, \quad |\theta_N + \theta_2 - \theta_F| = \left| \theta_N + \theta_2 - \frac{\theta_T}{2} \right| \quad (4-30)$$

$$\tau_{\theta} = \text{sinusoidal}, \quad |\theta_N + \theta_2 - \theta_F| = \left| \theta_N + \theta_2 - \frac{\theta_T}{2} \right|$$

In other words, for constant and sinusoidal shear stress distributions, equations (4-30) show that the deviation is equal to the deviation of the line of action of N from $\theta_T/2$. Figs. 4-6 and 4-7 show that $\theta_N + \theta_2$ is not likely to deviate much from $\theta_T/2$.

Inaccuracy Resulting from an Error in Selected Contact Angles

Observing equations (4-20) through (4-23), it appears that an error in selecting θ_N and associated θ_2 would have the greatest influence in the case of a towed wheel, equation (4-23). Therefore, only the case of a towed wheel will be considered. This case can be expressed more simply from Fig. 4-10 as

$$\frac{P_T}{W} = \tan \theta_N \quad (4-31)$$

The magnitude by which the computed pull differs from the correct pull can be expressed by the ratio

$$\frac{\left(\frac{P_T}{W}\right)_{\text{comp.}}}{\left(\frac{P_T}{W}\right)_{\text{correct}}} = \frac{\tan(\theta_N \text{ comp.})}{\tan(\theta_N \text{ correct})} \quad (4-32)$$

Based on the data in Figs. 4-6 and 4-8, it is most likely that a high value of $(\theta_N + \theta_2)/\theta_T$ is associated with a high value of θ_2/θ_T . Therefore, the deviation of θ_N from the mean can be expressed as a function of θ_T and θ_2 from

$$\frac{\theta_N + \theta_2}{\theta_T} = \frac{\theta_N}{\theta_T} + \frac{\theta_2}{\theta_T} = \text{mean} \pm \text{standard deviation}$$

giving

$$\frac{\theta_N}{\theta_T} = (.50 \pm .06) - \frac{\theta_2}{\theta_T} \quad (4-33)$$

Then we have for

$$\text{high } \frac{\theta_N + \theta_2}{\theta_T}, \frac{\theta_N}{\theta_T} = .56 - .3 = .26$$

$$\text{mean } " \quad , \frac{\theta_N}{\theta_T} = .50 - .2 = .30$$

$$\text{low } " \quad , \frac{\theta_N}{\theta_T} = .44 - .1 = .34$$

The pull ratio computed from equation (4-32), using the mean ($\theta_N = 0.3 \theta_T$) as the correct value, is presented in Table 4-1.

Table 4-1 Ratio of Computed to Correct Pull

$\frac{\theta_N + \theta_2}{\theta_T}$	θ_T					
	0	20°	40°	60°	90°	120°
high 0.5+0.06	1.00	0.87	0.86	0.86	0.85	0.84
low 0.5-0.06	1.00	1.13	1.14	1.15	1.16	1.18

Since for a normal distribution, the range from -(one standard deviation) to +(one standard deviation) contains 68.27% of the data, it can be concluded that for about 68% of wheel-soil interaction cases the computed

pull will be within about 15% of the correct value. This conclusion is, of course, based on the data presented in Figs. 4-5 through 4-9. With future careful testing of $(\theta_N + \theta_2)/\theta_T$ as a function of soil conditions and wheel conditions, it should be possible to reduce this theoretical error to a smaller value.

CHAPTER 5. WHEEL SINKAGE

WHEEL SINKAGE AND CONTACT ANGLES

The towed force (negative pull = $-P = P_T$) expressed by equation (4-23) is a function of W and θ_N only. As illustrated in Fig. 4-10, every state of slip of a wheel has associated with it a motion resistance, N_x . For a horizontal surface the N_x/N_y ratio can be expressed directly

$$\frac{N_x}{N_y} = \tan\theta_N \quad (4-31)$$

The sinkage, z , associated with this angle, θ_N , is illustrated in Fig. 5-1. Sinkage is here defined as the vertical distance between the bottom dead center of the wheel and the front wheel-soil contact

$$z = r(1 - \cos\theta_1) \quad (5-1)$$

from which

$$\theta_1 = \cos^{-1}\left(1 - 2\frac{z}{D}\right) \quad (5-2)$$

where D = wheel diameter. From Fig. 4-9, we note that θ_N/θ_1 is nearly constant and equal to 0.4 for most likely slip values. Therefore,

$$\theta_N = 0.4 \cos^{-1}\left(1 - 2\frac{z}{D}\right) \quad (5-3)$$

Combining equations (4-31) and (5-3) gives

$$\frac{N_x}{N_y} = \tan\left[0.4 \cos^{-1}\left(1 - 2\frac{z}{D}\right)\right] \quad (5-4)$$

Equation (5-4) relates sinkage to the motion resistance for a rigid cylindrical wheel. It is an approximate solution essentially independent of slip. Improvements to equation (5-4) should be sought from improved

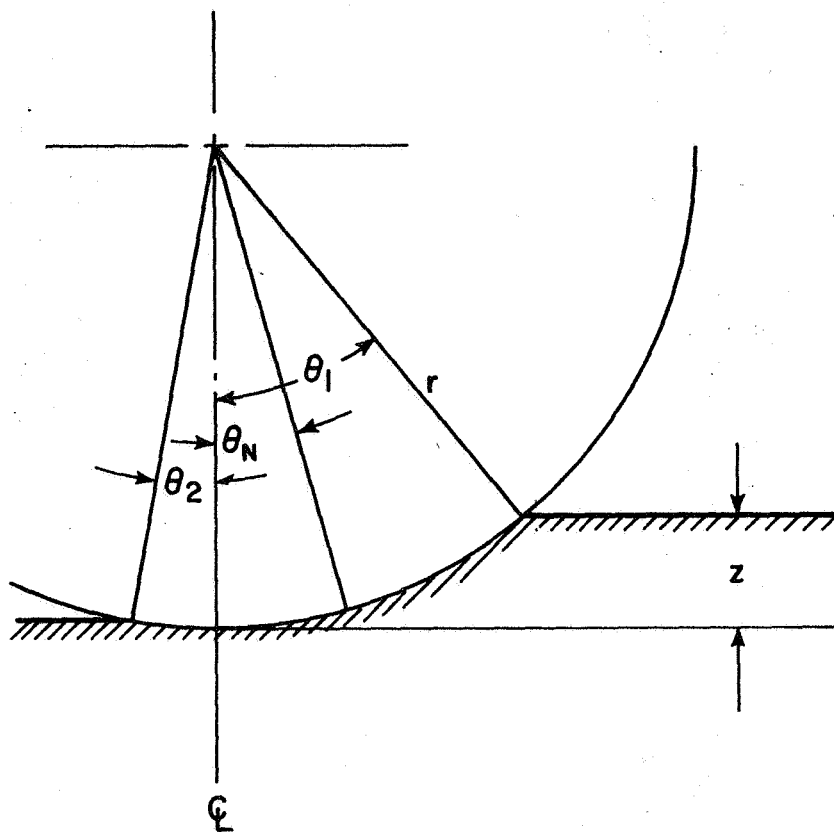


Fig. 5-1. Relationship between sinkage and wheel-soil contact angles.

data of the type plotted in Fig. 4-9. To check equation (5-4), experimental data from towed wheels are compared in Fig. 5-2.

Many relationships between sinkage and rolling resistance have been advanced previously, and many of these are conveniently summarized by Schuring (1972). He defines rolling resistance as $\rho = \sin\theta_N$. With this definition and equation (5-3), rolling resistance can be expressed as a function of sinkage. This leads to results which are almost identical with the Bernstein line (Schuring, 1972). The experimental data reported by Schuring in this paper deviate from the Bernstein line particularly for driven, pneumatic tires and low sinkage. (Actual rolling resistance appears to be considerably less than predicted.) Schuring proposes an explanation for this deviation: For low sinkage, the rear angle, θ_2 , tends to be proportionately larger, which leads to a smaller θ_N and smaller rolling resistance. He also proposes a relationship which seems to account for the influence of θ_2 rather well.

PRESSURE-SINKAGE RELATIONS

While equation (5-4) relates sinkage to motion resistance, N_x , it cannot be used to compute sinkage directly from soil parameters. To do this, an independent relationship is required.

Perhaps the most commonly used formula in the field of off-road mobility, to define vertical stress-strain relationships, is (Bekker, 1969)

$$q = \left[\frac{k_c}{w} + k_\phi \right] z^n \quad (5-5)$$

where q = bearing pressure on a plate of width, w , and sinkage, z . The constants k_c and k_ϕ , and exponent n are determined from testing and curve fitting. Bekker (1969) presents a thorough description of the use of

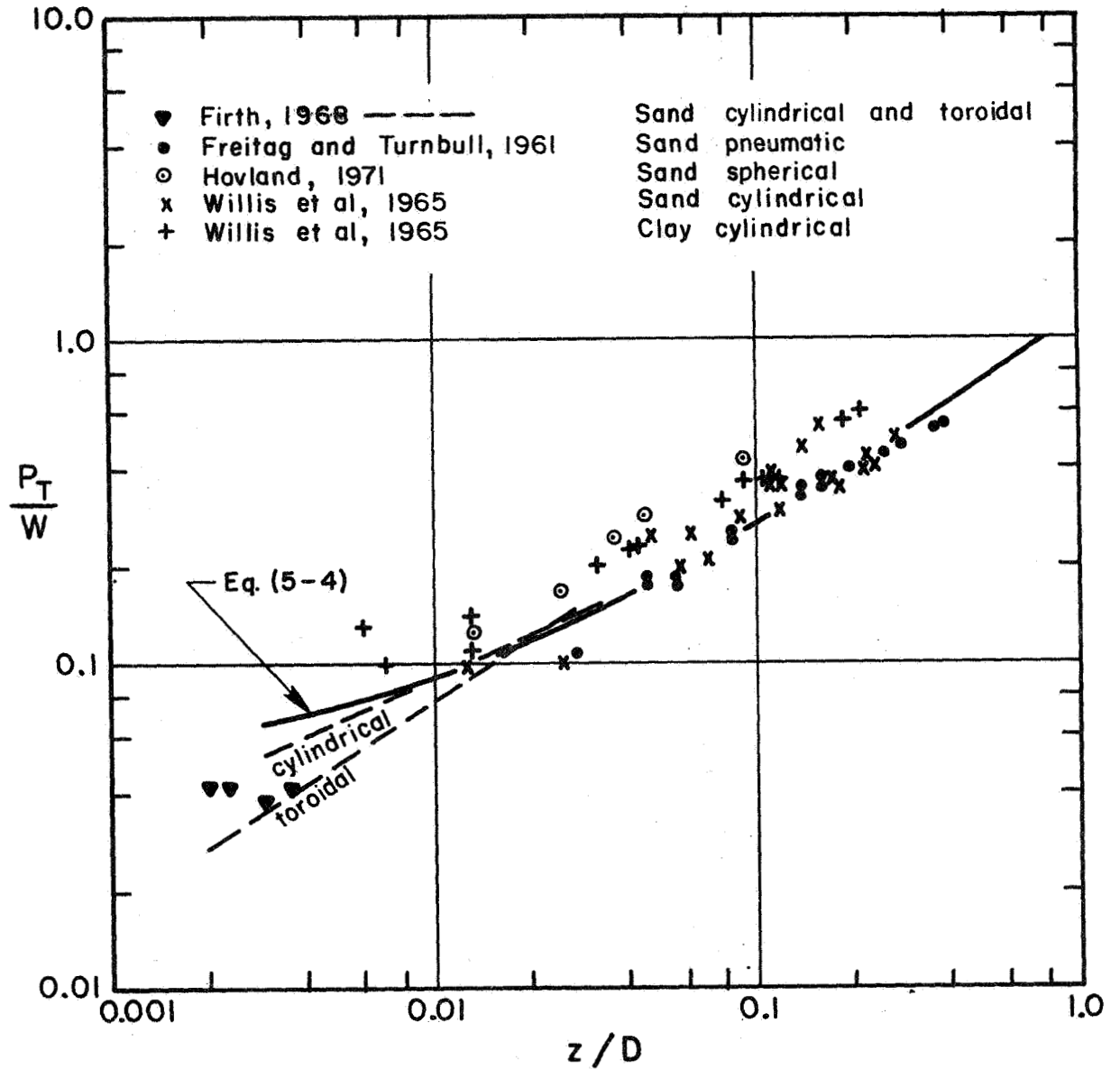


Fig. 5-2 Ratio of towed force to wheel load vs. ratio of sinkage to wheel diameter.

equation (5-5), and many experimentally determined pressure-sinkage curves.

A significant amplification of the type of pressure-sinkage relationship represented by equation (5-5) has been made by Firth (1968). On the basis of dimensional analysis, he derived a more general pressure-sinkage relationship.

$$\frac{W}{\gamma V} = \left(\frac{\ell^2}{A}\right)^m \left(\frac{z}{\ell}\right)^{n-1} f\left(\phi, \frac{c}{\gamma z}\right) \quad (5-6)$$

where V = volume of probe below plane of original surface

A = cross-sectional area of probe in plane of original surface

ℓ = major dimension of area, A

m and n are exponents to be determined from testing

Some separately postulated relationships, such as equation (5-5), are, in fact, special cases of equation (5-6) (Firth, 1967).

Alternatively, it is possible to use plasticity theory for pressure-sinkage relationships. A notable application of plasticity theory to the wheel-soil interaction problem has been made by Karafiath (1971) in an effort to predict stress distribution beneath wheels. His studies have also provided valuable information on the effect of soil pore water pressures in wheel-soil interaction (Karafiath, 1972).

Bearing capacity theory (a special solution based on plasticity theory) can also be used for pressure-sinkage relationships. The bearing capacity equation

$$q = \frac{\gamma_s w}{2} N_\gamma + cN_c + q'N_q \quad (5-7)$$

was first derived by Terzaghi (1943). Equation (5-7) is a function of sinkage by 1) $q' \approx \gamma_s z/2$, and 2) $q \approx N/A$, where A , the wheel-soil contact area, is a function of sinkage.

The main assumption in both Karafiath's analysis and equation (5-7) is that of two-dimensionality (an infinite dimension perpendicular to the plane of rolling in the case of wheel-soil interaction). Analysis based on this assumption, therefore, may be, at best, adequate for relatively wide wheels and for those cases where theory is substantiated or modified by experiments.

It is customary to modify the bearing capacity equation by shape factors (s_γ and $s_c = s_q$) for other than an infinitely long load-soil contact area. Using shape factors, and noting that $N_q = N_c \tan\phi + 1$, equation (5-7) can be expressed for rectangular loaded areas as

$$q = \frac{\gamma_s w}{2} s_\gamma N_\gamma + s_{cq} [(c + q' \tan\phi) N_c + q'] \quad (5-8)$$

where γ_s = soil unit weight, w = width of contact area, q' = surcharge, and N_γ , N_c , and N_q are bearing capacity factors which are functions of soil friction angle, ϕ , and slope angle, α , (Meyerhof, 1951).

While equation (5-8) has some empirical backing and considerable precedent in soil mechanics practice, it has not, to the author's knowledge, been experimentally modified or substantiated for rectangular wheel-soil contact areas. Although equation (5-8) will be suggested for long, rectangular, wheel-soil contact areas, its use in wheel-soil interaction must be considered hypothetical.

Bearing capacity theory can, however, be modified by experiments for specific cases of wheel-soil interaction. Extensive testing (Hovland, 1970) demonstrates that bearing capacity theory can be used to evaluate pressure-sinkage relationships of rolling spheres and spherical wheels. Fig. 5-3 shows a comparison between theoretical (modified bearing capacity theory) and experimental values of the density ratio, γ_r/γ_s ,

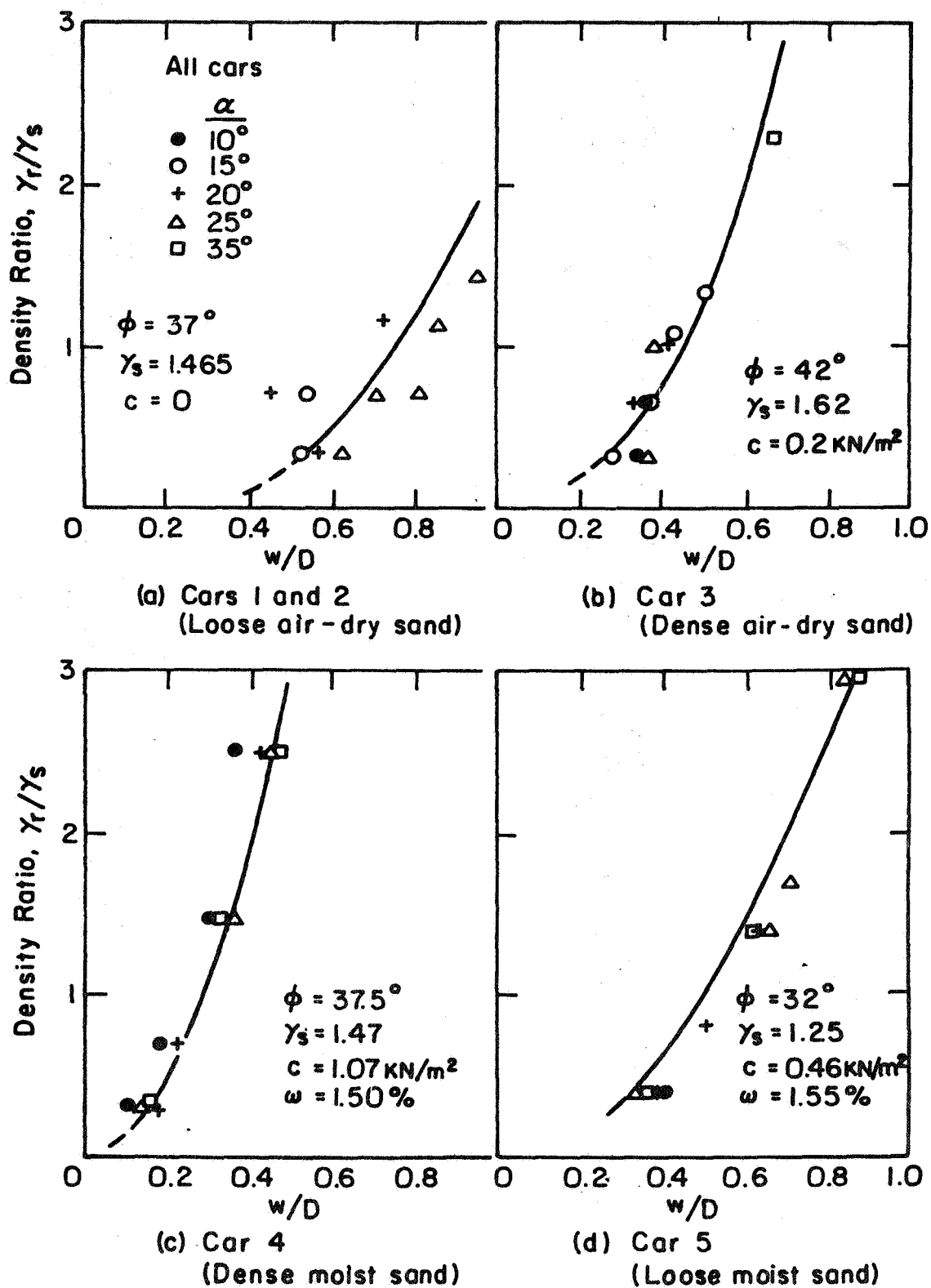


Fig. 5-3. Density ratio vs. w/D ratio for spheres rolling on Yuma sand (curves are theoretical for constant velocity rolling; points are experimental).

vs. track width to diameter ratio, w/D . Fig. 5-4 shows a comparison between theoretical and experimental values of sphere diameter vs. track width to diameter ratio, w/D . In these figures $\gamma_r =$ sphere unit weight. Fig. 5-5 shows a comparison between theoretical (calculated) and experimental friction angle values. The theoretical values were again calculated from bearing capacity theory modified to the rolling sphere-soil interaction problem (see equation (7-12)).

Such testing showed that, for the sphere-soil interaction problem, the bearing capacity factors (Meyerhof, 1951) need to be modified in equation (5-8). Specifically, for a sphere or spherical wheel

$$N_{\gamma \text{ sphere}} \approx \frac{1}{4} N_{\gamma}$$

and

$$N_{c \text{ sphere}} \approx \frac{1}{2} N_c$$

Substituting these bearing capacity factors into equation (5-8) gives for a spherical wheel

$$q = \frac{\gamma_s w}{2} s_{\gamma} \frac{N_{\gamma}}{4} + s_{cq} \left[(c + q' \tan \phi) \frac{N_c}{2} + q' \right] \quad (5-9)$$

We have, therefore, matched bearing capacity theory in an approximate way to two end-points of the wheel-soil interaction problem; 1) a rather narrow cylindrical wheel for which equation (5-8) applies, and 2) a spherical wheel, which is analogous to a wide wheel or a very light wheel, for which equation (5-9) applies. What about intermediate conditions?

Fig. 5-6a illustrates wheel-soil contact areas, as viewed from above, for various wheels:

- (1) A spherical wheel.

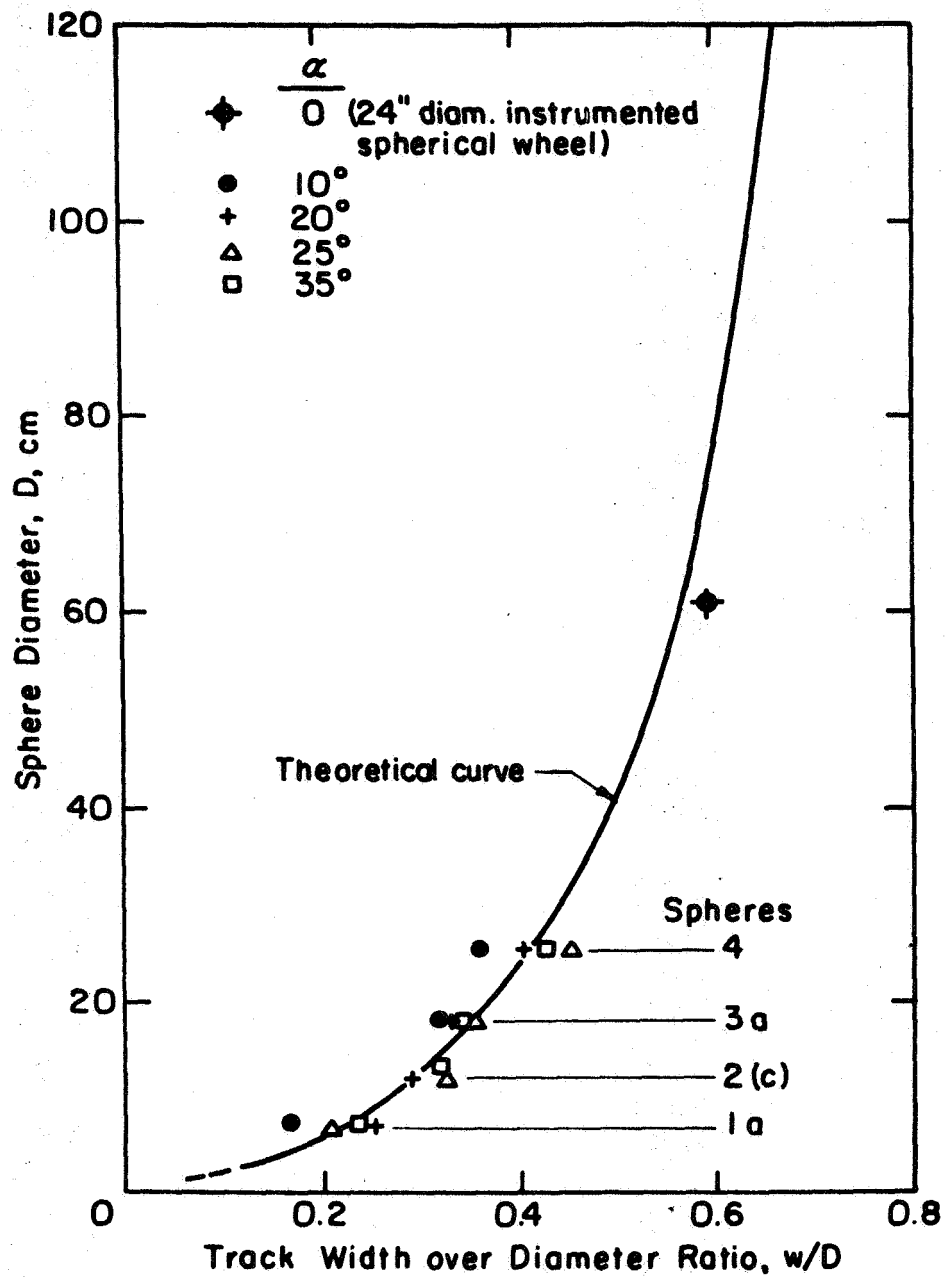


Fig. 5-4. Track width over diameter ratio as a function of sphere diameter.

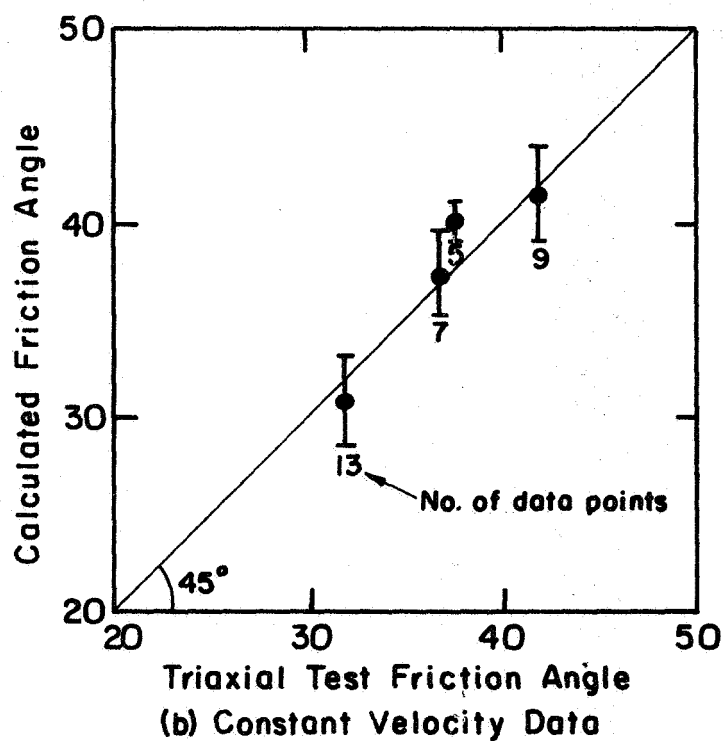
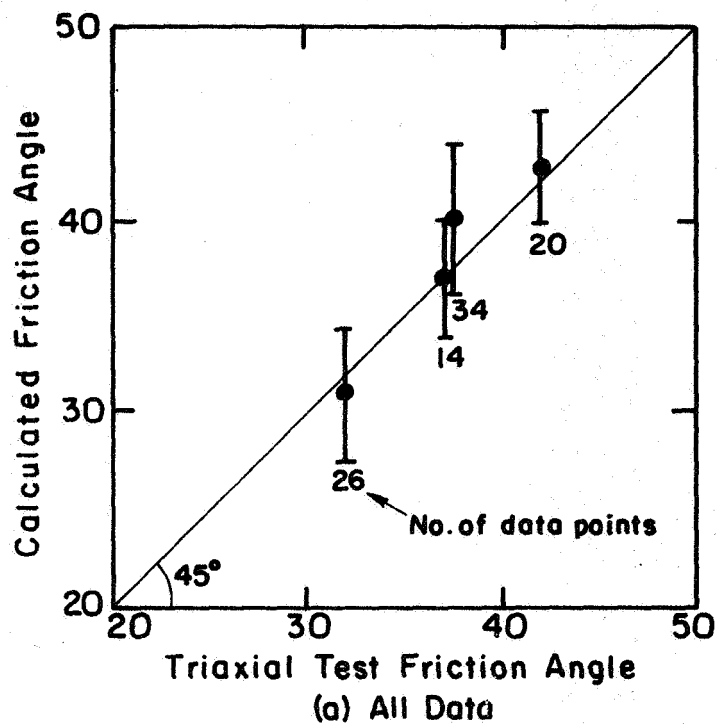
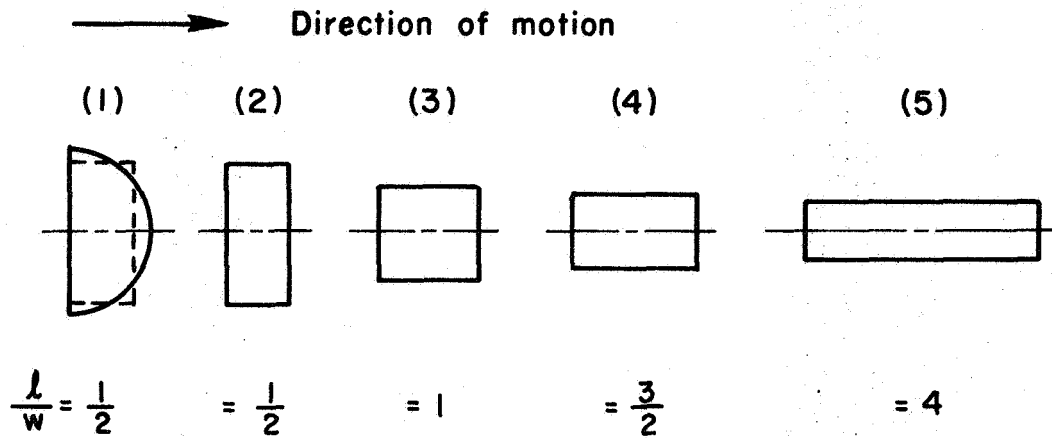
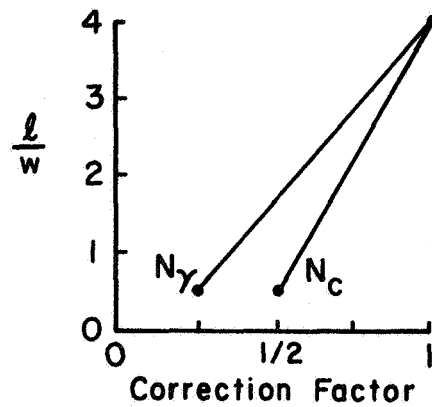


Fig. 5-5. Comparison between calculated and triaxial test friction angle values.



a) Wheel-soil contact areas for various wheels.



b) Correction factor to the bearing capacity factors of Eqs. (5-8) and (5-9).

Fig. 5-6. Suggested Correction of bearing capacity theory for wheel-soil interaction.

- (2) A wide cylindrical wheel with a contact area approximately equal in shape to that of a spherical wheel.
- (3) A cylindrical wheel with a square contact area, at which point the l/w ratio in the shape factor expressions

$$s_{\gamma} = \left(1 - .3 \frac{l}{w} \right)$$

and

(5-10)

$$s_{cq} = \left(1 + .2 \frac{l}{w} \right)$$

equals one.

- (4) A typical cylindrical wheel with sufficient sinkage for the l/w ratio to be larger than one, at which point the ratio must be inverted, giving

$$s_{\gamma} = \left(1 - .3 \frac{w}{l} \right)$$

and

(5-11)

$$s_{cq} = \left(1 + .2 \frac{w}{l} \right)$$

- (5) A rather narrow cylindrical wheel.

For the condition of Fig. 5-6a (1), equation (5-9) applies, using the ratio l/w in determining the shape factors. For the condition of Fig. 5-6a (5), equation (5-8) applies, using the ratio w/l in determining the shape factors. For intermediate cases, compute the shape factors from equations (5-10) and (5-11), and select from Fig. 5-6b the correction factor to the bearing capacity factors of equations (5-8) and (5-9). In all cases, select the bearing capacity factors from Meyerhof (1951) (Figs. 5-7, and 5-8), using $\theta_N = \text{Meyerhof's } \beta_m$.

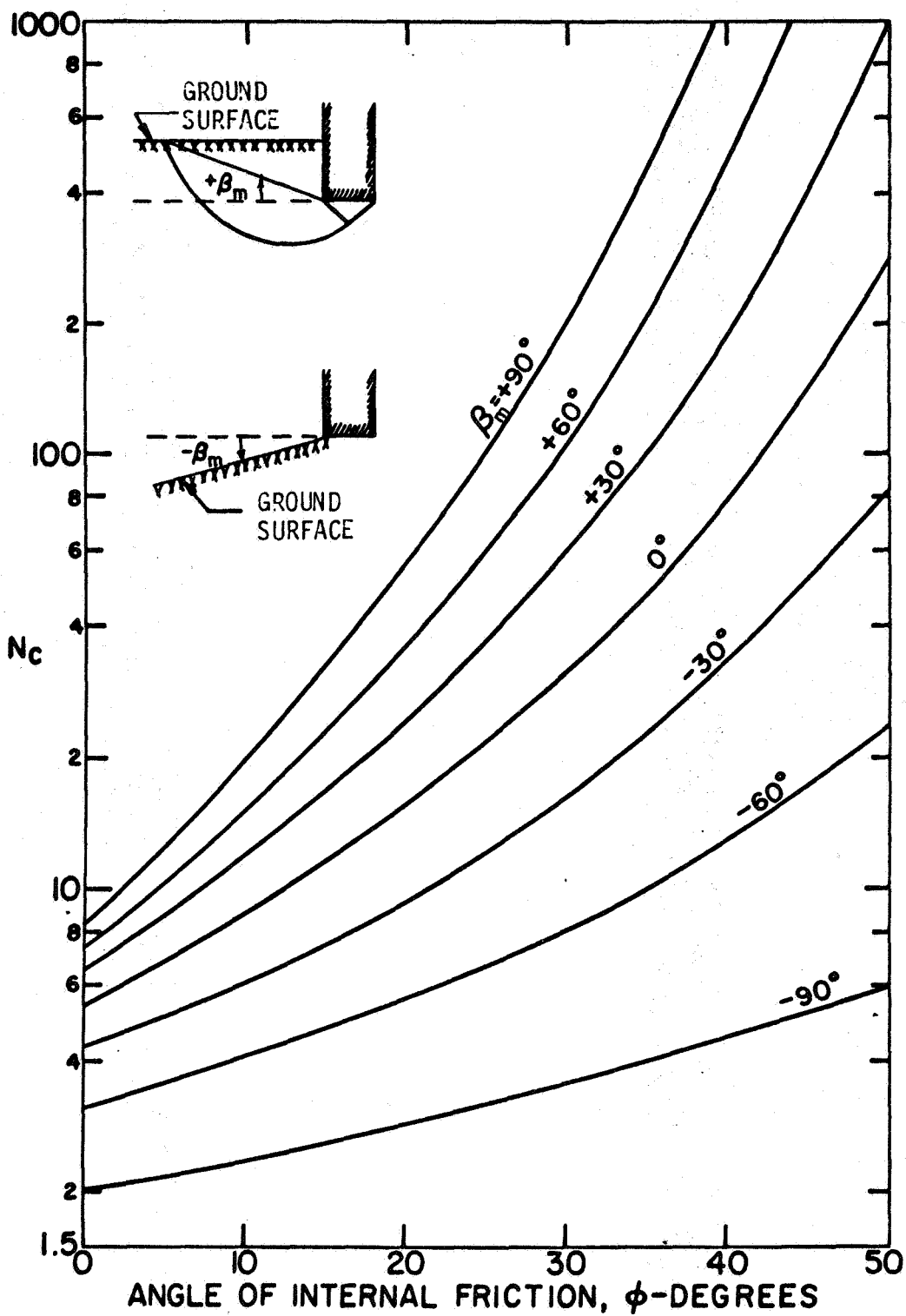


Fig. 5-7. General bearing capacity factor N_c for strip foundation (after Meyerhof, 1951).^c

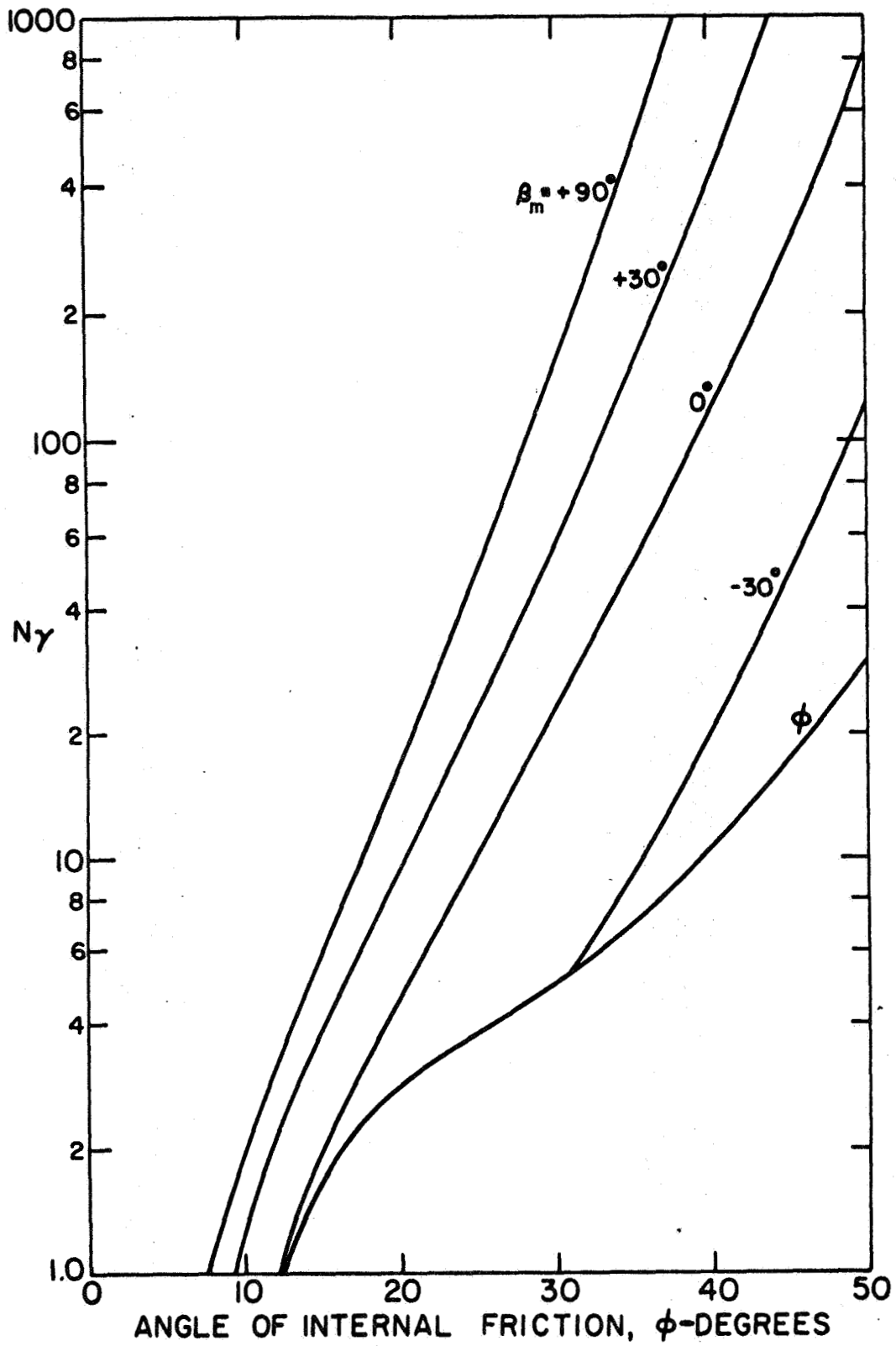


Fig. 5-8. General bearing capacity factor N_γ for strip foundation (after Meyerhof, 1951).

CHAPTER 6. MOBILIZATION OF SHEAR STRESSES

SLIP AT A POINT

The relationship between measured slip and slip at any point along the wheel-soil contact is illustrated in Fig. 6-1. Slip is established from measured distance through which the wheel revolved, DR, and distance through which the wheel traveled, DT. The measured slip (slip by its usual definition) takes place at the bottom dead center of the wheel, and may be expressed as

$$s = \frac{DR - DT}{DR + DT} \quad (4-9)$$

from which

$$\frac{DT}{DR} = \frac{1 - s}{1 + s} \quad (6-1)$$

Slip at a point, s_θ , is a function of θ , and may be expressed from Fig. 6-1 as

$$s_\theta = \frac{DR - DT \cos\theta}{DR + DT \cos\theta} \quad (6-2)$$

combining equations (6-1) and (6-2),

$$s_\theta = \frac{1 - \cos\theta + s(1 + \cos\theta)}{1 + \cos\theta + s(1 - \cos\theta)} \quad (6-3)$$

Because the expression of slip at a point (equation 6-3) may be new, it is desirable to see if predictions of its value are realistic. A surface of slip at a point, s_θ , is plotted in Fig. 6-2. The surface appears to be realistic and in accord with physical reasoning. Note particularly the cross-hatched area at the towed point; as the wheel load increases, the wheel-soil contact angle increases, and the towed point moves to a higher negative slip value. When the necessary relationships are established, later in this chapter, the towed point will be reconsidered.

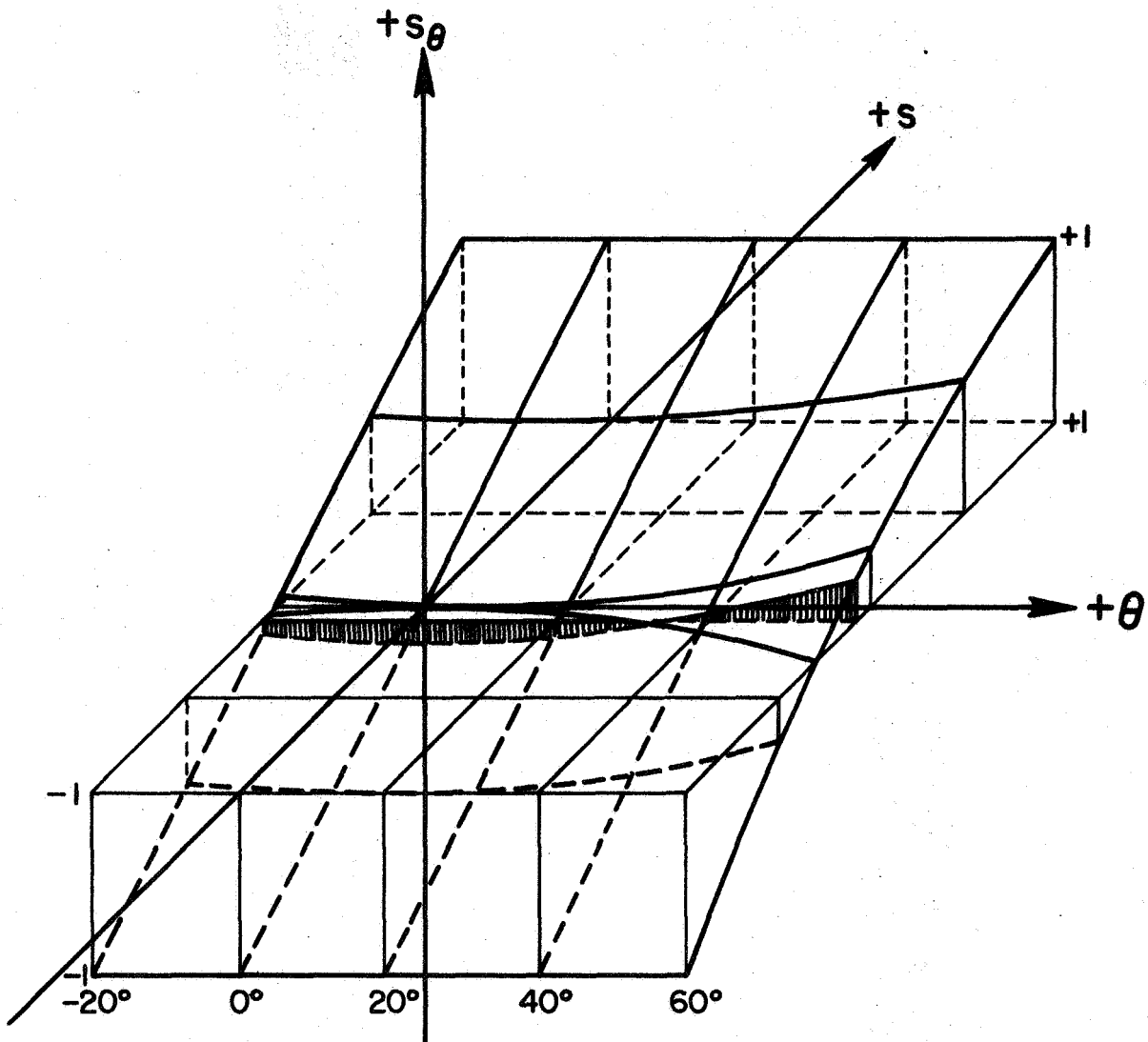


Fig. 6-2. Surface of slip, s_θ , at any point.

SOIL DISPLACEMENT VS. SLIP

A shear ring type of test (Bekker, 1969) (Fig. 6-3b) is probably most realistic for establishing wheel-soil interface strength parameters c_a and δ . In this type of test, soil is allowed to strain analogously to what happens to the soil under a wheel. Compare this test for example, to a direct shear test where strain is limited to a very narrow zone; peak strength would occur at a much smaller displacement in a direct shear test than in a ring shear type of test shown in Fig. 6-3b.

In this type of test, however, as in the case of the wheel, it is difficult to establish fundamental stress-strain relationships since strain cannot be defined. That is, the vertical distance, Δz , to which soil deforms is unknown. It is, however, possible to establish displacement relationships which may be useful.

Fig. 6-3 illustrates soil displacements and terminology for wheel- and ring-soil interaction. For the wheel, the rate of displacement can be expressed as

$$\frac{\Delta_w}{t_w} = \frac{DR - DT}{t_w} = \frac{\theta_w r_w - \theta_w r_w (1-i)}{t_w} = \frac{\theta_w r_w}{t_w} i \quad (6-4)$$

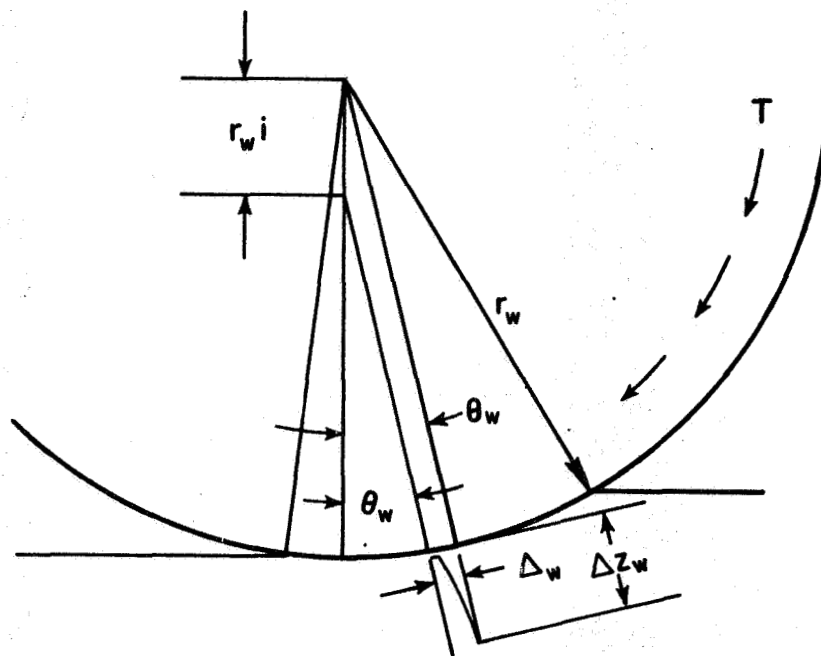
where t_w = time increment for wheel, and i = slip as defined by equation (3-16).

For the ring shear test (Fig. 6-3b)

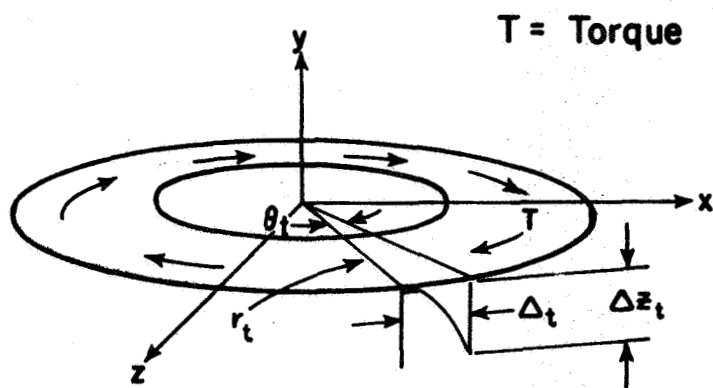
$$\frac{\Delta_t}{t_t} = \frac{\theta_t r_t}{t_t} \quad (6-5)$$

where t_t = time increment for test.

An equivalence may be written from equations (6-4) and (6-5) by assuming that the rate of soil displacement for the wheel and the test are the same



a) Wheel (side view)



b) Shear Ring Test (three dimensional view)

Fig. 6-3. Soil displacements for wheel and test.

$$\frac{\Delta_w/t_w}{\Delta_t/t_t} = 1 = \frac{\theta_w r_w t_t}{\theta_t r_t t_w} \quad (i) \quad (6-6)$$

If instead it is required that the strains for the wheel and the test be equal,

$$\frac{\epsilon_w}{\epsilon_t} = 1 = \frac{\theta_w r_w \Delta z_t}{\theta_t r_t \Delta z_w} \quad (i) \quad (6-7)$$

While these equations may be useful in selecting test setup and equipment, they do not tell us the slip, associated with a particular displacement.

From equation (6-4)

$$\Delta_w = \theta_w r_i \quad (6-8)$$

where r is the radius of the wheel, consistent with our earlier definition. Using equations (3-16) and (4-9), equation (6-8) can be expressed in terms of "s"

$$\Delta_w = \frac{2\theta_w r}{\frac{1}{s} + 1} \quad (6-9)$$

Solving for s from equation (6-3) and substituting for s into equation (6-9),

$$\Delta_w = \theta_w r \left[1 - \frac{(1 - s_\theta)}{(1+s_\theta) \cos\theta} \right] \quad (6-10)$$

Note that if $\theta = 0$, $s_\theta = s$, and equation (6-10) reduces to equation (6-9).

To facilitate certain comparisons and illustrative calculations to be presented in this report, equation (6-10) is plotted in Fig. 6-4 for $\theta = 0$, assuming $\theta_w = \theta_T$. In reality, θ_w could have any value; however, physical reasoning suggests that $\theta_w = \theta_T$ is a good first approximation, and it provides a convenient bridge from slip at a point to displacement.

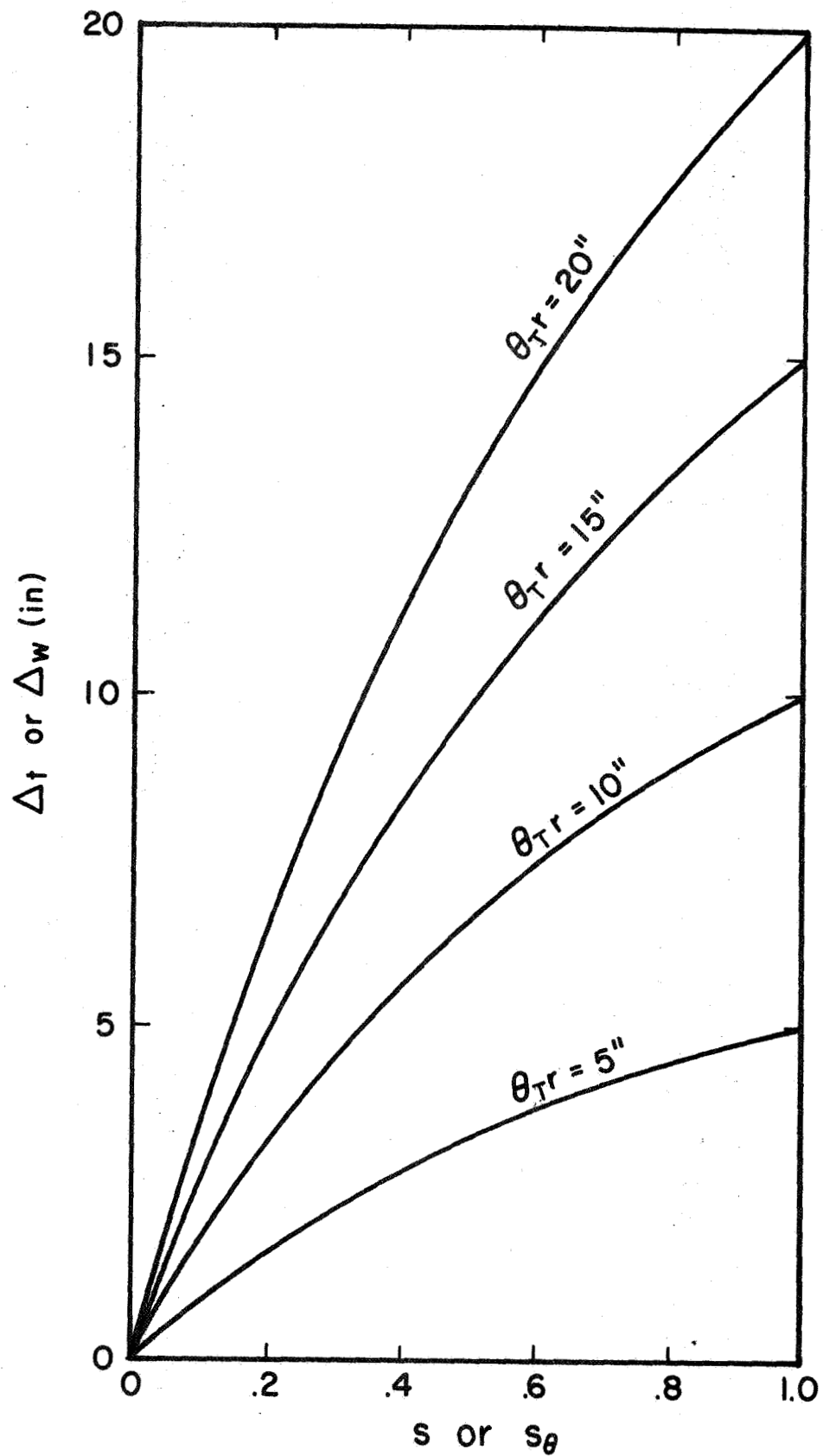


Fig. 6-4. Plot of equation (6-10).

With better understanding of the wheel-soil interaction process, the functional relationship expressed by equation (6-10) undoubtedly will need to be modified. For instance, Δ_w is probably a function of soil type; a coefficient, which would be very small for a brittle soil and relatively large for a very plastic soil, may be required. Further, it appears that soil elements influenced by the wheel are subjected to various states of shear; while some soil elements are in a state analogous to direct shear for high values of slip, some soil elements are in a state analogous to compression for low values of slip. These complexities also need to be considered.

WHEEL-SOIL INTERFACE STRENGTH PARAMETERS

As in many other engineering problems, the fundamental relationships to be obtained from testing are stress-displacement curves. Suppose that testing of a wheel surface material to soil, using a ring shear device, yields the curves shown in Fig. 6-5a (three tests - three different normal pressures - are adequate). From Fig. 6-5a shear stress vs. normal stress lines can be plotted for various displacements (Fig. 6-5b). From Fig. 6-5b strength parameters, c_a and δ , can be plotted as a function of displacement (Fig. 6-5c). These are the required wheel-soil strength parameters.

SHEAR STRESS SURFACE

Experimental wheel-soil interaction data suggest a shear stress surface, $\tau = f(s, \theta)$. An attempt will now be made to predict such a surface from the previously presented relationships. The procedure is as follows:

1. Testing yields soil strength parameters, c_a and δ as a function of displacement (Fig. 6-5).

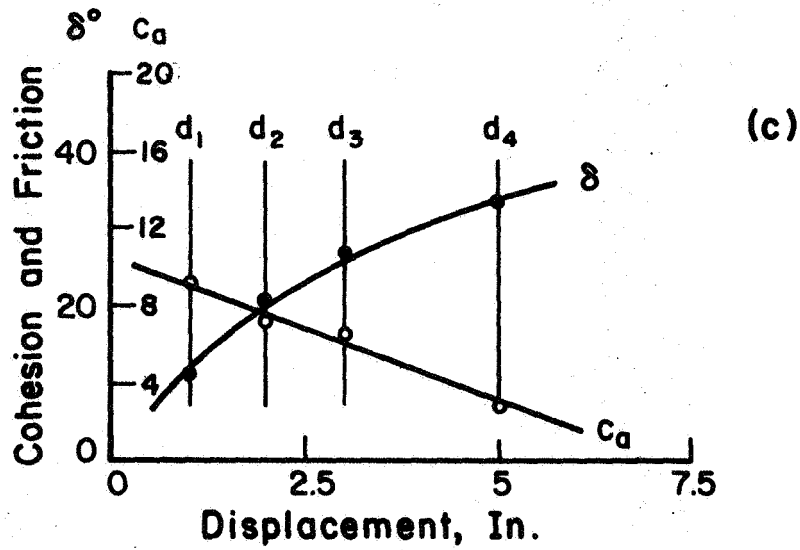
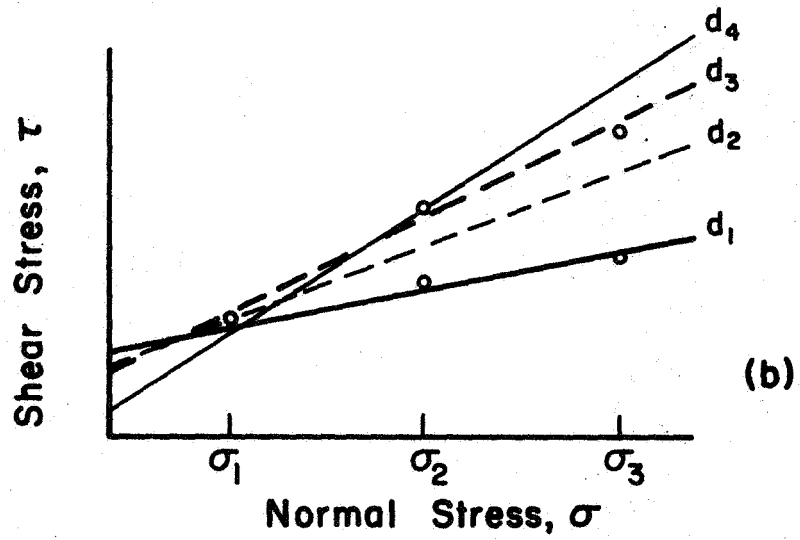
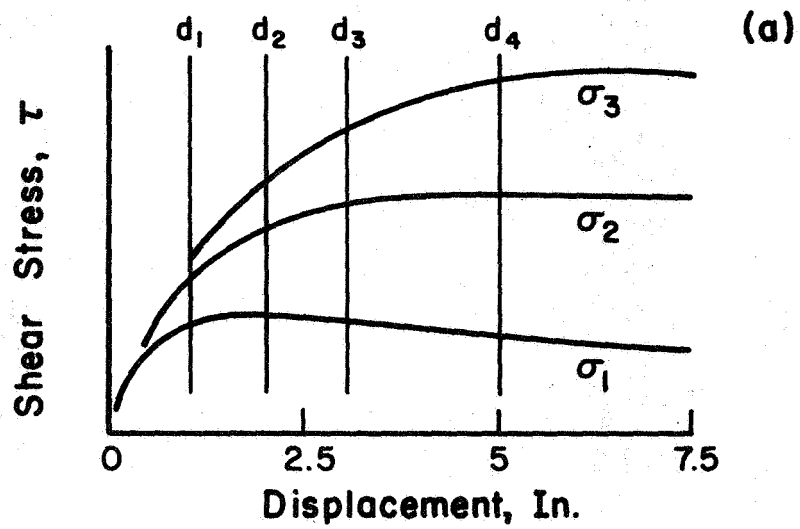


Fig. 6-5. Soil strength parameters, c_a and δ .

2. Slip, s , can be converted to slip, s_θ , using equation (6-3).
3. Displacement can be related to slip, s_θ , from Fig. 6-4.
4. The shear parameters are then known for slip at any point, s_θ , along the wheel-soil contact.
5. Therefore, the shear stress mobilized at any point along the wheel-soil contact can be computed from

$$\tau_{s\theta} = c_{as\theta} + \sigma_\theta \tan \delta_{s\theta} \quad (6-11)$$

In this prediction, the normal stress distribution, σ_θ , may be assumed sinusoidal for a sand and constant for a pure clay. For any real soil, the normal stress distribution is probably closer to sinusoidal.

The predicted shear stress surface is shown in Fig. 6-6, which shows a three-dimensional view. In this figure the contact angle, θ , is plotted on the horizontal axis, slip, s , is plotted on the diagonal axis, and shear stress is plotted on the vertical axis. The front part of the surface (dotted lines) is below the θ, s plane and the rear part (solid lines) is above the θ, s plane. The normal stress distribution was assumed to be sinusoidal. Soil strength parameters were obtained from Fig. 6-5, with $c_a = 10.0$ at displacement = 0. In Fig. 6-4, $\theta_T r$ was assumed to equal 10 inches. For a 20-inch diameter wheel, θ_T would then be approximately 60 degrees. The rear wheel-soil contact angle, θ_2 , was assumed to be 10 degrees.

The predicted shear stress surface appears quite realistic. The towed point for this case occurs approximately at $s = -0.08$; it is indicated by the cross-hatched area in Fig. 6-6. If friction at the wheel hub is zero, torque must be zero for a towed wheel (see also Yong and Webb, 1969), and the towed point is characterized by

$$\int \tau_\theta d\theta = 0 \quad (6-12)$$

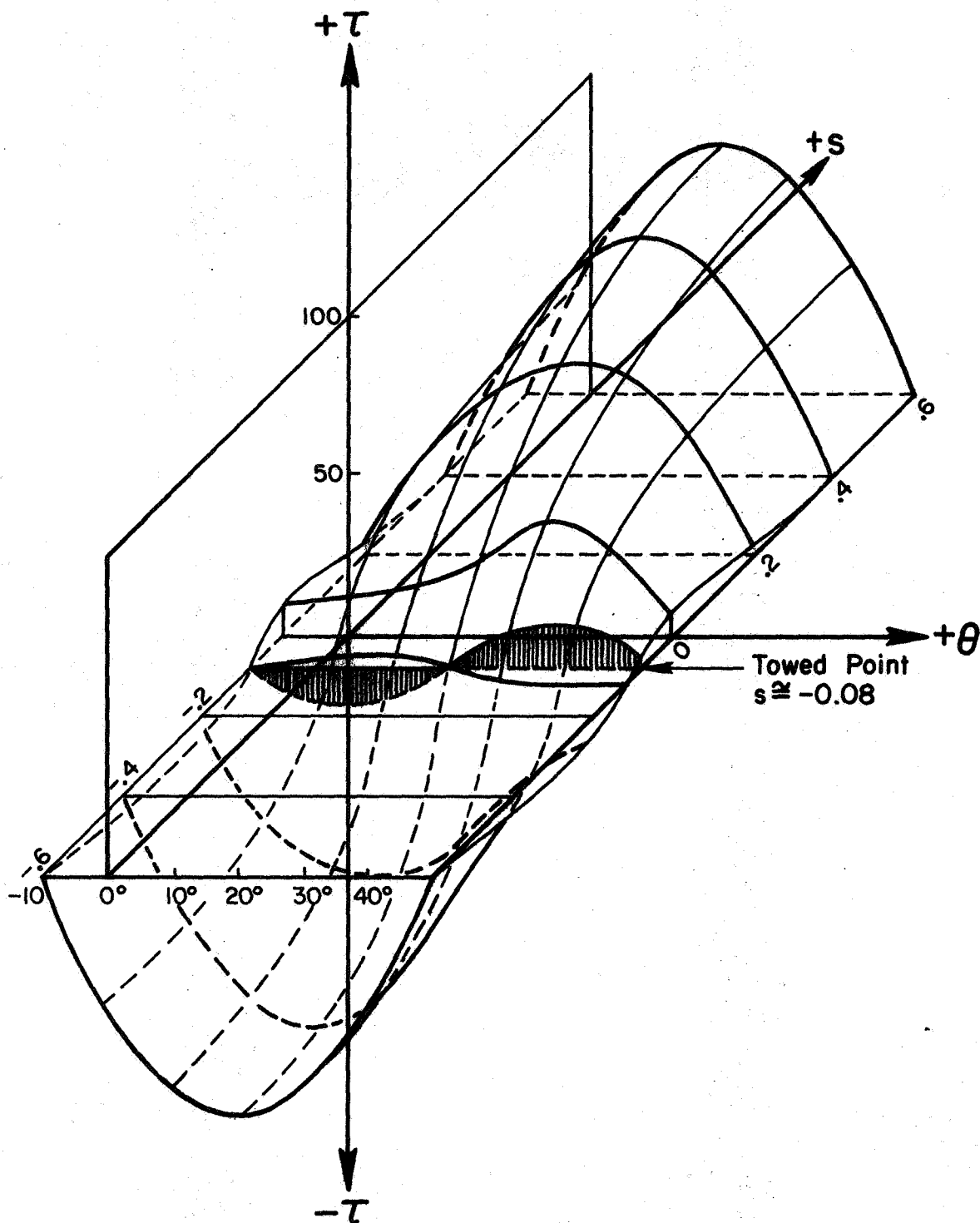


Fig. 6-6. Shear stress surface, $\tau = f(s, \theta)$.

In summary, given three stress-displacement curves, it is possible to estimate the shear stress mobilized at any point along the wheel-soil contact, for any value of slip.

CHAPTER 7. SOIL INERTIA IN WHEEL-SOIL INTERACTION

In previous investigations of wheel-soil interaction phenomena, the influence of inertia forces of moving soil have usually been assumed to be negligible. Although this assumption is probably valid for many wheel-soil interaction problems, it is supported by limited investigations and experimental data.

The investigations described in this chapter present a universally applicable hypothesis, to be tested experimentally. The hypothesis is based on the concept of a soil wedge being continuously formed and accelerated in front of the wheel.

Fig. 2-1 illustrates a track and associated shear surfaces resulting from pulling a 24-inch (61-cm) diameter wheel on Yuma sand. The extent of the shear surfaces is evaluated, and theory is presented from which the mass and acceleration of the moving soil can be deduced, thus forming the basis for evaluation of soil inertia forces.

THEORETICAL ANALYSIS

The resistance to a rolling wheel caused by the inertia of the soil set into motion by the wheel, R_I , is the product of the mass of soil involved, m_s , and its acceleration, a_s ,

$$R_I = m_s a_s \quad (7-1)$$

Mass of Moving Soil

Boundary of soil wedge:

A mechanism of shear in front of and below a wheel rolling down a soil slope is shown in Fig. 7-1. Imagine that the wheel center is at position 1. As the wheel center moves from position 1 to 2 and then to 3, the front of the wheel moves respectively from 1' to 2' then 3'. As the wheel moves

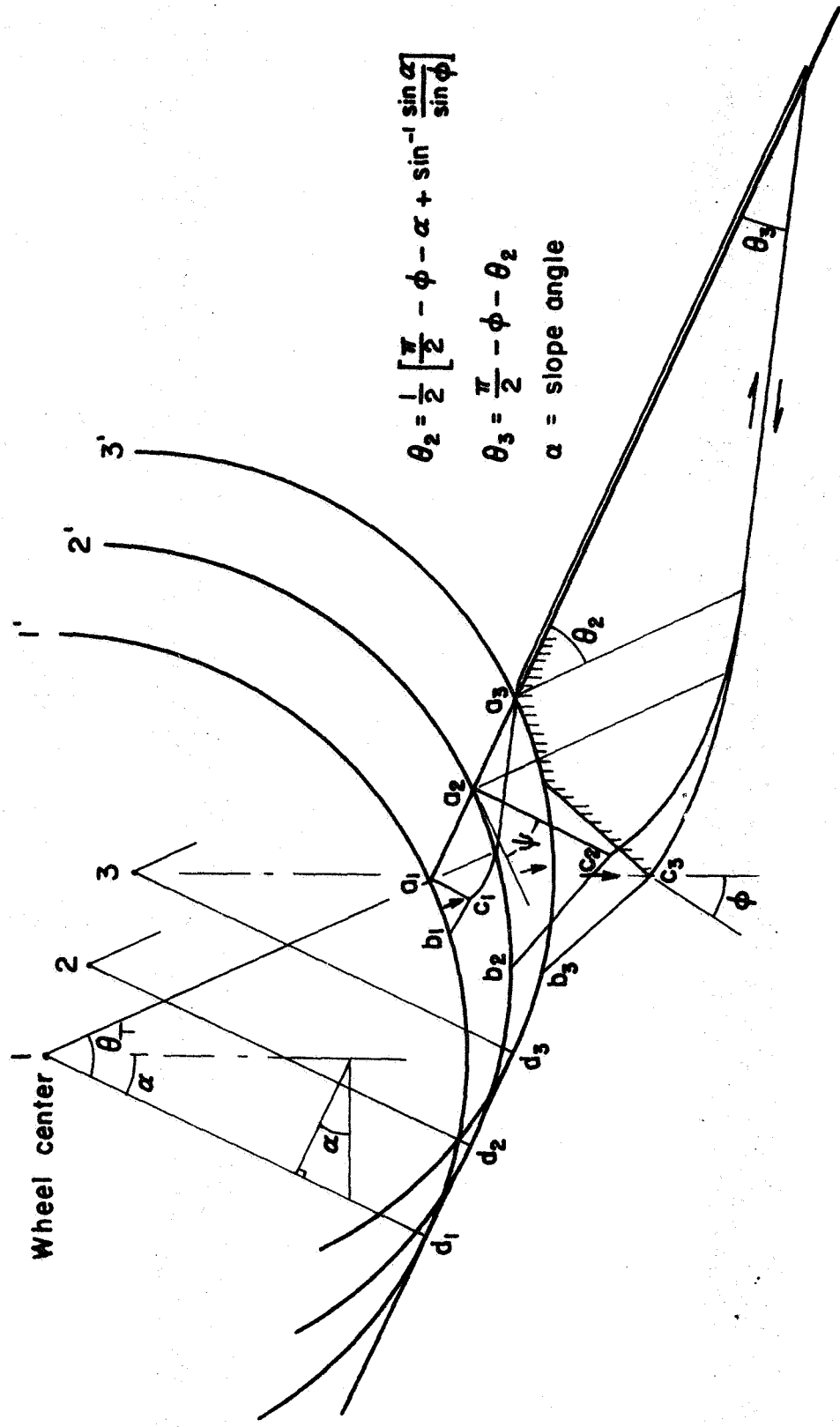


Fig. 7-1. Mechanism of shear in wheel-soil interaction.

from position 1, a shear surface confining an incremental soil wedge forms with an active Rankine zone $a_1b_1c_1$, a radial shear zone with log-spiral center at a_1 , and a passive Rankine zone. As the wheel continues to move (roll), the active Rankine zone grows and new shear surfaces form. Evidence for such shear surfaces is shown in Fig. 2-1; shear surfaces have also been observed in model tests (Hovland and Mitchell, 1972). The active Rankine zone and the corresponding soil wedge continue to grow until a limiting (maximum) size of wedge is formed. Beyond that point, new limiting (maximum) soil wedges will continue to form as the wheel rolls forward. It has been found that the maximum soil wedge (see Fig. 7-1) can be defined approximately by

1. An active Rankine zone, $a_2b_2c_2$, where distance (a_2b_2) equals one-half the soil-wheel contact or $1/2 (a_2d_2)$, with angle $\psi \approx 1.2 \phi$ (Meyerhof, 1955)
2. A radial shear zone with log-spiral center at a_2
3. A passive Rankine zone with θ_2 and θ_3 as indicated (Sokolovski, 1969; Karafiath and Nowatzki, 1968)

As the wheel moves from 2 to 3, the limiting soil wedge will deform and move out with relative motion, as shown by the arrows in Fig. 7-1. At this point, the active Rankine zone will be more compressed and the center of the log-spiral will be located at the intersection of the θ_2 line, with the vertical drawn through c_3 . At this point, with the center of the log-spiral directly above c_3 , motion along this ultimate shear surface will stop, since the angle between the direction of motion of the active Rankine zone and the normal to the shear surface is ϕ . For the wheel at position 3, the limiting soil wedge, constructed with the center of the log-spiral at 3, has the same size as that constructed for the wheel at 2 with the center of the log-spiral at a_2 .

To investigate how well the soil wedge selected by the procedure outlined above describes the actual soil wedge, a 24-inch (61 cm) diameter spherical wheel was rolled on Yuma sand, and the extent of the shear zones in front of and to the sides of the wheel were measured. Fig. 7-2 gives the results of this comparison. Predicted distance of forward shear (the distance at which the shear surface exits the slope) is plotted in comparison with measured distance of forward shear for different wheel loads. The measured distance of forward shear is the distance from the crest of the track to the furthest shear surface. The measured distance of side shear is also shown. It is the width of the shear zone on the side of the track measured from the crest of the track. The selected shear surface geometry appears to be adequate.

Mass of soil wedge:

Due to mathematical complexities in expressing exactly the mass of soil bounded by a log-spiral shear surface, and inherent assumptions in applying plasticity theory to the wheel-soil interaction problem, an approximation for the mass of soil is developed.

A longitudinal section of the boundary confining the moving soil, and an approximation to that boundary confining approximately the same mass of soil are shown in Fig. 7-3a. The ratio of d/d_o is plotted in Fig. 7-3b; this ratio was determined graphically. The curve in Fig. 7-3b can be expressed by

$$\frac{d}{d_o} = 1 + 0.002\phi^{1.77} \quad (7-2)$$

where ϕ is the soil friction angle in degrees.

From Fig. 7-3a, it follows that

$$d_o \approx \frac{r\theta_T}{4} \sqrt{2} \quad (7-3)$$

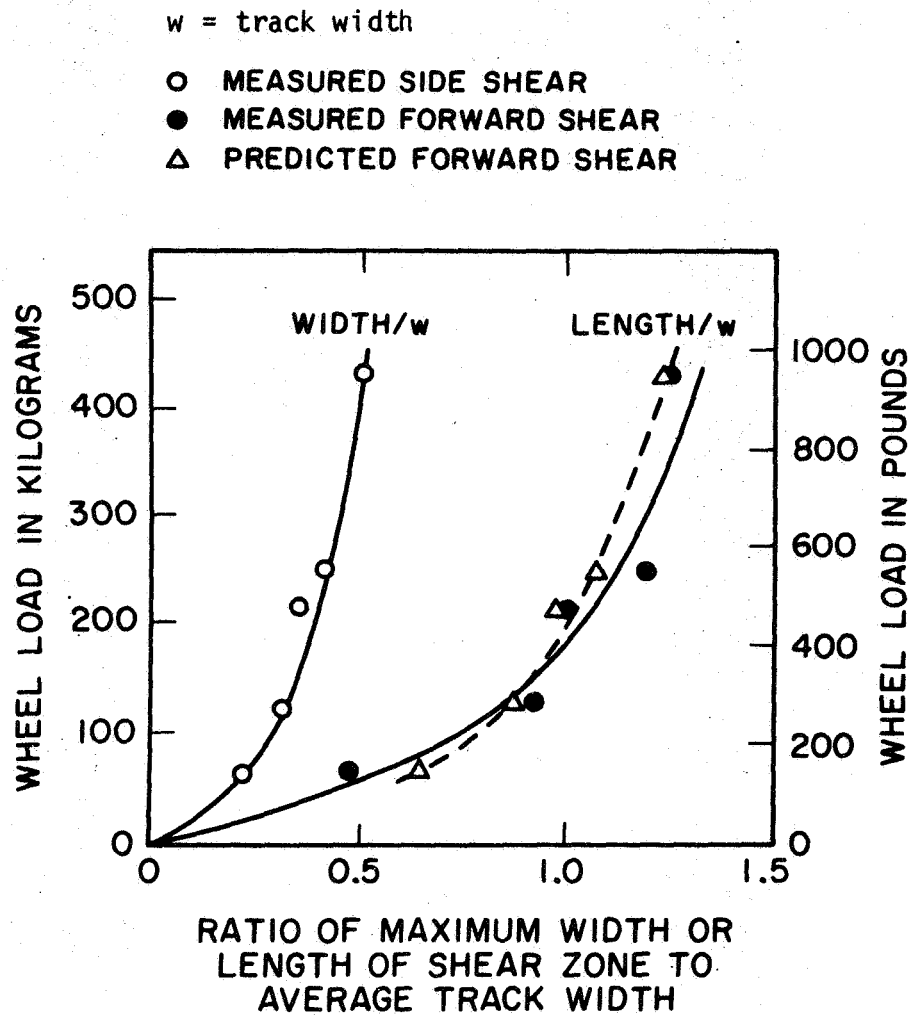
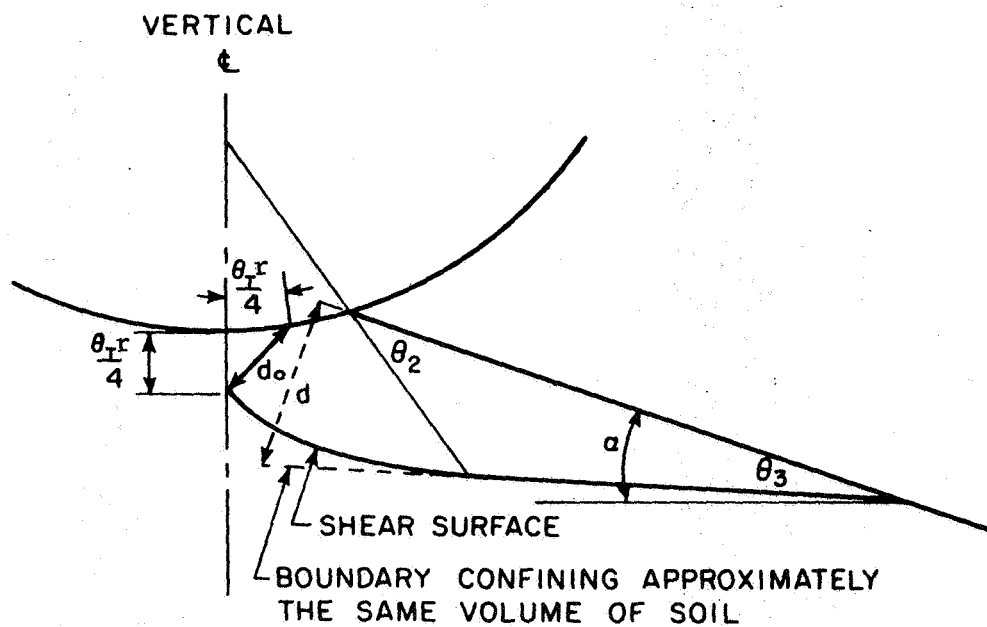
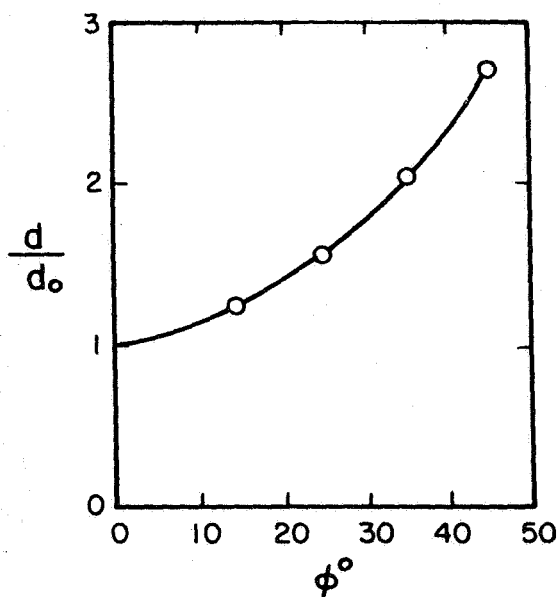


Fig. 7-2. Wheel load vs. predicted and measured dimension of soil wedge.



- a) Boundary confining approximately the same volume of soil as the actual shear surface.



- b) Ratio of d/d_o as a function of ϕ .

Fig. 7-3. Geometry for volume of moving soil.

where r = radius of wheel, θ_T = wheel-soil contact angle (see Fig. 7-1).

Fig. 7-2 suggests that the width of the moving soil wedge can be approximated by $1.4 w$, where w is the track width. Then, the mass of soil can be expressed as

$$m_s = \rho_s V_s = 0.7 \frac{\rho_s w d^2}{\tan \theta_3} \quad (7-4)$$

where ρ_s = soil mass density and V_s = soil volume.

Acceleration of Moving Soil

Acceleration of the moving soil wedge is related to its velocity. Velocity of the soil wedge is, in turn, related to the velocity of the wheel, which is known. It is, therefore, of interest to express the soil acceleration in terms of the velocity of the wheel.

Maximum soil acceleration as a function of average soil velocity:

Since motion of the soil wedge starts from rest and stops after the rolling wheel has passed, the initial and final soil velocities are known to be zero. Somewhere in between, the velocity of the shearing soil reaches a maximum. Fig. 7-4 shows experimentally determined distance, velocity, and acceleration relationships for shearing soil wedges. The plots were made from films taken of rolling spheres. Some 200 spheres were rolled on Yuma sand carefully prepared to desired densities in large soil cars at the U. S. Army Waterways Experiment Station (WES) (Hovland and Mitchell, 1971), and in some cases it was possible to determine the motion of soil wedges.

The relationships shown in Fig. 7-4 can be approximated theoretically by various assumed functions as listed in Table 7-1 and plotted in Fig. 7-5. The indicated accelerations, a_s ; velocities, v_s ; and distances, x_s ; are derived from the assumed function by simple differentiation and integration.

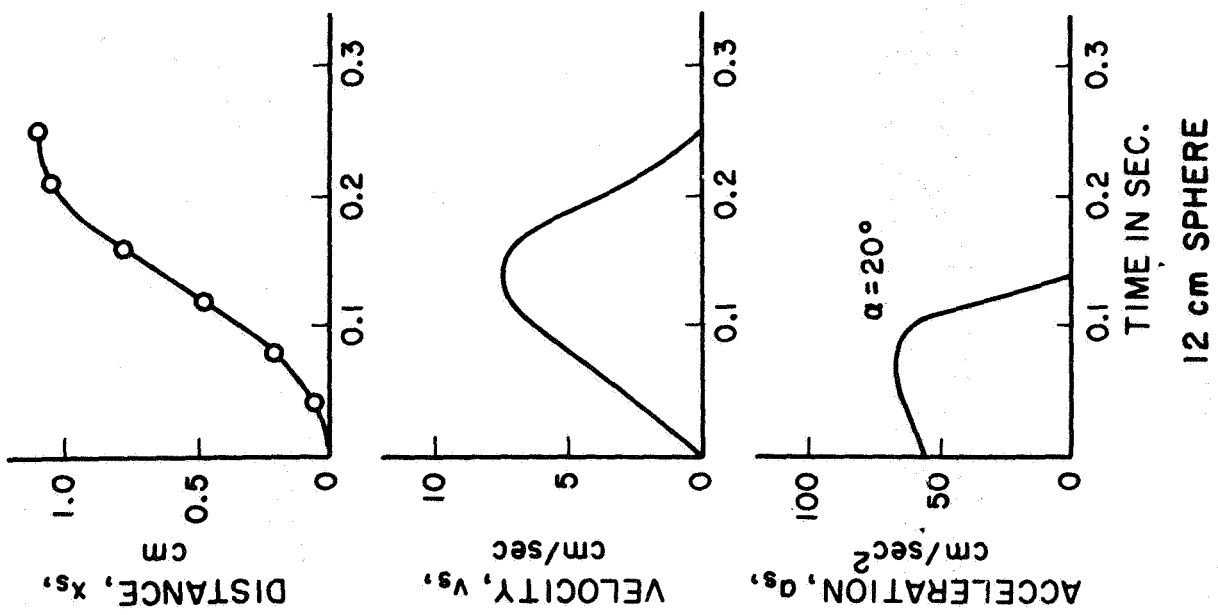
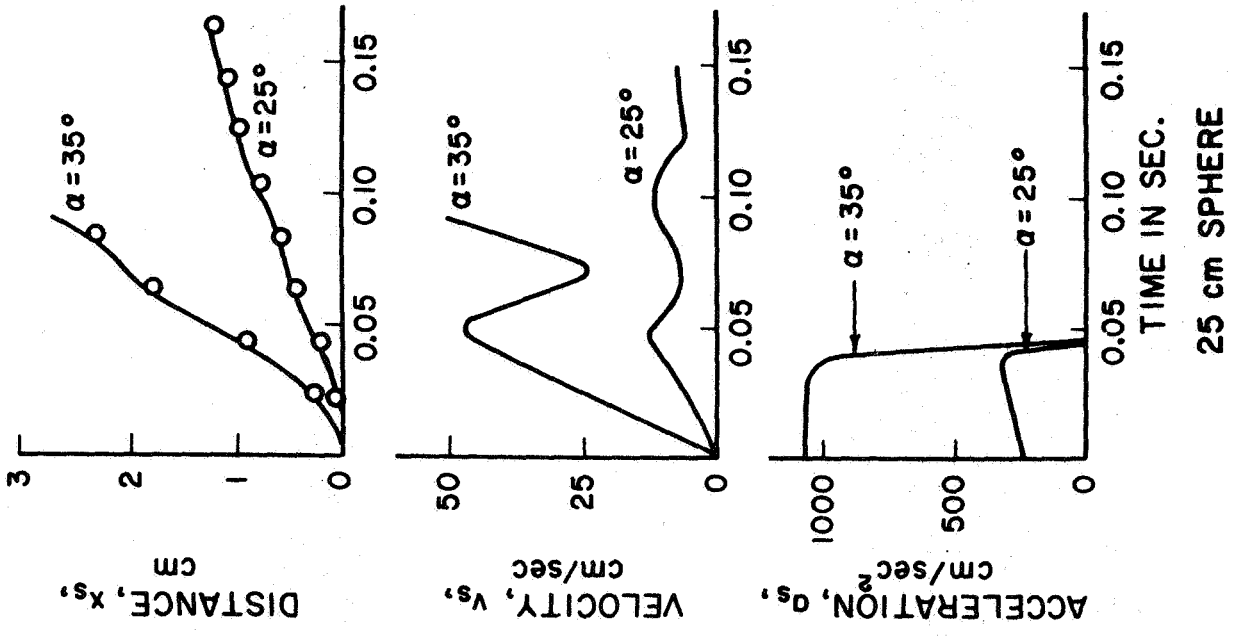


Fig. 7-4. Soil movement as a function of time (Hovland and Mitchell, 1971).

Table 7-1

Functions Approximating Motion of Soil Wedge

Assumed Function	Resulting Expressions	Maximum acceleration
Linear acceleration $a_s = -B_1 t + B_2$ -----	$a_s = 6 \left(1 - 2 \frac{t}{t_s}\right) \frac{v_a}{t_s}$ $v_s = 6 \frac{t}{t_s} \left(1 - \frac{t}{t_s}\right) v_a$ $x_s = 6 \frac{t^2}{t_s} \left(\frac{1}{2} - \frac{1}{3} \frac{t}{t_s}\right) v_a$	$6 \frac{v_a}{t_s}$
Sinusoidal velocity $v_s = B_1 \sin(B_2 + B_3 t)$ -----	$a_s = -\frac{\pi^2}{2} \cos\left[\pi \left(1 - \frac{t}{t_s}\right)\right] \frac{v_a}{t_s}$ $v_s = \frac{\pi}{2} \sin\left[\pi \left(1 - \frac{t}{t_s}\right)\right] v_a$ $x_s = \frac{t_s}{2} \left[\cos\left[\pi \left(1 - \frac{t}{t_s}\right)\right] + 1\right] v_a$	$4.9 \frac{v_a}{t_s}$
Step acceleration $a_s = \text{constant}$ -----	$a_s = 4 \frac{v_a}{t_s}$ $v_s = 4 v_a \frac{t}{t_s}$ $x_s = 2 v_a \frac{t}{t_s}$	$4 \frac{v_a}{t_s}$
Sinusoidal acceleration $a_s = a_{\max} \sin(B_1 t + B_2)$ -----	$a_s = 2 \pi \sin\left(2\pi \frac{t}{t_s}\right) \frac{v_a}{t_s}$ $v_s = \left(1 - \cos\left(2\pi \frac{t}{t_s}\right)\right) v_a$ $x_s = \left(t - \frac{t_s}{2\pi} \sin\left(2\pi \frac{t}{t_s}\right)\right) v_a$	$6.28 \frac{v_a}{t_s}$

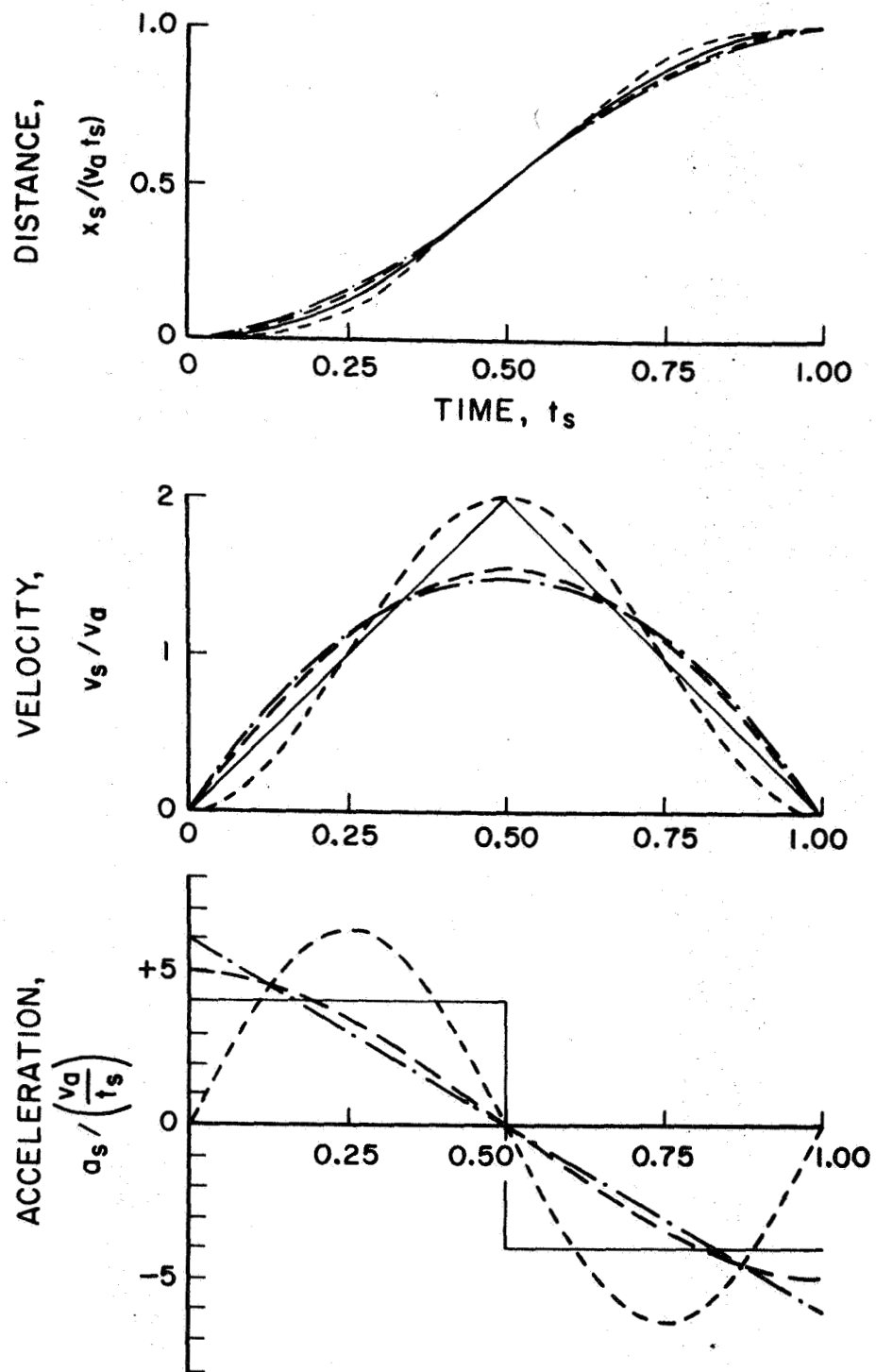


Fig. 7-5. Theoretical approximations to soil movement as a function of time.

In Table 7-1, v_a = average soil velocity, t_s = time in which soil moves, and B_1 , B_2 , and B_3 are integration constants.

By comparing the experimental curves (Fig 7-4) and the theoretical curves (Fig. 7-5), and the values of maximum acceleration listed in Table 7-1, the following conclusions can be made:

1. Since a small difference in the distance vs. time curve (Fig. 7-5) can lead to a drastic difference in the acceleration curve, it is difficult to interpret the exact acceleration function from an experimentally measured distance vs. time curve.
2. Since the maximum accelerations for the various functions (Table 7-1, Fig. 7-5) only vary from $4 v_a/t_s$ to $6.28 v_a/t_s$, it is not necessary to know the exact acceleration function, for a first approximation.
3. The curves in Fig. 7-4 show greatest resemblance to the step acceleration and sinusoidal velocity functions in Fig. 7-5 for which $a_{\max} = 4 v_a/t_s$ and $4.9 v_a/t_s$, respectively.

In the following development, $a_{\max} = 5 v_a/t_s$ will be used. Deviations from this value will then be within $\pm 20\%$ of the range of functions considered.

Average soil velocity as a function of wheel velocity:

Fig. 7-1 indicates that in the time the wheel moves from 2 to 3, the soil wedge (midpoint of a_2c_2) moves approximately 1/6 that distance in the same direction. Therefore, the average soil velocity is

$$v_a = \frac{v}{6} \quad (7-5)$$

where v = velocity of the wheel parallel to the slope. The maximum soil acceleration may then be expressed as

$$a_s = \frac{5 v}{6 t_s} \quad (7-6)$$

To have a useful expression for a_s it is necessary to eliminate t_s from equation (7-6). Observations of wheel-soil interaction show that the soil at a_1 , Fig. 7-1, begins to move before the wheel reaches position 1. With the very limited experimental data available on this problem, it will be assumed that the soil moves in the time the wheel moves twice the distance from position 1 to 3 in Fig. 7-1. Then we can say that $t_s = \theta_T r/v$, and

$$a_s = \frac{5}{6} \frac{v^2}{\theta_T r} \quad (7-7)$$

It is now possible to compare experimental maximum soil accelerations shown in Fig. 7-4 and theoretical values determined using equations (7-6) and (7-7). This comparison is shown in Table 7-2.

Table 7-2

Comparison Between Experimental and Theoretical Accelerations

Identification			Experimental			Theoretical	
Soil car	Slope °	Sphere Diam. (cm)	v (cm/sec)	t_s (sec)	a_s (cm/sec ²)	a_s (Eq.7-6) (cm/sec ²)	a_s (Eq.7-7) (cm/sec ²)
1	20	12	19	.25	67	63	51
4	25	25	27	.085	320	265	102
4	35	25	106	.085	1060	1040	1675

In Table 7-2, the theoretical accelerations computed using equation (7-6) and experimental values for t_s compare well. The theoretical accelerations computed using equation (7-7) and the assumed value for t_s compare less well.

Soil Inertia Resistance to a Rolling Wheel

Combining equations (7-4) and (7-7) gives

$$R_I = \frac{0.58 \rho_s w d^2 v^2}{\tan \theta_3 \theta_T r} \quad (7-8)$$

This inertia force can be expressed as force per unit area of wheel to soil contact, analogous to unit bearing capacity, by dividing by the contact area, $\theta_T r w$,

$$q_I = \frac{0.58 \rho_s d^2}{\tan \theta_3} \left(\frac{v}{\theta_T r} \right)^2 \quad (7-9)$$

A convenient dimensionless expression results by dividing both sides by $\rho_s g w$ and substituting for d , equations (7-2) and (7-3)

$$\frac{q_I}{\rho_s g w} + \frac{(1 + 0.002 \phi^{1.77})^2}{13.8 \tan \theta_3} \frac{v^2}{w g} \quad (7-10)$$

or

$$\frac{q_I}{\rho_s g w} = \beta \frac{v^2}{w g} \quad (7-11)$$

where

$$\beta = \frac{(1 + 0.002 \phi^{1.77})^2}{13.8 \tan \theta_3}$$

As an aid in solving equation (7-11), values of β are presented in Fig. 7-6. As α approaches ϕ , θ_3 approaches zero and β approaches infinity. Since such values of β are unreasonable, Fig. 7-6 is considered valid for $\alpha \leq \phi - 5^\circ$ only; i.e., the solid portion of the curves only.

SCHURING'S ANALYSIS

It is also possible to study the effects of inertia forces by considering the flotation provided a moving wheel by soil inertia and soil static forces (bearing capacity). It is to be noted that while the volume of the soil wedge is not a function of cohesion (previous section), bearing capacity is a function of both cohesion and friction. Thus, at this point cohesion, c , is introduced.

Schuring (1968) studied inertia forces by moving plates at various

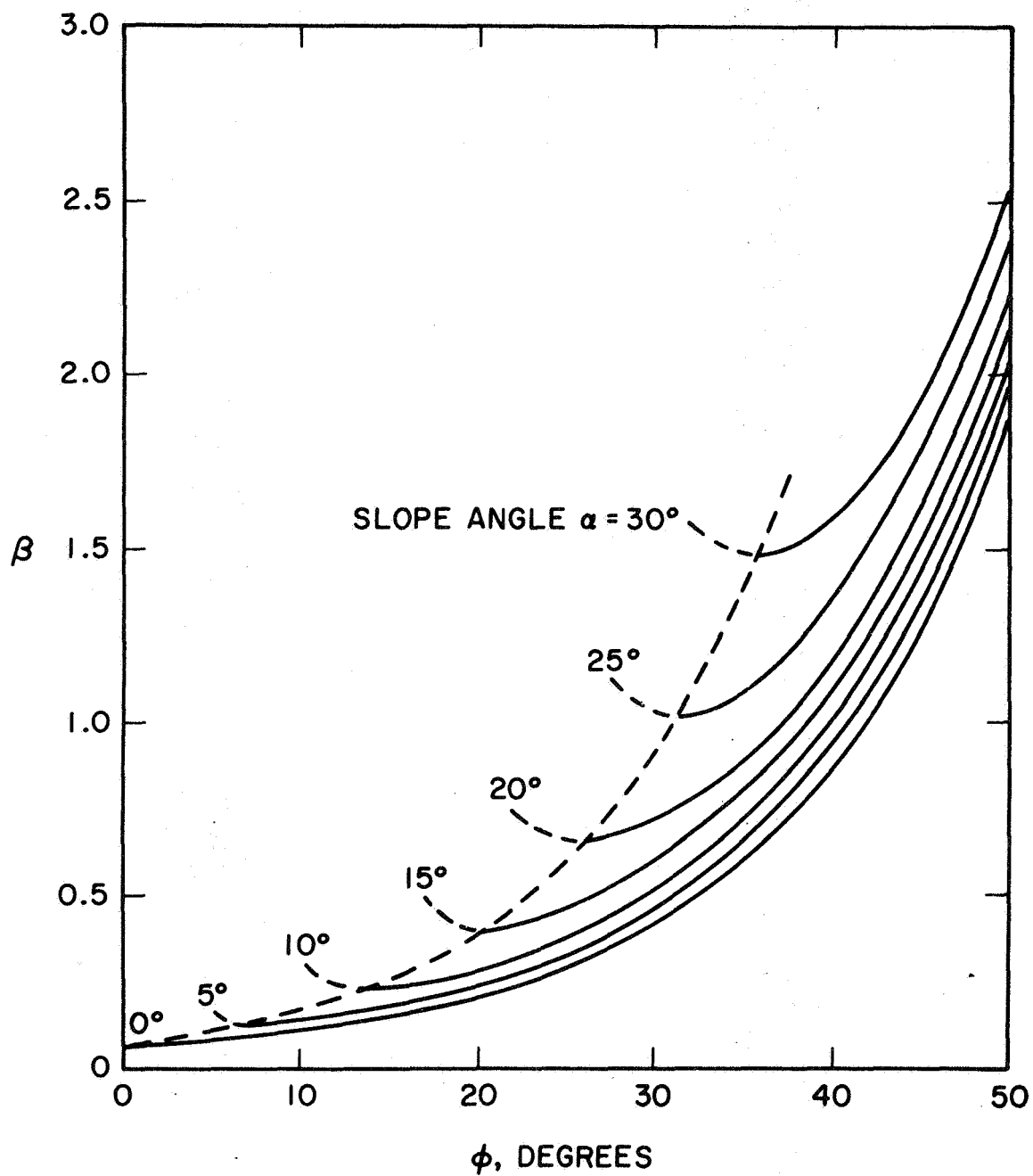


Fig. 7-6. Values of β for use in equation (7-11).

velocities and inclined at various angles to a bed of soft clay. He plotted his results as shown in Fig. 7-7. This plot is analogous to the familiar Moody diagram in fluid mechanics; the ratio plotted on the vertical axis is similar to the drag coefficient and the ratio plotted on the horizontal axis corresponds to Reynolds number. Schuring concluded that:

1. For ordinary vehicular speeds, inertia effects are likely to be insignificantly small.
2. "For special applications, such as dynamic testing and aircraft landing, inertia of accelerated soil may be the most important factor."

Wheel velocities which lead to either insignificant or significant (static range and dynamic range, respectively) inertia forces can be conveniently separated by plotting data as shown in Fig. 7-7. In the static range, where inertia forces are negligible, data plot along a 45° line. In the dynamic range, where inertia forces predominate, data become asymptotic to the horizontal axis. Thus, this approach places bounds on velocities for which inertia forces can be neglected and for which they predominate.

This ingenious approach appears to have two shortcomings, which Schuring also recognized. First, although the method is good for separating negligible and predominating inertia forces, it does not provide a basis for predicting performance for specific conditions, particularly in the transition range. Further, data for a $c - \phi$ soil cannot be accounted for. (ϕ represents an additional parameter, and the frictional force is further complicated by being a function of the normal force (see Schuring, 1968)). The theoretical analysis presented earlier in this paper attempts to overcome the first shortcoming. A concept of equivalent cohesion presented below attempts to overcome the second shortcoming.

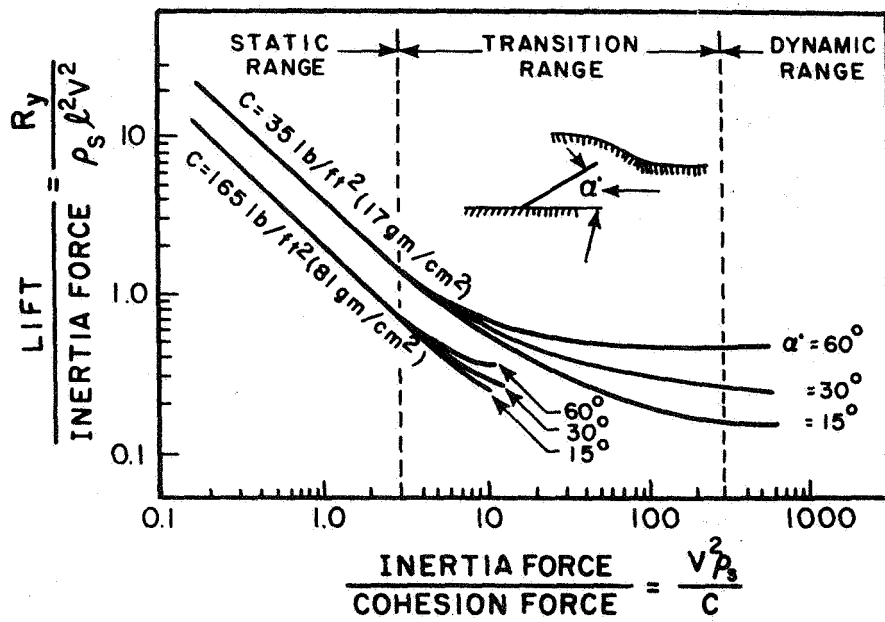


Fig. 7-7. Rectangular plate 5.5 x 2.76 in., moved at different inclination angles through very soft soil (Schuring, 1968).

EQUIVALENT COHESION

While a general relationship between cohesion, c , and friction, ϕ , is not possible (c and ϕ being independent soil parameters), it is always possible to express the total effect of the two by one strength parameter for any one type of problem. Soil resistance to a rolling wheel can be considered a bearing capacity type of problem. (It has been demonstrated that bearing capacity theory can be used as a basis for analyzing soil resistance to freely rolling spherical wheels and spheres (see Chapter 5 and Hovland and Mitchell, 1971). It is believed that phenomenologically bearing capacity theory can provide the basis for analyzing soil resistance of rolling wheels in general). Thus, for this specific problem, an equivalent cohesion is developed below.

The general bearing capacity equation (5-7), was adapted to the rolling sphere problem (Hovland and Mitchell, 1971)

$$\frac{q}{w\gamma_s} = 0.188 N_{\gamma_s} + 1.1 \frac{c}{w\gamma_s} N_{cs} + 0.55 \frac{z}{w} N_{qs} \quad (7-12)$$

where

q = soil bearing capacity

N_{γ} , N_c , N_q = bearing capacity factors (Meyerhof, 1951)

$$N_{\gamma_s} \approx 0.25 N_{\gamma}$$

$$N_{cs} \approx 0.50 N_c$$

$$N_{qs} = N_{cs} \tan\phi + 1$$

z = sinkage

$$\gamma_s = \text{soil unit weight} = \rho_s g$$

If a soil (x) is to give the same resistance as a soil (1),

$$\frac{\left(\frac{q}{w\gamma_s}\right)_x}{\left(\frac{q}{w\gamma_s}\right)_1} = 1 = \frac{\left[.188N_{\gamma_s} + 1.1 \left(\frac{c}{w\gamma_s}\right) N_{cs} + 0.55 \left(\frac{z}{w}\right) N_{qs}\right]_x}{\left[.188N_{\gamma_s} + 1.1 \left(\frac{c}{w\gamma_s}\right) N_{cs} + 0.55 \left(\frac{z}{w}\right) N_{qs}\right]_1} \quad (7-13)$$

Rearranging equation (7-13) and substituting $N_{\gamma_s} = 0.25 N_{\gamma}$, $N_{cs} = 0.5 N_c$, and $N_{qs} = N_{cs} \tan\phi + 1$ leads to an expression for c_x/c_1

$$\frac{c_x}{c_1} = \frac{w\gamma_s}{c_1} \left[\frac{1}{2} \left(\frac{z}{w} \right) \left(\frac{N_{c_1}}{N_{cx}} \tan\phi_1 - \tan\phi_x \right) + 0.085 \frac{(N_{\gamma_1} - N_{\gamma_x})}{N_{cx}} \right] + \frac{N_{c_1}}{N_{cx}} \quad (7-14)$$

In this equation geometrical parameters are held constant ($w_x = w_1 = w$), and $\gamma_{sx} = \gamma_{s1} = \gamma$. A $c-\phi$ soil can be treated as an equivalent c_e soil by letting ϕ_x in equation (7-14) equal zero

$$\frac{c_e}{w\gamma_s} = \left[\frac{1}{2} \frac{z}{w} \tan\phi_1 + \frac{c_1}{w\gamma_s} \right] \frac{N_{c_1}}{N_{cx}} + 0.085 \frac{N_{\gamma_1}}{N_{cx}} \quad (7-15)$$

where N_{c_1} and N_{γ_1} are determined for $\phi = \phi_1$, and N_{cx} is determined for $\phi = 0$.

Using equivalent cohesion as determined from equation (7-15), experimental data for any $c - \phi$ soil can be analyzed on the type of plot shown in Fig. 7-7. Comparing theory and experimental data on this type of plot has certain important implications, which are discussed subsequently.

DISCUSSION

Theory Compared with Schuring's Data

To compare predictions of the theoretical analysis presented in this paper with Schuring's data, load-soil interaction must be expressed for comparable geometries. The geometries of a rolling wheel and Schuring's plate are illustrated in Fig. 7-8. The geometries are comparable, and the wheel geometry is defined, if the length and orientation of the chord-length for a wheel-soil contact is the same as the length, l , and the orientation of the plate.

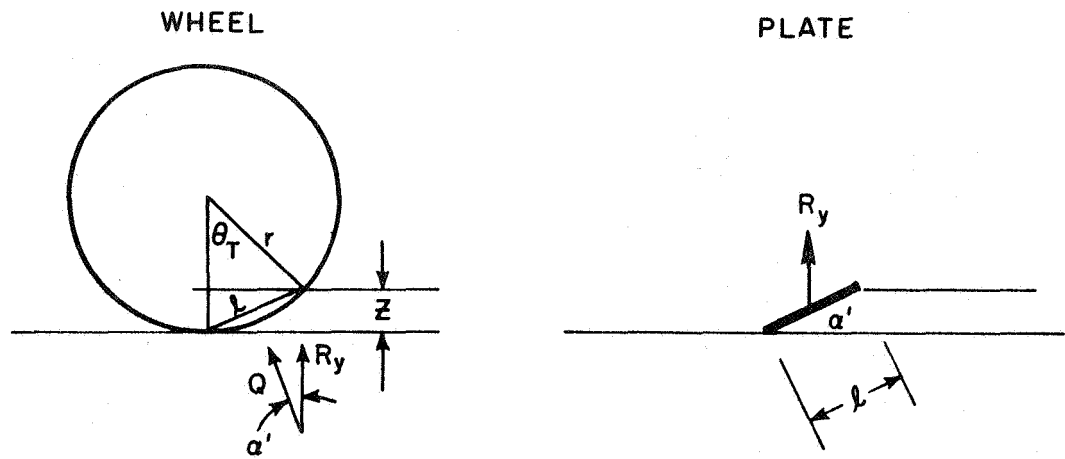


Fig. 7-8. Comparable geometries for wheel and plate.

The axes of Fig. 7-7 can now be expressed in terms of developed theory using equation (7-11) and Fig. 7-8:

$$\frac{\text{lift}}{\text{inertia force}} = \frac{R_y^*}{\rho_s \ell^2 v^2} = \frac{(q + q_I)}{q_I} \beta \cos \alpha', \text{ and}$$

$$\frac{\text{inertia force}}{\text{cohesion force}} = \frac{v^2 \rho_s}{c} = \frac{q_I}{\beta c_e}$$

where α' = inclination of plate; ℓ = length of plate in the plane of the paper, equal to the chord distance of θ_T ; and R_y = lift, equal to the vertical component of the total bearing capacity. In working out the parameters of these axes, q_I is computed from equation (7-11), q is computed from equation (7-12), assuming α' = slope angle in determining the bearing capacity factors (Meyerhof, 1951), and c_e is computed from equation (7-15).

Ordinates and abscissas were computed as described above for the soil conditions of Schuring's tests. His experimental curves are compared with theoretical predictions, curves A and A', in Fig. 7-9. While for Schuring's experimental curves, the separation in the static range is caused by a change in cohesion, c , the separation for the theoretical curves A and A' is primarily caused by the change in α' from 15° to 30° . Schuring's data for $c = 165$ psf (8.1 kN/m^2) are very close to the theoretical curves. For the data for $c = 35$ psf (1.7 kN/m^2), the experimental ordinate is more than twice the theoretical ordinate for high velocities. Since the mechanisms of soil shear under a rolling wheel (theoretical analysis) and a bulldozing plate (Schuring's data) are somewhat different, a close agreement for this comparison should not be expected.

The influence of changes in soil parameters on inertia forces is also illustrated in Fig. 7-9. If ϕ_1 is increased from zero to 10° , 20° and 30° ,

*In Schuring's analysis, ℓ^2 = area of plate (verbal communication with Mr. Schuring).

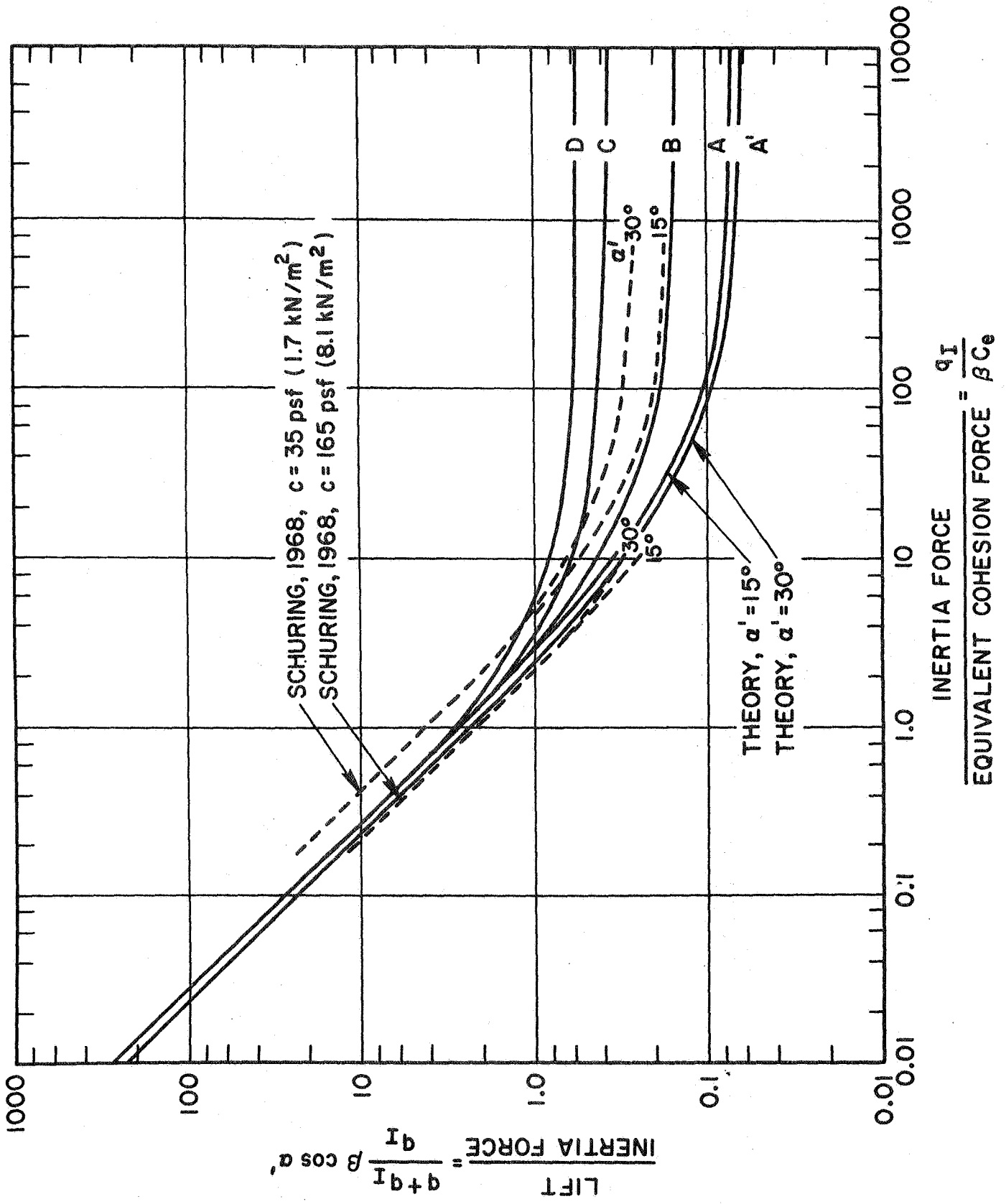


Fig. 7-9. Comparison between theoretical analysis and Schuring's (1968) data.

keeping all other soil parameters in curve A constant, c_e increases from 165 psf to 250, 420, and 780 psf (8.1 kN/m² to 12.2, 20.6, and 38.2 kN/m²) respectively, and we obtain curves B, C, and D. Therefore, in the dynamic range, curves A, B, C, and D separate with an increase in ϕ . If, instead, c_1 is increased, keeping $\phi_1 = 0$, curve A remains unchanged. This behavior is consistent with plasticity theory, which predicts that the volume of a soil wedge is a function of ϕ but is not a function of c .

Theory Compared with Data from Rolling Sphere Tests

An experimental comparison can also be made for spheres rolled on Yuma sand (Hovland and Mitchell, 1971). In this case, experimental values for the ordinates and abscissas for the type of plot shown in Fig. 7-7 are most conveniently determined as $R/(\rho_s \ell^2 v^2)$ and $(\rho_s v^2)/c_e$, respectively. Dynamic equilibrium of a freely rolling sphere (Hovland and Mitchell, 1971) (see also Fig. 4-1 and equation (4-5)) shows that

$$R = W \left[\left(\sin \alpha - \frac{a}{g} \right)^2 + \cos^2 \alpha \right]^{1/2} \quad (7-16)$$

where R = vertical force or lift, W = sphere weight, and a = sphere acceleration. Since W , a , and α are known, R can be calculated from equation (7-16). The sphere-soil contact area is $\ell^2 = 0.393 w^2$ (Hovland and Mitchell, 1971), where w = track width. Theoretical values for the ordinates and abscissas are determined as $\beta(q + q_I)/q_I$ and $q_I/(\beta c_e)$, where q_I is computed from equation (7-11), q is computed from equation (7-12), and c_e is computed from equation (7-15). Note that for a freely rolling sphere, the forces are vertical as determined, and the $\cos \alpha$ correction of the ordinate values is not necessary. Table 7-3 lists the type of data compared and Fig. 7-10 shows the comparison.

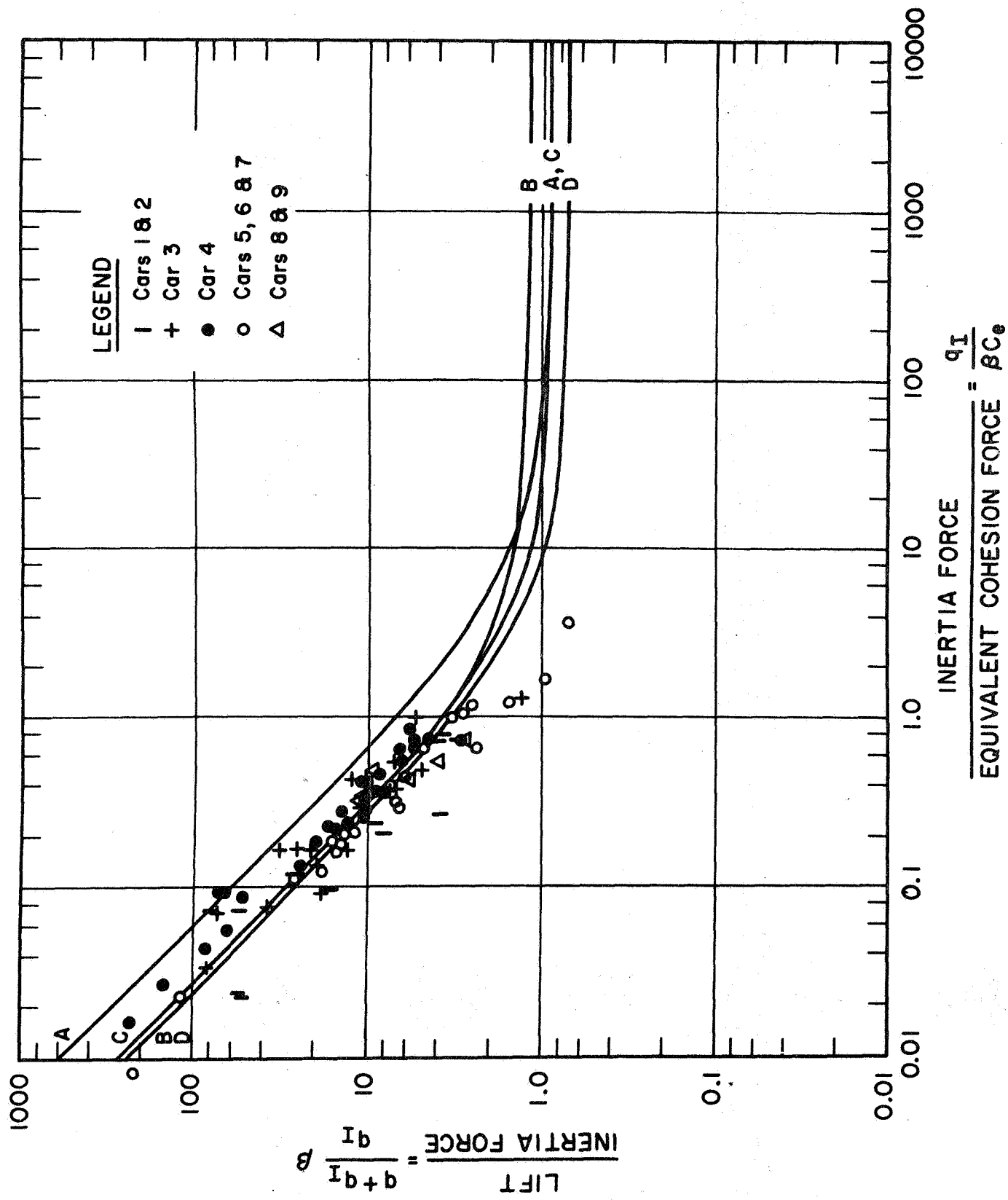


Fig. 7-10. Comparison between theoretical analysis and spheres rolled on Yuma sand.

Table 7-3

Data for Spheres Rolled on Yuma Sand

Curve on Fig. 7-10	Soil Cars	Experimental Data		Basis for Theoretical Curves					
		Range of α°	Range of $\frac{w}{D}$ (cm)	α_{ave}°	$\frac{w}{D}_{ave}$ (cm)	ρ_s ($\frac{gm-sec^2}{cm^4}$)	ϕ_1°	c_1 (gm/cm^2)	c_e (gm/cm^2)
A	1,2	15-25	.45-1.00	20	.68	.00150	37	0	12
B	3	10-35	.30-.65	20	.40	.00165	42	2.1	36
C	4,8,9	10-35	.10-.47	20	.33	.00150	37	10.5	85
C	5,6,7	10-35	.32-.87	20	.61	.00128	32	4.8	28

If Figs. 7-9 and 7-10 are compared, it will be noted that the data for Yuma sand ($32^\circ < \phi < 42^\circ$) are approximately averaged by Schuring's $c = 165$ psf (8.1 kN/m^2) line, for which $\phi = 0$. This suggests that, in the static range, data plotted in terms of c_e tend to converge to a narrow zone.

While it has been argued that a change in cohesion has a minor effect, curves A and C in Fig. 7-10 suggest that a change in w/D can have a much larger effect. However, the curves in Fig. 7-10 provide only a general comparison between theory and experimental data. Note that while the curves were determined for an average w/D , for the experimental data, w/D changed from data point to data point.

A more direct comparison is shown in Fig. 7-11, where the actual w/D ratio for each point was used in computing the theoretical values. In general, the comparison is good. The data in both Figs. 7-10 and 7-11 particularly for cars 1, 2, and 3 show a relatively large amount of scatter. Most of the data for the spheres rolled on moist, dense Yuma sand (car 4) lie approximately 20% below the 45° line. Most of the data for the spheres

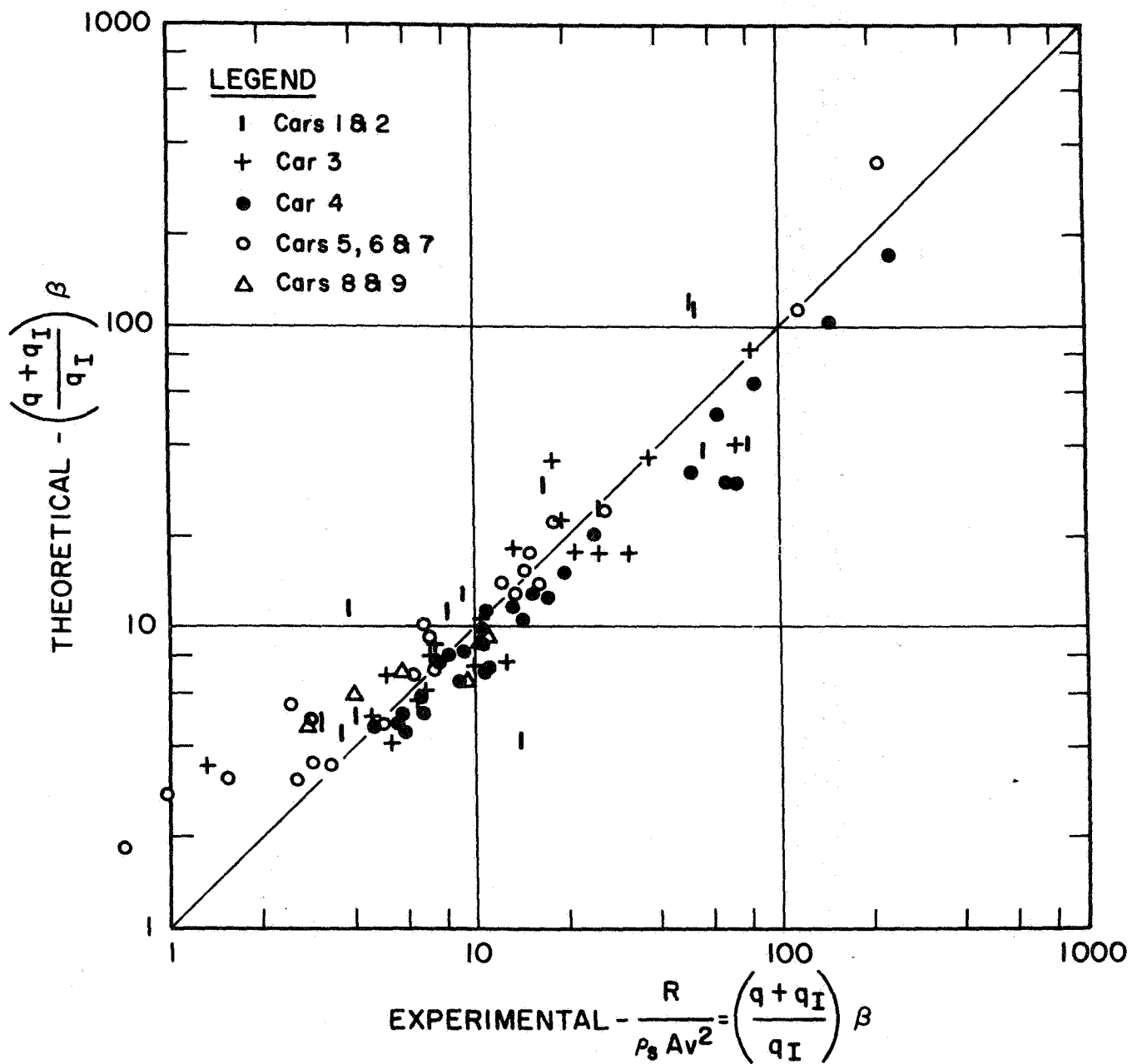


Fig. 7-11. Comparison between theoretical and experimental values of lift to inertia force ratio.

rolled on moist, loose Yuma sand (cars 5,6,7) lie approximately 20% above the 45° line.

Since for the soil conditions of these tests (Table 7-3) β varies approximately from 0.75 to 1.25 (Fig. 7-6) with an average value of 1.00, the relative contribution due to soil inertia is approximately the inverse of the value of the axes in Fig. 7-11. That is, for $R/(\rho_s Av^2) = 1, 10,$ and 100, inertia contribution to total soil resistance is approximately 100%, 10% and 1% respectively. Therefore, to the right of $R/(\rho_s Av^2) = 10,$ the comparison is indirect evidence for the applicability of bearing capacity theory in wheel-soil interaction. For all data to the left of $R/(\rho_s Av^2) = 10$ in Fig. 7-11, soil inertia forces were significant. This fact is not clearly revealed in Fig. 7-10, where the data essentially plot along a straight 45° line with no indication of bending into the transition range.

For low values of the abscissa in Fig. 7-11, the data tend to be above the 45° line. Although the data are limited, this suggests that for these rolling spheres, the theory underestimated the inertia effects by perhaps 50%.

Value of Theory to Experimental Work

While the agreement between theory and experimental data is generally good, although very preliminary, it is equally important that β can be determined experimentally. At high velocities (100 mi/hr.), as q_I becomes very large, $(q_I + q)/q_I$ approaches one, and the value of the ordinate (for example in Fig. 7-10) approaches β .

It will be recalled that the assumptions used in developing equation (7-11) are all incorporated into β . Therefore, as experimental data on β become available for various soils, the assumptions can be checked and better analysis will be possible.

The expression for β used in equation (7-11) can be generalized as

$$\beta = \frac{V_s \psi_a}{(\theta r)^2 w} \quad (7-17)$$

where V_s = volume of soil, and ψ_a is a function or coefficient relating the acceleration of the moving soil to the velocity of the wheel ($a_s = \psi_a \frac{v^2}{\theta r}$).

The only unknowns in equation (7-17) are V_s and ψ_a . Therefore, experimentally determining β is a way of backcalculating $V_s \psi_a$. Since ψ_a may be close to one (see equation (7-7)), experimentally determining β is a way of backcalculating the volume of moving soil.

Examples

To illustrate the practical implications of the theoretical analysis, consider first a Cessna 150 attempting a landing on a soft playa or marsh. If the gross weight of the airplane is assumed to be 1600 lb. (7300 N), at what velocity will severe and immobilizing sinkage of the wheels begin? (At what velocity will the wheel loads exceed the total lift?) Fig. 7-12 shows the velocity at which the wheels begin to sink severely into the soil, the total lift, and the lift provided by soil inertia forces as a percentage of total lift. (Soil and wheel conditions are indicated in Fig. 7-12.) The curve shown is computed in accordance with presented theory, and no experimental data are available at this time for comparison.

Consider now the inertial contribution to lift of the Lunar Roving Vehicle (LRV) operated on the surface of the moon. Estimates by the theoretical analysis are shown in Fig. 7-13. (Soil conditions are as indicated.) Inertia forces are shown to be significant at low velocities. Note that, on the moon, soil forces which are dependent on gravity are reduced by 1/6; therefore, the contributions due to inertia and cohesion are relatively six times more important.

CONDITIONS:

$$w = 7", \ell = 5.7", z = 2"$$

$$\phi = 10^\circ$$

$$c = 500 \text{ psf} = 24.5 \text{ kN/m}^2$$

$$\gamma_s = 100 \text{ pcf} = 16.0 \text{ kN/m}^3$$

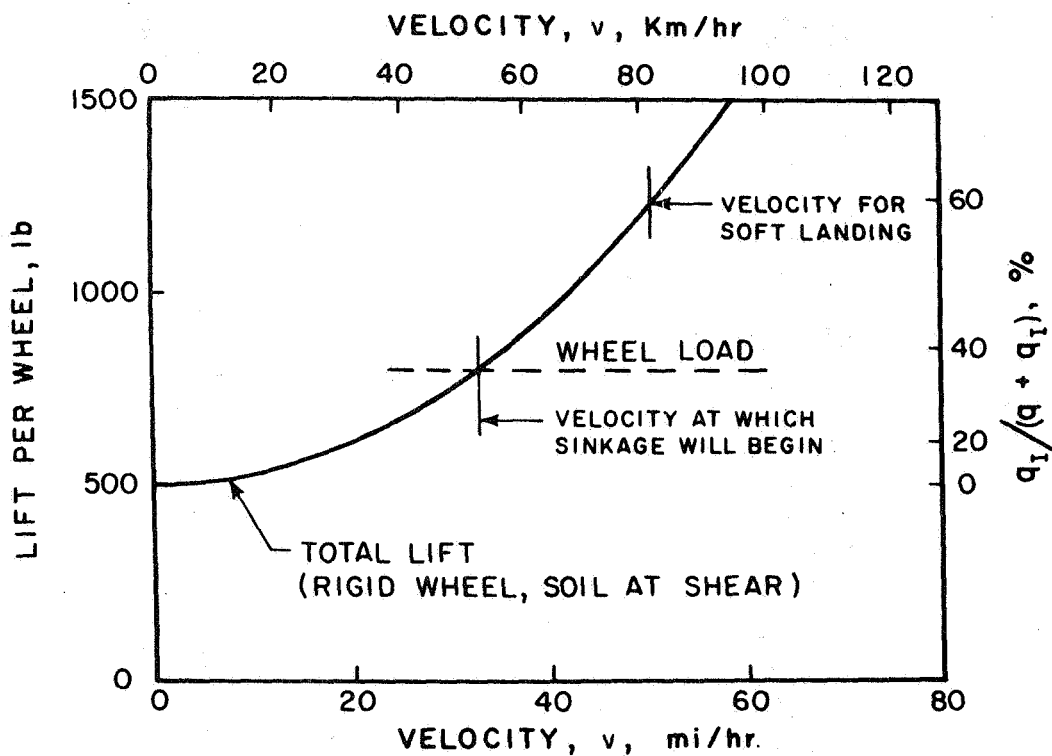


Fig. 7-12. Relative importance of soil inertia forces for a light airplane landing on a soft clayey soil.

CONDITIONS:

$$w = 9", l = 6", z = 0.5"$$

$$\phi = 40^\circ$$

$$c = 20 \text{ psf} = 0.98 \text{ kN/m}^2$$

$$\gamma_s = 100/6 \text{ pcf} = 16/6 \text{ kN/m}^3$$

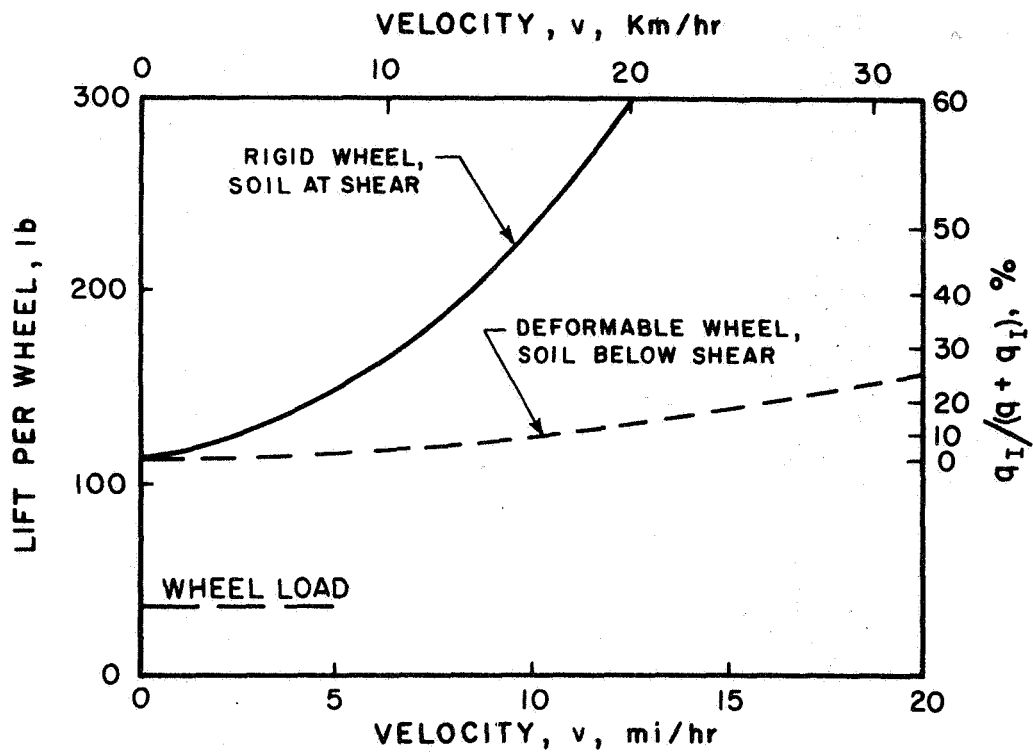


Fig. 7-13. Relative importance of soil inertia forces for the Lunar Roving Vehicle operated on the surface of the moon.

While in the first example (Fig. 7-12) the wheel load is higher than the static bearing capacity, the wheel load for the Lunar Roving Vehicle (appr. 35 lb = 160 N on the moon) is much less than the static bearing capacity (appr. 118 lb = 540 N on the moon). Therefore, not all the soil within the soil wedge defined by theory moves. The relative amount of soil that moves can, however, be estimated.

Radial pressure, σ , at a wheel-soil contact is proportional to the resistance to shear that is mobilized along a shear surface. Resistance to shear is proportional to the normal pressure along the shear surface. The normal pressure at any point along the shear surface (see Fig. 7-1) can be estimated by adding the pressure due to wheel load and the pressure due to soil weight. (The pressure due to the wheel load can be estimated from theory of pressure beneath a uniform load on an elastic half-space.) Assuming that for an increment of deformation, x , of the soil at the wheel-soil contact, shear stresses are mobilized along a related portion of the shear surface, we can estimate and plot resulting radial pressure, σ , vs. displacement, x . Such a plot suggests that the ratio of displacement, x , to displacement for full mobilization of shear stresses along the shear surface, x_{\max} , can be considered proportional to the ratio of σ to bearing capacity, q , squared. That is,

$$\frac{x}{x_{\max}} \propto \left(\frac{\sigma}{q}\right)^2 \quad (7-18)$$

Therefore, for the LRV wheel-soil interaction, the magnitude of soil inertia forces, which are proportional to the amount of moving soil, are reduced by approximately $(35/118)^2 \approx (1/11)$. This leads to the dashed line in Fig. 7-13.

The above example also clearly illustrates that the performance of a deformable wheel operating below soil bearing capacity is a different and a more complex problem than a rigid wheel, and Fig. 7-13 is intended as an example and a rough estimate only. Note that while for a rigid wheel, equilibrium is achieved by appropriate sinkage into the soil, for a deformable wheel, equilibrium is achieved mainly by appropriate flexure of the tire.

Based on the dashed curve in Fig. 7-13, soil inertia forces are likely to contribute from 10 to 20 percent of the total lift to the Lunar Roving Vehicle.

CONCLUSIONS

A theory has been presented from which inertia forces of moving soil, influencing the motion of a rolling wheel, can be estimated. The theory is compared with previous experimental analysis and experimental data from rolling spheres. These comparisons indicate that the theoretical predictions are reasonable, and that predictions specifically of the magnitude of inertial effects are within 50% of the measured values. These inertial effects are computed from equation (7-11)

$$\frac{q_I}{\rho_s g w} = \beta \frac{v^2}{wg}$$

where q_I = pressure due to inertia of moving soil (acting in the same direction as static bearing capacity, q), ρ_s = mass density of soil, g = acceleration of gravity, w = track width, v = velocity of wheel, and β is a function of soil friction angle, ϕ , and slope angle, α . Values of β are given in Fig. 7-6.

A concept of equivalent cohesion is introduced, which allows data for

and $c - \phi$ soil to be plotted and analyzed as shown in Figs. 7-7, 7-9, and 7-10. The main advantage of this type of plot is that β can be determined experimentally from tests at high wheel velocities (100 m/hr = 161 km/hr). Since all assumptions necessary in developing equation (7-11) are incorporated in β , refinements in values of β can be made as additional experimental data become available.

The studies presented show that soil inertia forces can be important (5 to 50% of total soil reaction) at even moderate wheel velocities.

CHAPTER 8. WHEEL-SOIL INTERACTION ANALYSIS

SUMMARY

A summary of the relationships derived in the previous chapters is given below. These relationships are related to:

1. Sinkage of a wheel
2. Pull that can be developed from a wheel
3. Mobilization of shear stresses at the wheel-soil contact
4. Soil inertia effects

The derivations are all based on the assumption that the wheel-soil interaction is two-dimensional in the sense that relevant interaction between soil particles and the wheel is all in the plane of rolling of the wheel. The presented relationships were based on two fundamental observations:

1. The line of action of the resultant of radial stresses approximately bisects the wheel-soil contact angle, θ_T , for all values of slip, s .
2. For developing general wheel-soil interaction theory, all parameters operating at the wheel-soil interface are functions of slip and position. This led to concepts such as 1) slip at a point, 2) the shear stress surface, and 3) the performance surface (to be presented). The general problem requires that all functional relationships be visualized in some three-dimensional way.

Summary of Basic Relationships

For a rigid cylindrical wheel operating in any soil, sinkage can be related to the towed force by

$$\frac{N_x}{N_y} = \tan \left[0.4 \cos^{-1} \left(1 - 2 \frac{z}{D} \right) \right] \quad (5-4)$$

where z = sinkage, D = wheel diameter, N_x = motion resistance, and N_y = vertical component of N associated with motion resistance (Fig. 4-10).

Sinkage can be estimated, using bearing capacity theory, from equation (5-8) or equation (5-9) by noting that the total bearing capacity, Q , must equal, N , giving

$$q = \frac{N}{A} = \frac{\gamma_s w}{2} s_{\gamma} N_{\gamma} + s_{cq} [(c + q' \tan \phi) N_c + q'] \quad (5-8)$$

where

q = unit bearing capacity

q' = $z \gamma_s / 2$ or surcharge

N = resultant of radial stresses

A = wheel-soil contact area = $\theta_T r w$

w = wheel width

γ_s = soil unit weight

c = soil cohesion

ϕ = soil friction angle

s_{γ} , s_{cq} = shape factors which can be determined from equations (5-10) and (5-11)

N_{γ} , N_c = bearing capacity factors which can be determined from Figures 5-7 and 5-8, using θ_N = Meyerhof's β_m

Sinkage can also be estimated from

$$q = \left[\frac{k}{w} + k_{\phi} \right] z^n \quad (5-5)$$

using procedures outlined by Bekker (1969), and taking into account experience gained from the use of these procedures.

Pull, P , negative or positive, can be determined from a force polygon (Fig. 4-10) or from the following equations

For a soil with both cohesion and friction, where the wheel-soil cohesion $c_a > 0$, and the wheel-soil friction angle $\delta > 0$,

$$\begin{aligned} \left(\frac{P}{W}\right)^2 &= \left(\cos\theta_N - \frac{P}{W} \sin\theta_N\right)^2 \left[1 + \left(\frac{\tan\delta}{r/r}\right)^2\right] \\ &+ 2\left(\cos\theta_N - \frac{P}{W} \sin\theta_N\right) \frac{\tan\delta}{(r/r)^2} \frac{Ac_a}{W} + \left(\frac{Ac_a}{W r/r}\right)^2 - 1 \end{aligned} \quad (4-20)$$

For a pure sand ($c_a = 0$),

$$P^2 = \left[\frac{r}{r_f'/r_f} \int \frac{\sigma_\theta}{\cos\delta} d\theta\right]^2 - W^2 \quad (3-34)$$

or

$$\left(\frac{P}{W}\right)^2 = \left(\cos\theta_N - \frac{P}{W} \sin\theta_N\right)^2 \left[1 + \left(\frac{\tan\delta}{r/r}\right)^2\right] - 1 \quad (4-21)$$

For a pure clay ($\delta = 0$),

$$\left(\frac{P}{W}\right)^2 = \left(\cos\theta_N - \frac{P}{W} \sin\theta_N\right)^2 + \left(\frac{Ac_a}{W r/r}\right)^2 - 1 \quad (4-22)$$

For a towed wheel in any soil,

$$\left(\frac{P}{W}\right)^2 = \left(\cos\theta_N - \frac{P}{W} \sin\theta_N\right)^2 - 1 \quad (4-23)$$

The towed force can also be analyzed from

$$\left(\frac{P}{W}\right) = \tan\theta_N \quad (4-31)$$

Soil inertia forces influencing the wheel can be evaluated from

$$\frac{q_I}{\rho_s g w} = \beta \frac{v^2}{g w} \quad (7-11)$$

where β can be estimated from Fig. 7-6.

In the above equations, δ and c_a are functions of position, θ , and slip, s , but the subscripts were omitted to shorten the expressions. (The use of δ and c_a and the mobilization of shear stresses are discussed in detail in Chapter 6.) The ratios \bar{r}/r and r_f'/r_f , which turn out to be equal, can be determined from Fig. 3-7. The terms in the above equations are defined as follows:

- c_a = wheel-soil cohesion
- g = acceleration of gravity
- P = pull (negative or positive) for any slip
- q_I = soil inertia pressure
- r = radius of wheel
- \bar{r} = radius to line of action of F (vectorial)
- r_f = moment arm to dR (see Fig. 3-1)
- r_f' = moment arm to R (see Fig. 3-1)
- v = translational velocity of wheel
- W = wheel load
- β = abbreviation used in solving equation (7-11), see Fig. 7-6
- δ = wheel-soil friction angle
- θ = angle identifying any position at the wheel soil contact (see Fig. 3-1)

θ_N = angle to the line of action of the resultant of radial (normal) stresses

σ_θ = radial stress at the wheel-soil contact

ρ_s = soil mass density

ANALYSIS PROCEDURE

Suppose that we are to determine performance of a wheel in a given soil at a particular state of slip of the wheel. In solving all forces of the force polygon (Fig. 4-10), two separate procedures may be considered: 1) sinkage known, 2) sinkage unknown. These cases will be described in detail below. The written outline follows the block diagram and graphical solutions in Figs. 8-1 and 8-2.

Sinkage Known (Fig. 8-1)

Given: Wheel load

Procedure:

1. Determine wheel-soil strength parameters, δ and c_a , as a function of displacement from 3 ring-shear tests, as shown in Fig. 6-5.
2. Select the appropriate strength parameters, δ and c_a , for desired slip, using Fig. 6-4 and the test data.
3. Compute θ_N from equation (5-3), and draw to scale W and θ_N .
4. Assume a value of N and compute F using equations (4-18) and (4-19). Draw F perpendicular to the θ_N line, and draw N parallel to the θ_N line, from F .
5. Compare F and N to the required closure. The resultant of F and N must reach the line of action at P , which is a horizontal line drawn from the top of W . If the force polygon does not close, a wrong N value was used.

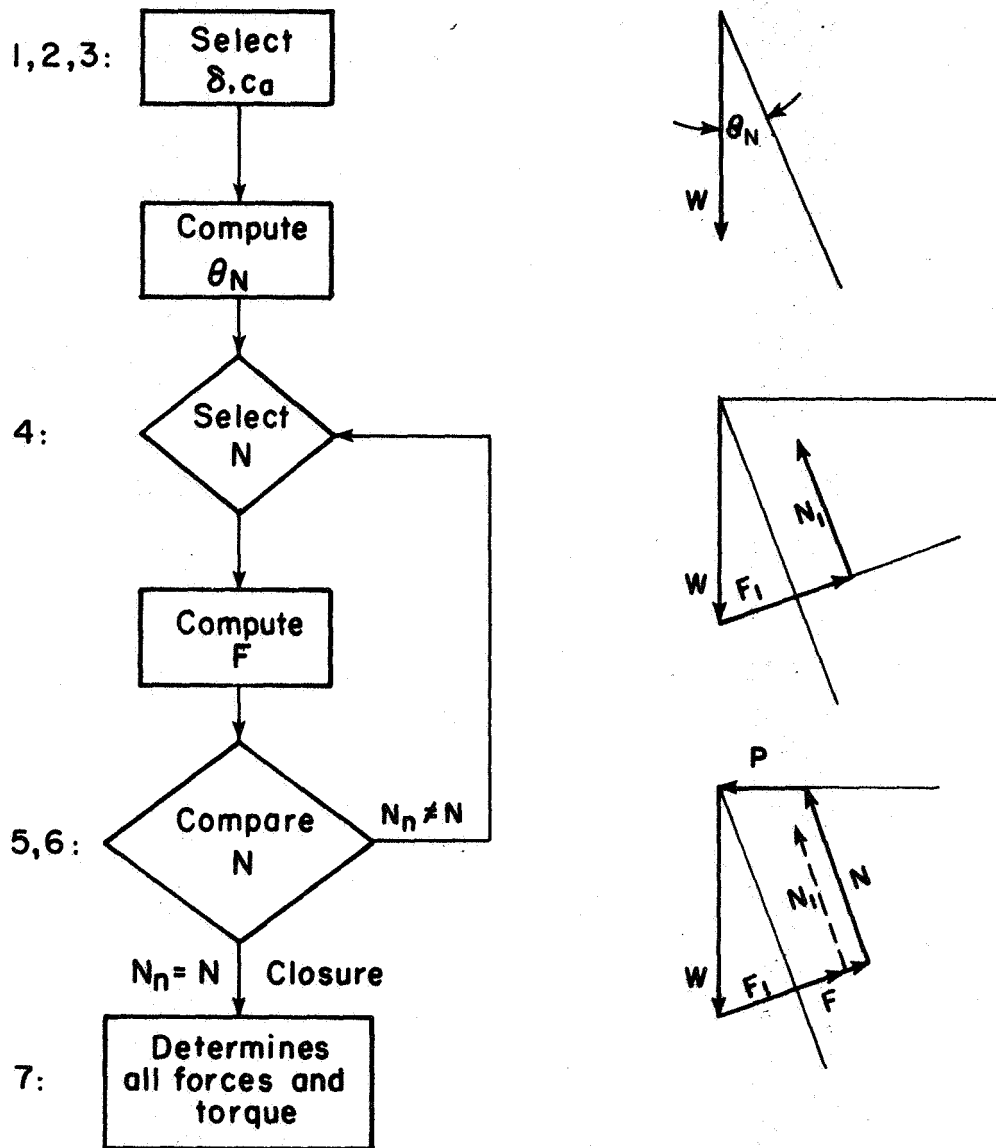


Fig. 8-1. Solution of the wheel-soil interaction force polygon for known sinkage.

6. Select a new N and compute F ; continue steps 4, 5 and 6 until the force polygon closes.
7. Closure of the force polygon determines the pull, P , and all other forces associated with the force polygon. Once all these forces are known, the required torque, or torque associated with F , can also be determined.

Weakest Link:

The weakest link or step in the above procedure is probably that of relating soil parameters to slip (Fig. 6-4). This requires further research.

Sinkage Unknown (Fig. 8-2)

Given: Wheel load

Procedure:

1. Determine soil strength parameters, ϕ and c , and/or coefficients associated with equations (5-5) or (5-6).
2. Compute q vs. θ_N from equations (5-8) or (5-9) or equations (5-5) or (5-6), using also equation (5-3).
3. Assume a value of N giving a value for θ_N . Draw to scale W and θ_N .
4. Determine wheel-soil strength parameters, δ and c_a , as a function of displacement from 3 ring-shear tests, as shown in Fig. 6-5.
5. Select the appropriate strength parameters, δ and c_a , for desired slip, using Fig. 6-4 and the test data.
6. Compute F using equation (4-18) and (4-19), and draw F perpendicular to the θ_N line. Draw N parallel to the θ_N line, from F .
7. Compare F and N with the required closure.

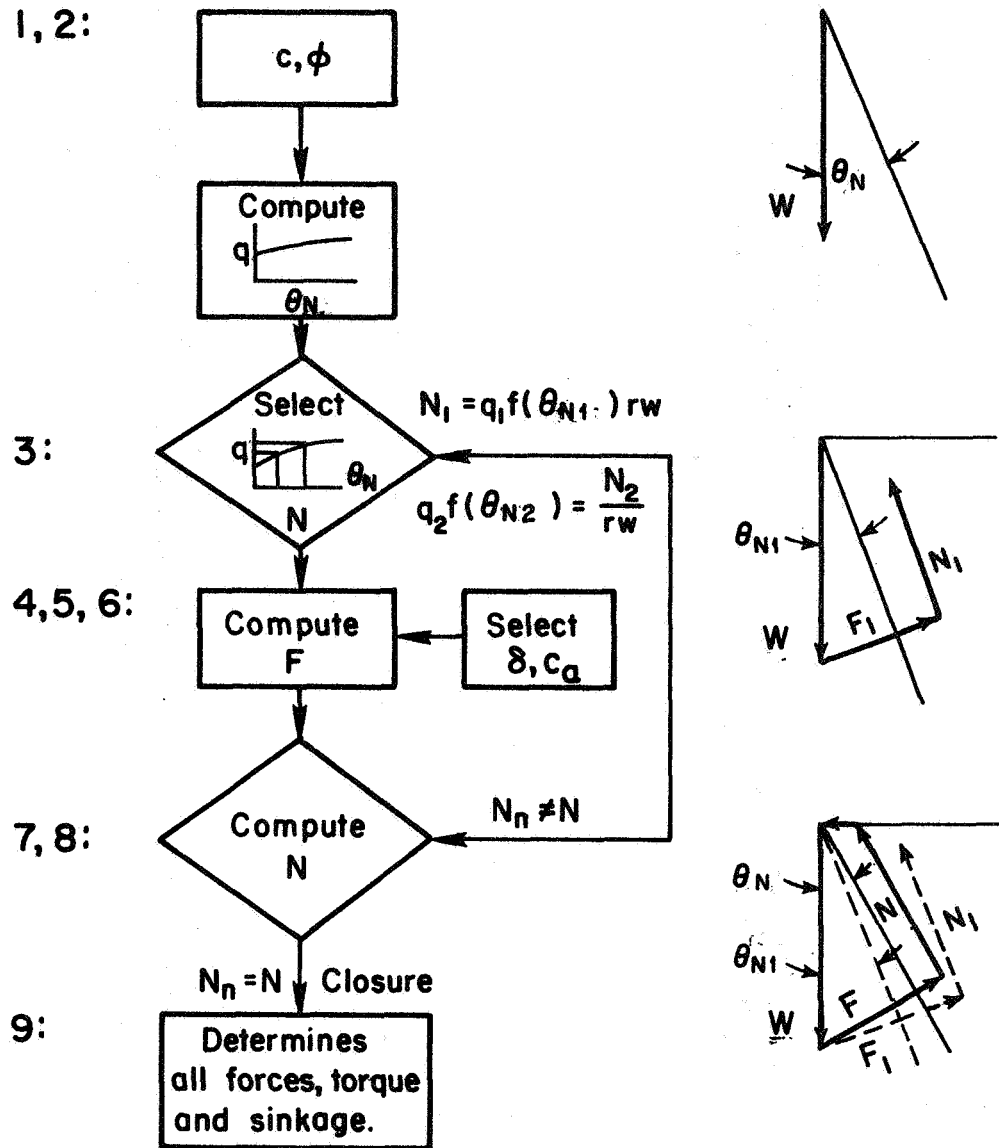


Fig. 8-2. Solution of the wheel-soil interaction force polygon for unknown sinkage.

8. If the force polygon does not close, select a new N , compute a new F , and continue steps 3, 6, 7, and 8 until appropriate closure is achieved.
9. Closure of the force polygon determines all the forces consistent with the computed sinkage and wheel-soil contact angles. Again, the torque, T , associated with F can now be determined.

Weakest Link:

The weakest link or step in the above procedure (sinkage unknown) is probably that of estimating sinkage (step 2), either using bearing capacity theory or equations (5-5) or (5-6). This requires further research. In addition, step 5, which relates soil parameters to slip (Fig. 6-4), requires further research.

COMPARISONS

It has not been possible to compare predictions based on the procedures outlined above directly with experimental data, because the type of displacement dependent wheel-soil strength parameters (Fig. 6-5) required have not been found in the literature. It is possible, however, to make some general comparisons.

A common expression for developed pull (Bekker, 1969) is

$$P = H - R_b \quad (8-1)$$

$$H = Ac + W \tan \phi$$

$$R_b = \frac{W^x}{k w D}$$

where H = traction developed by the wheel, R_b = motion resistance, k = a sinkage coefficient, and the exponent x varies between 1 and 2.

Consider the simple case of a pure sand with $\delta = 45^\circ$, $k = k_\phi \cong 3$, and a wheel with $w = 5$ and $D = 20$. Equation (8-1) then reduces to

$$P = W - \frac{W^x}{300} \quad (8-2)$$

Based on theory presented in this report, the same simple case can be studied using equation (4-21). For the same soil conditions used above, and assuming $\bar{r}/r = 1$, equation (4-21) reduces to

$$P^2 = 2(W \cos \theta_N - P \sin \theta_N)^2 - W^2 \quad (8-3)$$

While equation (8-2) is a function of the width of the wheel, equation (8-3) is just an equilibrium solution of forces in the plane of rolling. Equation (8-3) incorporates also the case of an undeformable surface, such as may be the case with a rail. Note that in this case $\theta_N = 0$, and equation (8-3) reduces to $P/W = 1$. This is obviously correct for $\delta = 45^\circ$.

For a deformable surface, such as a soil, θ_N is a function of W . Assume for the sake of this comparison that θ_N increases linearly from 0 to 20 degrees as W increases from 0 to 300. On this basis, equations (8-2) and (8-3) are compared in Fig. 8-3. As shown, the two theories lead to similar P vs. W relationships for this simple case. In the use of equation (8-2), the trick is to select the proper x . In the use of equation (8-3), the trick is to select the proper θ_N .

The influence of the uncertainty in selecting θ_N was also evaluated by solving equation (8-3) for $\theta_N \pm$ one standard deviation, based on data in Figs. 4-5 to 4-9. The range suggested by these solutions is shown by the cross-hatched area in Fig. 8-3. The same range can also be defined by $x = 1.87$ and $x = 1.91$. While it may be difficult to even distinguish between 1.87 and 1.91 by curve-fitting techniques, this range represents

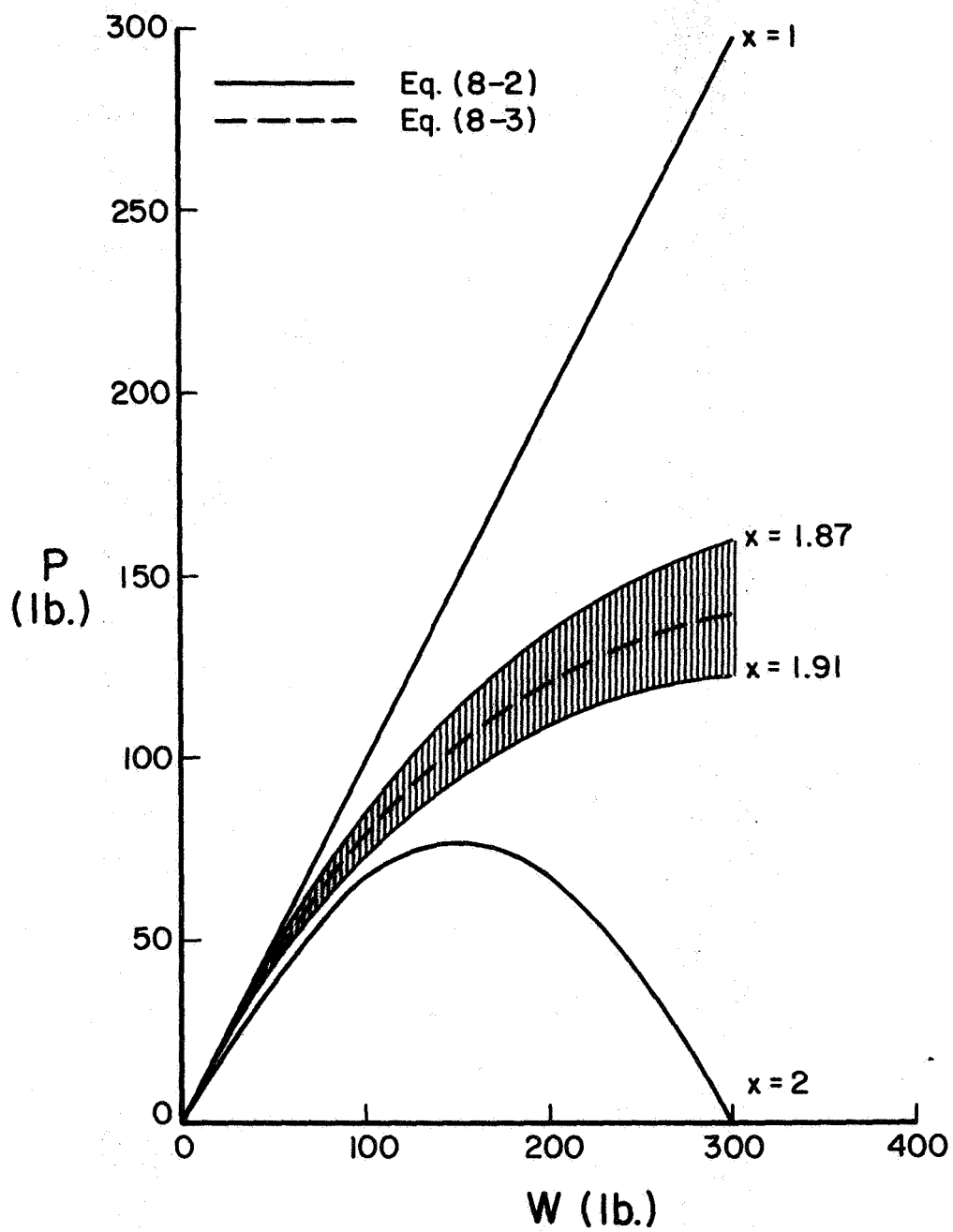


Fig. 8-3. Comparison between equations (8-2) and (8-3).

approximately 68% of the data shown in Figs. 4-5 to 4-9. The potential value of presented theory, rather than theory based on an exponential equation, is therefore demonstrated. Solutions can be more accurately bracketed by θ_N rather than x .

Consideration of pull as a function of both slip, s , and position, θ , suggest a performance surface as illustrated in Fig. 8-4. Reanalysis of data by Leflaive, 1967, demonstrates experimentally the same type of surface, as shown in Fig. 8-5. There is a separate P vs. s relationship for each value of W . Therefore, P/W by itself, although very frequently given in the literature, may not be a very meaningful dimensionless parameter.

It is also possible to predict a performance surface from theory presented in this report. Such a surface (Fig. 8-6) was computed on the basis of Leflaive's wheel and sinkage data, and Figs. 6-4 and 6-5. It is to be noted that Figs. 8-5 and 8-6 are not comparable; a comparable theoretical prediction could only be made using soil strength parameter relationships based on actual testing instead of Fig. 6-5. Fig. 8-6 illustrates, however, the general and realistic nature of the prediction. Also, the performance surface of Fig. 8-6 suggests a more plastic soil than that of Fig. 8-5, where there is essentially no increase in pull, P , beyond $s = + .15$.

CONCLUSIONS AND RECOMMENDATIONS

Conclusions

Approximate and general solutions have been developed for a rigid cylindrical wheel operating in soil. A detailed summary of these developments was presented earlier in this chapter. The solutions deal with

1. Sinkage of a wheel
2. Pull that can be developed from a wheel

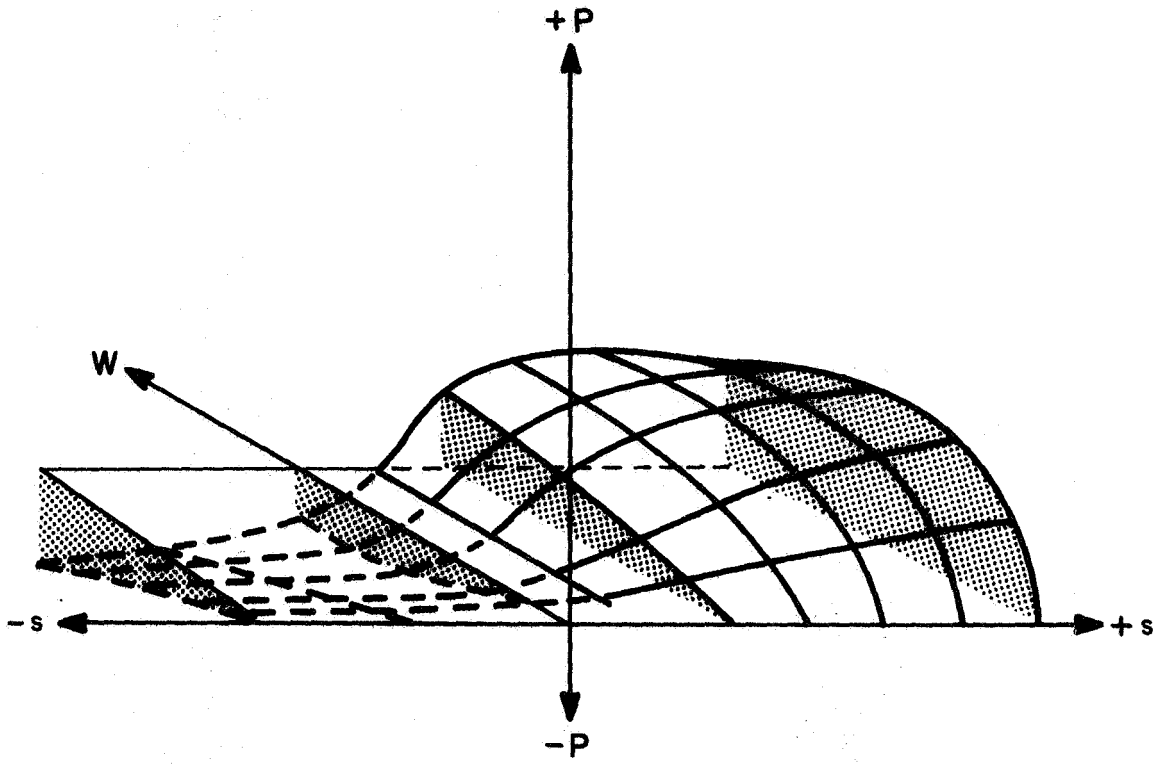


Fig. 8-4. Performance surface; pull as a function of wheel load and slip.

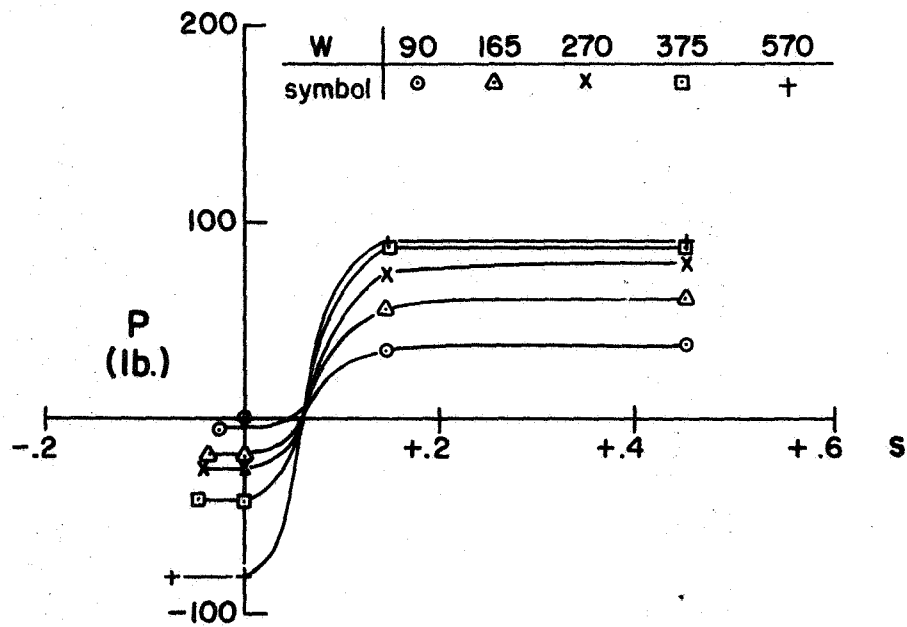
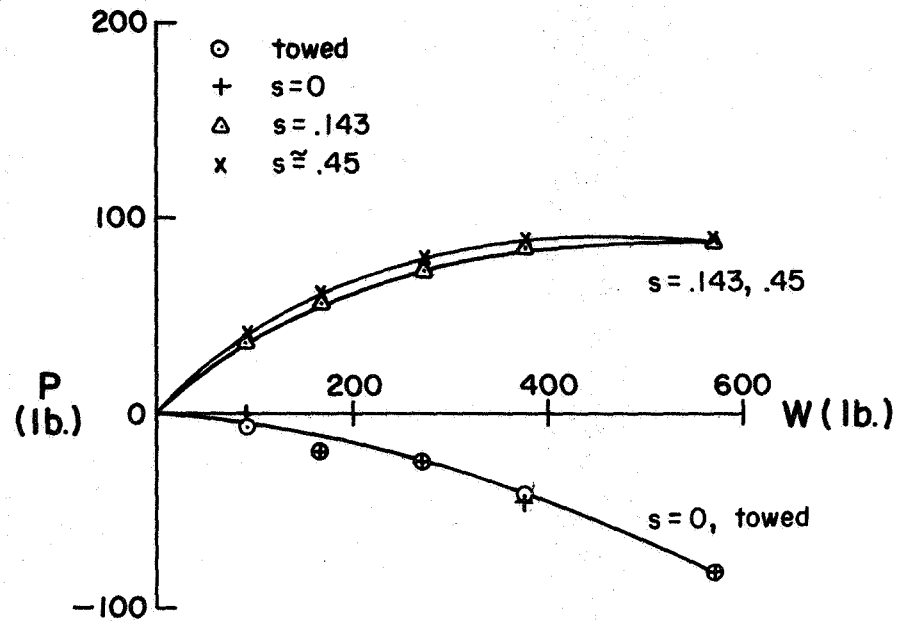


Fig. 8-5. Performance surface, rigid wheel data, Leflaive (1967)

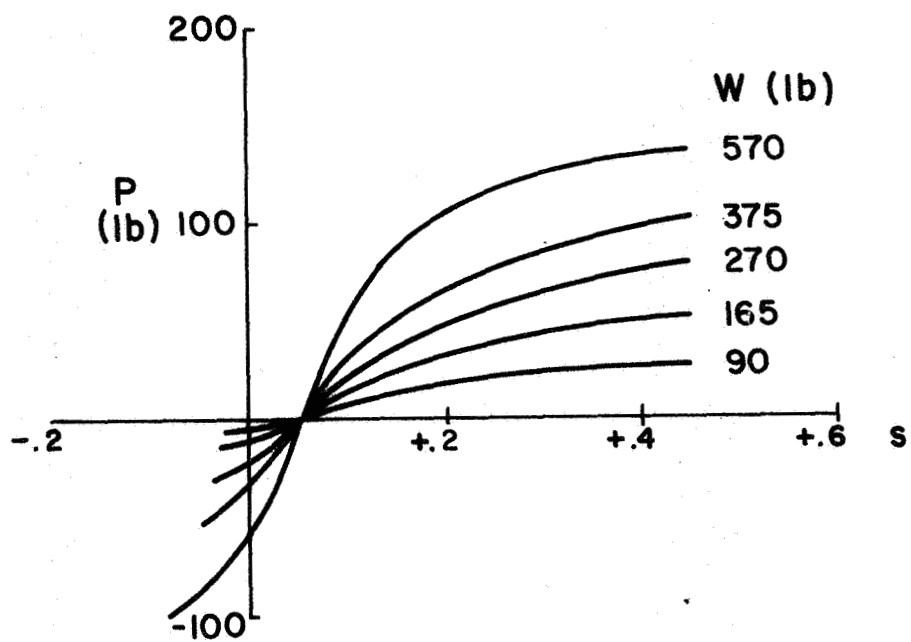
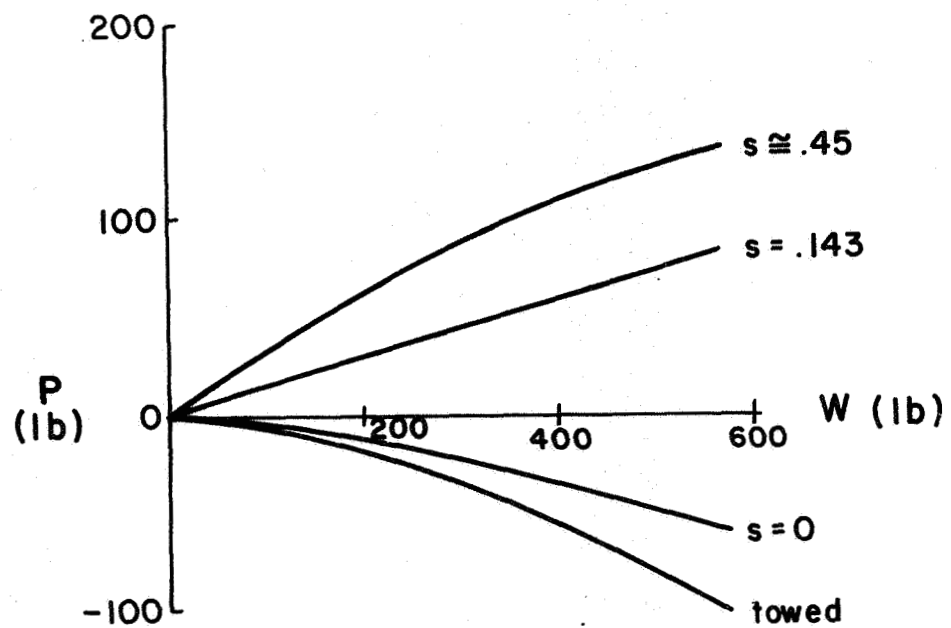


Fig. 8-6. Predicted performance surface.

3. Mobilization of shear stresses at the wheel-soil contact
4. Soil inertia effects

The solutions are primarily the result of simple considerations of statics and dynamics. The error associated with the solutions can be evaluated, and theoretical predictions are likely to be within 15% of the correct value.

For each of the four phenomena listed above, the developments suggest how prediction of wheel-soil interaction can be improved, and these items are discussed below.

Recommendations

Sinkage of a wheel:

Sinkage, as computed from equation (5-7), is subject to typical limitations of bearing capacity theory. Because the wheel-soil interaction problem requires an exact solution as opposed to an upper or lower bound, if bearing capacity theory is to be used, it must be tailored specifically to fit the problem. This is possible, as was demonstrated by modifying the bearing capacity equation to the case of rigid spherical wheels (Fig. 5-3, 5-4, and 5-5). The intermediate cases (3) and (4) in Fig. 5-6a, require further research.

Tests should be conducted where soil conditions are controlled, and careful measurements are made of wheel-soil contact angles, θ_1 , θ_2 , θ_T , and θ_N as these are influenced by the state of slip of the wheel. Then the measured wheel load and pull or towed force can be compared to predictions by the bearing capacity equation, and more realistic shape factors and correction factors to the bearing capacity factors can be developed.

The observation that the line of action of the resultant of radial stresses approximately bisects the wheel-soil contact angle for all values of slip, which is substantiated by data in Figs. 4-5 and 4-6, clearly

suggest that the mobilization of shear stresses along the wheel-soil contact, and the mobilization of radial stresses, are associated with two separate mechanisms. It is believed that the resultant of radial stresses, N , should be related to bearing capacity for all values of slip.

Pull that can be developed from a wheel:

Further, while much data has been accumulated on performance parameters, much less detailed data is available on wheel-soil contact angles. Since it has been demonstrated that, knowing θ_N , the wheel-soil interaction problem becomes determinate, careful data on θ_N should be collected. With the data presented in Figs. 4-5 through 4-9, it is probable that about 68% of predictions of pull will be within approximately 15% of the correct value. Improved data, adequate to separate out variables associated with the states of the wheel and the soil, should reduce the error to an acceptable value in probably all cases.

Mobilization of shear stresses at the wheel-soil contact:

Further theoretical contemplation should be first undertaken to relate soil test displacements to slip at a point, s_θ , as was attempted in Fig. 6-4. This could lead to a general and rigorous relationship. Contemporaneously, shear stress surfaces (Fig. 6-5) should be plotted from experimental data whenever possible to further our understanding of the general problem:

Soil inertia effects:

The developments in Chapter 7, and particularly Figs. 7-9 and 7-10, show that β in equation (7-11)

$$\frac{q_t}{\rho_s g w} = \beta \frac{v^2}{wg}$$

can be experimentally determined. Since all assumptions necessary in developing equation (7-11) are incorporated in β , our dependence on these

assumptions need only be temporary. Tests conducted by running a wheel at relatively high velocity on a soil, and measuring the lift provided the wheel by the soil, will allow determination of β for desired soil conditions from the type of plots shown in Figs. 7-9 and 7-10.

REFERENCES

- Bekker, M. G., Theory of Land Locomotion, University of Michigan Press, Ann Arbor, 1956.
- Bekker, M. G., Introduction to Terrain-Vehicle Systems, University of Michigan Press, Ann Arbor, 1969.
- Crenshaw, B., "Soil/Wheel Interaction at High Speed," SAE paper No. 710181, January 1971.
- Crenshaw, B., Butterworth, C., and Truesdale, W., "Aircraft Landing Gear Dynamic Loads from Operation on Clay and Sandy Soil," AFFDL-TR-69-51, February, 1971.
- Firth, B. W., "Resistance of Soils to Sinkage and Translation of Rigid Bodies: A Study by Means of Dimensional Analysis," SAE paper No. 670172, January, 1967.
- Firth, B. W., "Direct Demonstration of Dimensional Analysis," Bull. Mech. Engng, Educ., Vol. 8, pp. 65-70, 1969.
- Hovland, H. J., "Mechanics of Rolling Sphere-Soil Slope Interaction," Ph.D. Dissertation, Civil Engineering Department, University of California, Berkeley, 1970.
- Hovland, H. J. and Mitchell, J. K., "Mechanics of Rolling Sphere-Soil Interaction," Final Report, Vol. 2, Space Sciences Laboratory, University of California, Berkeley, 1971.
- Hovland, H. J. and Mitchell, J. K., "Model Studies of the Failure Mechanism Associated with a Sphere Rolling Down a Soil Slope," Journal of Terramechanics, Vol. 9, No. 1, pp. 37-50, 1972.
- Karafiath, L. L. and Nowatzki, E. A., "A Study of the Effect of Sloping Ground on Bearing Strength and the Landing Performance of Space Vehicles," Memorandum RM-407, Grumman Research Department, New York, 1968.
- Karafiath, L. L. "Plasticity Theory and Stress Distribution Beneath Wheels," Journal of Terramechanics, Vol. 8, No. 2, 1971.
- Karafiath, L., "On the Effect of Pore Pressures on Soil-Wheel Interaction," Proceedings Fourth International Conference for Terrain Vehicle Systems, Stockholm, April, 1972.
- Karafiath, L. L. and Nowatzki, E. A., "The Effect of Speed on Wheel Drag in Soil," Memorandum RM-546, Grumman Research Department, New York, 1972.
- Krick, G., "Druck-und Schubverteilung Unter Rädern und Reifen auf Naehgiebigem Boden Unter Berücksichtigung der Reifendeformation," Proceedings of the 3rd Intern. Conference, ISTVS, pp. 50-75, 1969.

Leflaive, E. M., "Mechanics of Wheels on Soft Soils, Report 2; Effect of Width on Rigid Wheel Performance," U.S. Army Engineer Waterways Experiment Station, Technical Report No. 3-729, 1967.

Meyerhof, G. G., "The Ultimate Bearing Capacity of Foundations," *Geotechnique*, Vol. 2, p. 301, 1951.

Meyerhof, G. G., "The Bearing Capacity of Foundations Under Eccentric and Inclined Loads," *Proc. Third Int. Conf. Soil Mech.*, Vol. 1, p. 440, 1953.

Onafeko, O. and Reece, A. R., "Soil Stresses and Deformations Beneath Rigid Wheels," *Journal of Terramechanics*, Vol. 4, No. 1, pp. 59-80, 1967.

Sela, A. D., "The Shear to Normal Stress Relationship Between a Rigid Wheel and Dry Sand," U.S. Army Land Locomotion Laboratory, Report No. 8524, June, 1964.

Schuring, D., "A Contribution to Soil Dynamics," *Terramechanics*, Vol. 5, No. 1, pp. 31-37, 1968.

Schuring, D., "Rolling Resistance of Wheels in Soft Soil," *American Society of Automotive Engineers*, Paper No. 72-633, Dec., 1972.

Söhne, W. and Sonnen, F. J., "Comparison Between Relationships of Agricultural Tractors and Mechanical Soil Values," *Proc., 1st Intern. Conf. on the Mechanics of Soil-Vehicle Systems*, Edizioni Minerva Tecnica, Torino, Italy, No. 33, 1961.

Sokolovski, V. V., Statics of Soil Media, Butterworths, London, 1969.

Taylor, D. W., "Stability of Earth Slopes," *Journal of the Boston Soc. of Civil Engineers*, Vol. 24, No. 3, 1937.

Terzaghi, K., Theoretical Soil Mechanics, John Wiley and Sons, Inc., New York, 1943.

Uffelmann, F. L., "The Performance of Rigid Cylindrical Wheels on Clay Soil," *Proc., 1st Intern. Conf. on the Mechanics of Soil-Vehicle Systems*, Edizioni Minerva Tecnica, Torino, Italy, No. 8, 1961.

U. S. Army Engineer Waterways Experiment Station, "Tests on Natural Soils with Self-Propelled Vehicles, 1951-53," *Tech. Memo No. 3-240, 12th Suppl.*, Nov., 1954.

Vincent, E. T., "Pressure Distribution on and Flow of Sand Past a Rigid Wheel," *Proc. 1st Intern. Conf. on the Mechanics of Soil-Vehicle Systems*, Edizioni Minerva Tecnica, Torino, Italy, No. 50, 1961.

Yong, R. N. and Webb, G. L., "Energy Considerations in Wheel-Clay Soil Interaction," *McGill University, Montreal, Canada, Soil Mech. Series No. 25*, 1969.

Yong, R. N. and Windisch, E. J., "Contact Stresses and Soil Strain-Rate Behaviour in Wheel-Soil Interaction," *McGill University, Montreal, Canada, Soil Mech. Series, No. 28*, 1970.

LIST OF SYMBOLS

A	wheel-soil contact area
$A_1 A_2$	$A_1 = A_2 - \theta$
a	linear acceleration of wheel
a_s	linear acceleration of soil
a_{max}	maximum acceleration of soil
$B_1 B_2 B_3$	integration constants
b	width of footing in the bearing capacity equation
c	soil cohesion
c_a	wheel-to-soil cohesion or adhesion
c_e	equivalent cohesion
c_1	cohesion of soil (1)
c_x	cohesion of soil (x)
D	wheel diameter
DR	distance revolved
DT	distance traveled
d	dimension defining triangle base proportional to d_o
d_o	dimension of cone (active Rankine zone) underneath wheel
e	base of natural logarithm
F	vectorial sum of shear stresses at wheel-soil contact
F_a	algebraic sum of shear stresses at wheel-soil contact
F_x	x component of F
F_y	y component of F
g	acceleration of gravity
H	traction developed by wheel, equation (8-1)
I	mass moment of inertia of wheel

i	slip = $1 - DT/DR$
k_c	cohesion parameter in equation (5-5a)
k_ϕ	friction parameter in equation (5-5a)
l	length of wheel-soil contact in direction of motion
m	mass of wheel
m_s	mass of soil set in motion by wheel
N_Y , N_c , N_q	Meyerhof (1951) bearing capacity factors
N_{Ys} , N_{cs} , N_{qs}	bearing capacity factors for rolling spheres
N	vectorial sum of normal stresses at wheel-soil contact
N_x	x component of N (motion resistance)
N_y	y component of N
P	pull developed by the wheel (negative or positive)
P_T	towed force
Q	total bearing capacity
q	unit bearing capacity
q_I	unit resistance due to soil inertia
q^1	surcharge pressure
R	vectorial sum of all stresses at the wheel-soil contact
R_a	algebraic sum of all stresses at the wheel-soil contact
R_b	motion resistance, equation (8-1)
R_I	soil inertia force
R_x	x component of R
R_y	y component of R
r	wheel radius
r_e	wheel effective radius
r_f	moment arm to any dR , but $r_f \neq f(\theta)$
$r_{f\theta}$	moment arm to any dR from wheel center
r_f^1	moment arm to R from wheel center

r_t	radius of shear ring test, chapter 6
r_w	radius of wheel, chapter 6
r_z	wheel radius as a function of z
\bar{r}	radius, or distance from wheel center, to action of F
s	slip = $(DR - DT)/(DR + DT)$
s_θ	slip, s , as a function of θ
s_γ s_c s_q	shape factors used in bearing capacity theory
T	input torque
t	time
t_s	time of soil movement
t_t	time increment for ring shear test
t_w	time increment for wheel
u	angular acceleration of wheel
V_s	volume of moving soil
v	linear velocity of wheel
v_a	average soil velocity
v_s	velocity of soil
$v_{c/x}$	velocity of wheel center w.r.t. x
$v_{p/c}$	velocity of point p w.r.t. c
$v_{p/x}$	velocity of p w.r.t. coordinate system, x , fixed in soil
W	wheel load or weight
w	track width
x, y, z	coordinates
x_s	distance of soil displacement
x_w	distance of wheel displacement
y	vertical distance to instantaneous center of rotation
z	sinkage

α	slope angle
α^1	inclination of plate
β	abbreviation used in solving equation (7-1)
β_m	angle defining Meyerhof's free surface
δ	wheel-soil friction angle
$\delta_{\theta s}$	δ as a function of θ and s
γ_s	unit weight of soil
γ_r	unit weight of sphere or rock
θ	angle identifying any position at the wheel-soil contact
θ_F	angle defining the line of action of F
θ_T	total wheel-soil contact angle
θ_n	angle to the line of action of the resultant of normal (radial) stresses
θ_t	contact angle associated with ring shear test, chapter 6
θ_w	contact angle associated with wheel, chapter 6
θ_1	wheel-soil contact angle forward of vertical centerline
θ_2	wheel-soil contact angle rear of vertical centerline
θ'_2	angle of intersection of slope and upper end of passive Rankine zone
θ'_3	angle of intersection of slope and shear surface
Φ	angle defining the direction of any dR in a $c - \phi$ soil
ϕ	soil friction angle, or angle of shearing resistance
ϕ_1	friction angle of soil (1)
ϕ_x	friction angle of soil (x)
ψ	angle defining frictional resistance at wheel-soil contact
ψ_a	function or coefficient relating soil acceleration to wheel velocity

ρ_s	soil mass density
σ	radial pressure at wheel-soil contact
$\sigma_{\theta z}$	as a function of θ and direction perpendicular to the paper, z
τ	shear stress at the wheel-soil contact
$\tau_{\theta z}$	shear stress as a function of θ and z
ϵ_w	soil strain associated with wheel
ϵ_t	soil strain associated with a ring shear test
Δt	soil displacement associated with a ring shear test
Δw	soil displacement associated with wheel
Δz_t	depth of soil strained in the ring shear test
Δz_w	depth of soil strained by wheel
ω	angular velocity of wheel